AD-752 057

A PROBABILISTIC APPROACH TO THE DESIGN OF HEAT PIPES

C. C. Roberts, et al

New Mexico University

Prepared for:

Office of Naval Research

September 1972

DISTRIBUTED BY:

NTIS

National Technical Information Service
U. S. DEPARTMENT OF COMMERCE
5285 Port Royal Road, Springfield Va. 22151

AD752057

THE UNIVERSITY OF NEW MEXICO

Bureau of Engineering Research

Albuquerque

A PROBABILISTIC APPROACH TO
THE DESIGN OF HEAT PIPES

by
C. C. Roberts
and
K. T. Feldman

Technical Report ME-55(72)ONR-012

September 1972

*This work supported by Office of
Naval Research Contract N00014-68-A-0155-0002.*

A PROBABILISTIC APPROACH TO
THE DESIGN OF HEAT PIPES

by

C. C. Roberts
and
K. T. Feldman

Technical Report ME-55(72)ONR-012

September 1972

ABSTRACT

The design of heat pipes involves knowledge of phenomena such as surface tension forces, wick permeability, and fluid vaporization and condensation. Considerable variability in these phenomena has been observed in heat pipe experiments. Thus, a probabilistic design model for predicting heat pipe heat transfer rate has been developed taking into consideration uncertainty in the prediction of the above phenomena. The probabilistic model yields a mean, a standard deviation, and the distribution of heat transfer rate based on the means, standard deviations, and distributions of the design parameters. The probabilistic method is compared to experimental data from heat pipes with wire mesh wicks. Mean values, standard deviations, and distributions are presented for wick permeability, critical radius, area, porosity, tortuosity, and heat transfer rate. A technique is described for making wire mesh wicks. The probabilistic design model indicates the range of design without the use of safety factors.

Preceding page blank

TABLE OF CONTENTS

LIST OF FIGURES

NOMENCLATURE

A	cross sectional area of liquid saturated wick, ft^2, cm^2
A_v	cross sectional area of vapor passage, ft^2, cm^2
b	tortuosity or wick geometry constant, dimensionless
D	diameter, ft, cm
d	characteristic dimension, ft, cm
e	porosity of capillary structure or wick, dimensionless
F	force term
g	gravitational acceleration constant, 32.2 ft/sec^2
g_c	dimensional conversion constant, 32.2 lbm $ft/lbf\ sec^2$
H	gravity head, inches H_2O
h	elevation distance, ft, cm
h_{fg}	latent heat of vaporization, BTU/lbm, cal/gm
J	mechanical equivalent of heat, 778 ft lb/BTU
k	thermal conductivity, BTU/hr ft^2 °F, watts/cm °C
K	permeability, ft^2, cm^2
L	pipe length, ft, cm
L'	effective length, $L_e/2 + L_a + L_c/2$, ft, cm
m	mass flow rate, lbm/hr, gm/sec
M	momentum, lbm ft/sec
N_ℓ	liquid transport factor, BTU/hr ft^2, $watts/cm^2$
P	pressure, lb/ft^2 $dynes/cm^2$ mm Hg
p	probability
q	heat flux, BTU/hr ft^2, $watts/cm^2$
Q	maximum heat transfer rate, BTU/hr, watts
r	radius or radial coordinate, ft, cm

r_e	pore radius in evaporator wick, ft, cm
r_c	pore radius in condenser wick, ft, cm
r_{pi}	inside radius of heat pipe, ft, cm
R	miniscus radius of curvature at liquid vapor interface, ft, cm
t	thickness
t_w	wick thickness, ft, cm
T	temperature, °F, °C
u	axial velocity, ft/sec, cm/sec
v	radial velocity, ft/sec, cm/sec
V	volume, ft^3, cm^3
w	work, lbf
x	axial coordinate
y	vertical coordinate
z	coordinate
α	accommodation coefficient
γ	specific weight, lbf/cu.ft.
ε	emissivity of radiation heat transfer
Δ	difference symbol
θ	wetting angle, degrees
μ	dynamic viscosity, lbm/ft sec, gm/cm-sec
ρ	density, ft^3/lbm, cm^3/gm
σ	surface tension, lbf/ft, dynes/cm
ϕ	angle of inclination

Subscripts

a	adiabatic
c	condenser
c_a	calculated

e	evaporator, or arbitrary wick pore
g	gravity effect
i	inside
ℓ	liquid
max	maximum
fr	fully recessed
f	friction
N	dimension
v	vapor
w	wick
p	pressure
r	recessed
P_i	pipe
o	outside surface
Ob	observed
s	steel
v	vapor
w	wick or wall

STATISTICAL NOTATION

$\bar{x}$	estimate of the mean of a population of random variables, x.
S_x	estimate of the standard deviation of a population of random variables, x
x_i	a particular random variable (K_i is a random K)
μ	the mean (general)
σ	standard deviation (general)
n	sample size

E( ) expected value of

~ distributed

$N(\bar{x},S_x)$ normal distribution with mean $\bar{x}$ and standard deviat- tion, S_x

$ZZ(\bar{x},S_x)$ ZZ distribution with mean $\bar{x}$ and standard deviation S_x

CHAPTER 1

INTRODUCTION

1.1 Design Methodology

Optimization and reliability of design have been the topics of growing interest to engineers in recent years. A critical review of present design methodology, that based on arbitrary "ignorance factors" or safety factors, is under way.[1] The realization that design parameters are usually characterized by some statistical distribution of values rather than by a single value indicates that probabilistic methodology is a logical alternative. The present deterministic (single valued) methods are special cases of the probabilistic methodology when the parameter variabilities are set equal to zero. Figure 1.1 shows a comparison between the conventional deterministic design and probabilistic design methodologies. In actual physical systems, the absence of design parameter variability is indeed a rare case.

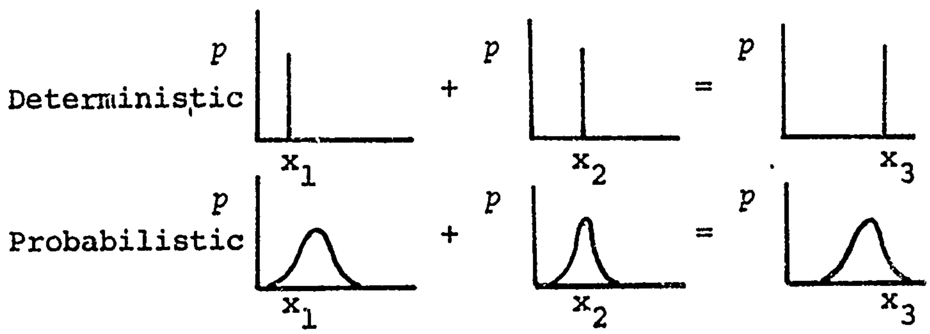

Figure 1.1. Design Methodology.

It is not difficult to find examples of design parameter variation. For instance, in heat transfer we describe the rate of energy radiation from a body as

$$\frac{Q}{A} = \varepsilon\sigma_b T^4 \quad (1.1)$$

where Q is the rate of energy radiated, T is the absolute temperature of the body, σ_b is a universal physical constant, ε is a property of an emitting surface, and A is the surface area of the emitting body. Values of ε are quite variable.[2] Values of σ_b and T may depend on the accuracy of the instrumentation used. The functional variation of Q will grow as the fourth power of the temperature variation. It is indeed optimistic to believe that the calculated Q and actual Q are identical. Yet that is what the deterministic model implies. The objective of this discussion is not to undermine the deterministic model but to improve upon it. The deterministic model has been an engineering tool for many years and has worked well. The probabilistic model uses the deterministic equation to find the mean value of the design result. But the added feature of the probabilistic methodology is that it yields a statistical distribution of the occurrence of the design result. This determines the expected range of the design result or, in the particular example mentioned (Equation 1.1), the probabilistic design yields a bound on the variation of Q. We are now able to determine a range in which the actual energy radiated, Q, may lie instead of calculating a single value of Q and hoping that it is similar in magnitude to the actual Q. In many cases, an agreement of plus or minus 30% between the calculated result and the actual result is considered to be normal. This is in itself an admission of the uncertainty in modeling natural phenomenon. The probabilistic approach to design gives us a logical measure of this uncertainty.

1.2 Design of Heat Pipes

The application of deterministic design techniques to the design of heat pipes has indicated a need for an improved technique. Uncertainties in wick pore size, wick permeability, surface conditions, liquid inventory, and fluid properties has rendered the classical deterministic design approaches inaccurate. Probabilistic design, which treats the design parameters as random variables, has been used successfully to describe the integrity of structural components.[1] Thus, it is logical to consider the use of probabilistic techniques in the design of heat pipes.

Haring and Greenkorn[3] used a statistical distribution to describe the pore radius in a porous medium. Figure 1.2 shows the beta distribution which was used to model the uncertainty of pore radius in a porous medium. Pore radius is so variable that deterministic descriptions cannot be made. It is virtually impossible to randomly choose a particular pore and accurately calculate its radius. The probability distribution enables the researcher to do the next best thing. That is one will be able to describe a range of radii in which a particular pore radius might be observed. One is able to observe

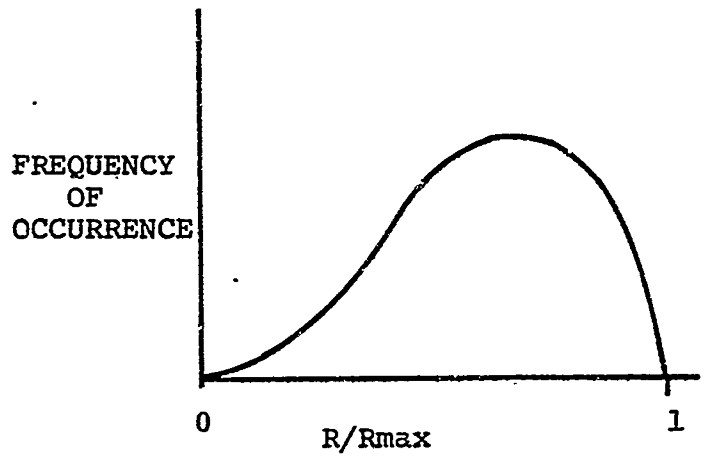

Figure 1.2. Beta Distribution Model of Pore Radius in a Porous Medium

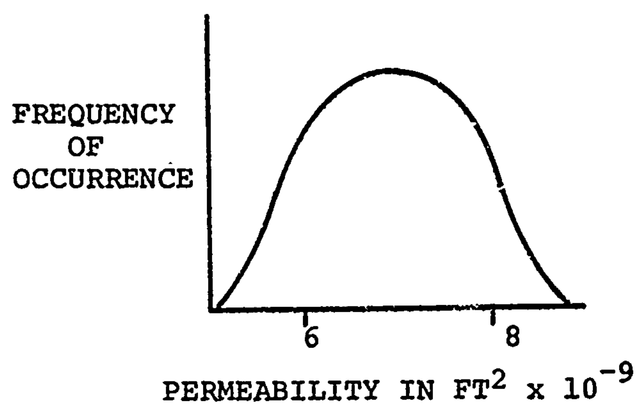

Figure 1.3. Permeability Distribution of 100 Mesh Stainless Steel Screen

the range of variation and the probabilities of residing in certain locations of the range. Also, experiments at The University of New Mexico have shown the wide variability of wick permeability data.[20]

Figure 1.3 is a plot of a continuous distribution approximation of experimental permeability data and illustrates the high variability in this heat pipe design variable. The measured permeability of wick samples taken from the same material is not exactly the same even though great care may be taken to uniformly clean and assemble each sample in an identical way. Choosing one particular value of wick permeability or even the average value would be erroneous in light of the high scatter between samples. Therefore, it is more correct to describe wick permeability using the average of all samples as an estimate of the mean permeability, $\bar{K}$, and the standard deviation, S_k, as a measure of scatter.

Heat pipe operation is a function of permeability, surface tension, wetting angle, fluid properties and geometrical configuration.[6] If any of these parameters are distributed and, therefore, described by a probability distribution, the resulting heat flux capability of the heat pipe will be distributed with a mean heat flux, $\bar{Q}$, and a standard deviation, S_q, as a measure of variability.

Plotting of typical design results, as in Figure 1.4, shows the power of the probabilistic design method. The deterministic method gives an acceptable answer and a factor of safety while the probabilistic method indicates a finite probability of failure. One minus the probability of failure (1-p) is the probability of a successful design. The probability of obtaining a successful design is usually termed the reliability

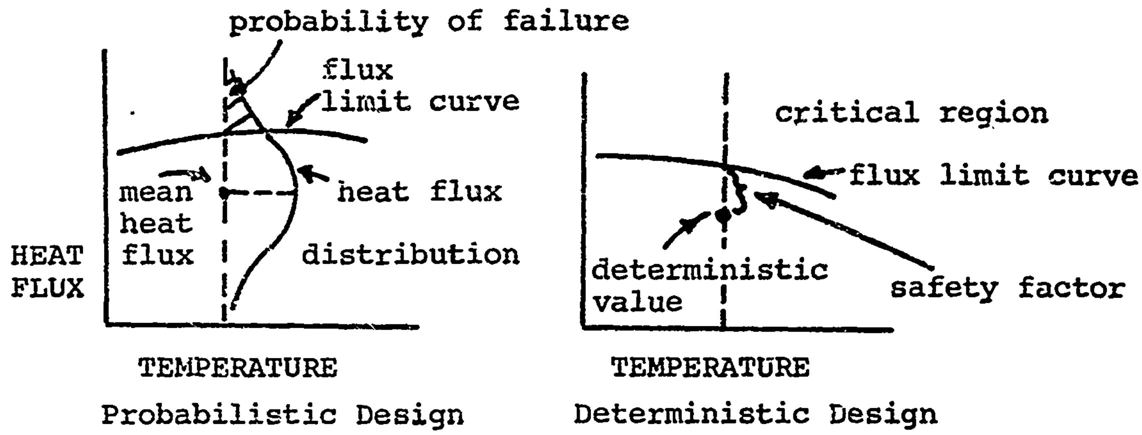

Figure 1.4. Design Methodology Comparison

The usefulness of the probabilistic design technique may be extended to heat exchanger design. There may be hundreds of heat pipes in a heat exchanger system, each having a different heat transfer capability. Conventional deterministic design dictates that the minimum heat transfer capability be used as characteristic of each heat pipe. This is essentially a "worst case" analysis. Another conventional design technique uses the mean heat transfer rate multiplied by a safety factor based on experience. The calculated performance of the heat exchanger, using either the "worst case" values or the mean values with a safety factor, no doubt will give a design safety factor which works. But typically, such a design is very conservative and the overdesigned heat exchanger is larger and more expensive than necessary. The probability of manufacturing one hundred heat pipes that have a performance decidedly worse than average, and, therefore, a "worst case," may be very small. For example, if the probability of occurrence of the worst case is .05, then the probability of manufacturing a heat exchanger with 100 "worst case" heat pipes is $(.05)^{100}$, which is a very rare event.

The purpose of this research project is to:

1. Measure statistical data on water heat pipes using wire mesh wicks.
2. Develop a probabilistic model of heat pipe operation.

Based on the literature, it appears that heat pipe design considerations have been purely deterministic. The publication of Holm[4] indicates some realization of experimental uncertainty in the collection of data. Holm presents his data using an error bound but does not mention anything about repeatability and distribution theory. Phillips[5] presents data on nominal pore diameter for 200 mesh stainless steel screen. It is optimistic to hope that this deterministic pore diameter value is representative of the sample. A mean pore diameter, standard deviation and distribution will better represent the physical characteristics of this wick. Also, it has been observed at UNM that permeabilities of screen samples have large standard deviations despite many efforts to obtain uniform samples.[20]

A survey of the literature reveals no effort to account for parameter variability in the field of heat transfer. Little information is available on the statistical behavior of heat transfer parameters such as convection coefficient, conductivity, and permeability. The author has not yet found any literature which applies probabilistic approaches to heat transfer design.

CHAPTER 2

THEORY

To develop the probabilistic theory for heat pipe design, it is necessary to derive the deterministic model on which the probabilistic model is based. The classic derivation of the heat pipe design equation appears in the literature.[8] In this chapter, the classic derivation of the fully saturated wick model is described. This derivation is based on the principles of conservation of momentum, energy, and mass for a differential element in the wick. The fully saturated wick model is later modified for the partially saturated wick condition and will be used as the basis of the probabilistic design equation.

2.1 Deterministic Model of Heat Pipe Operation

The heat pipe to be considered in this work is cylindrical in shape with an annular wick, as shown in Figure 2.1. The major assumptions used in the development of the deterministic model are:

1. The system is treated as one-dimensional.
2. The wick is fully saturated with liquid.
3. The heat flux is uniform over the evaporator and condenser sections.
4. The liquid-vapor interface meniscus can be characterized by one radius of curvature.
5. The liquid and vapor are at the same temperature along the entire length of the pipe.
6. Wick properties are isotropic.

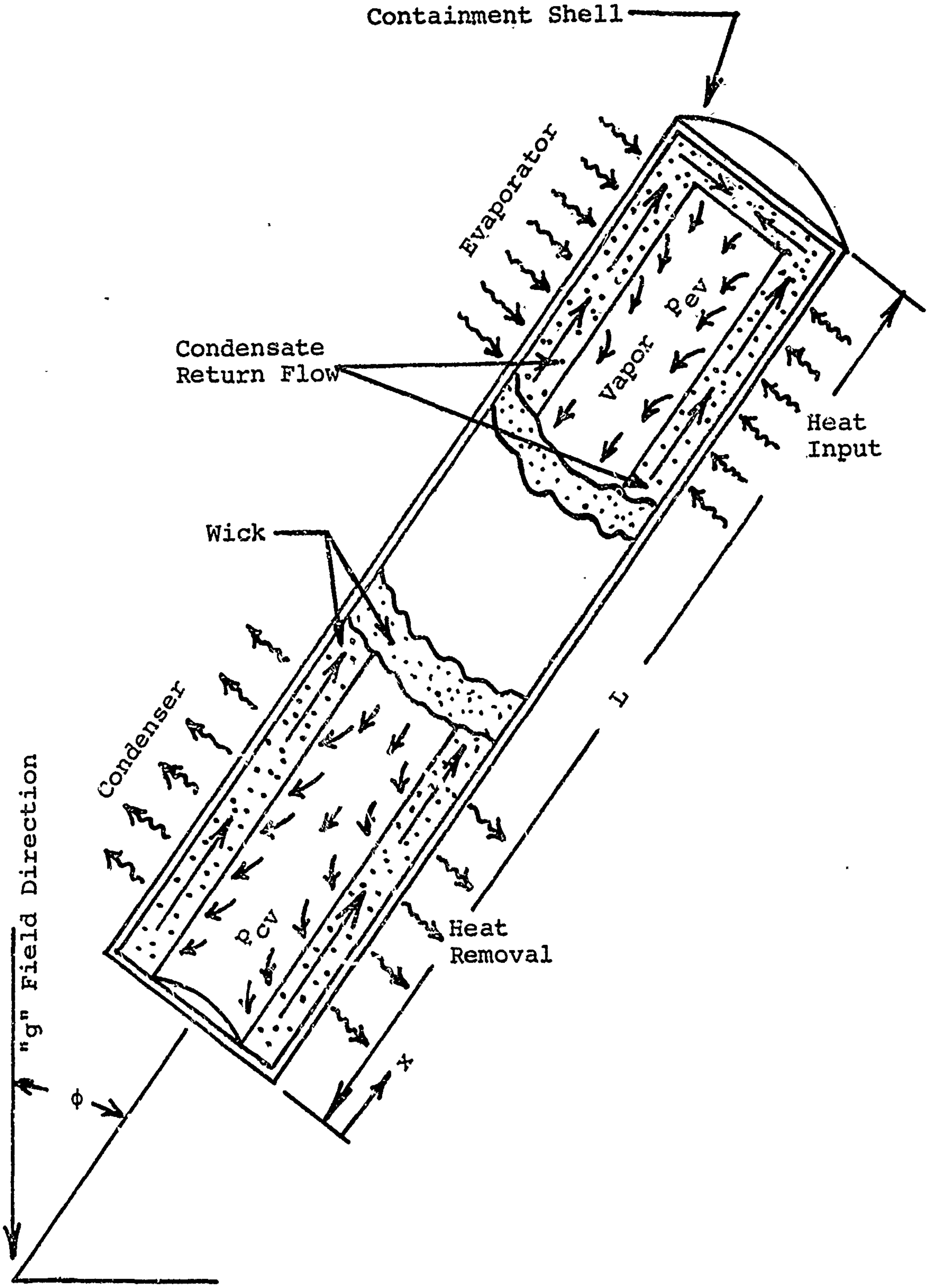

Figure 2.1. Operating Heat Pipe

7. Differentials raised to the second or higher powers are neglected.

8. The heat pipe is wick limited, that is, viscous pressure drops in the liquid saturated wick are so much larger than those in the vapor that the viscous pressure drop in the vapor is negligible.

9. The vapor condensing on the liquid-vapor interface has a velocity in the y direction only. Therefore, there is no contribution to momentum changes in the x and z directions.

A differential fluid element taken in the condenser section of the heat pipe wick may be used for the analysis. Applying conservation of mass to the element shown in Figure 2.2, the relationship between liquid and vapor flow rates is obtained

$$\dot{m}_{\ell_x} + \dot{m}_v = \dot{m}_{\ell(x+dx)} \tag{2.1}$$

where

$$\dot{m}_{\ell_x} = \rho_\ell e(\bar{t}_w Z_w) u_\ell \tag{2.2}$$

$$\dot{m}_{\ell(x+dx)} = \rho_\ell e(\bar{t}_w Z_w)\left(u_\ell + \frac{du_\ell}{dx} dx\right)^* \tag{2.3}$$

Combining Equations 2.1, 2.2, and 2.3, and solving for $\dot{m}_v$

$$\dot{m}_v = \rho_\ell \frac{du_\ell}{dx} dx e(\bar{t}_w Z_w) \tag{2.4}$$

From the liquid-vapor interface of the differential element

$$\dot{m}_v = \rho_v u_v Z_w dx \tag{2.5}$$

---

*where $\bar{t}_w$ is the average wick thickness as would be measured by a micrometer.

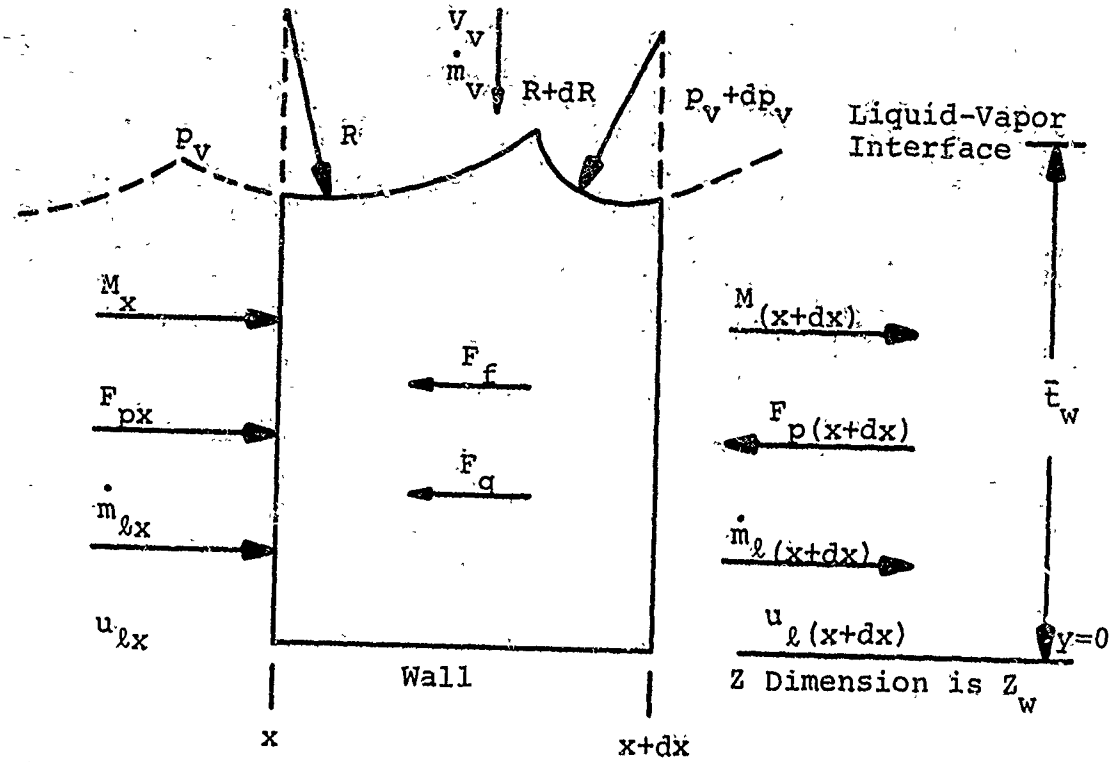

Figure 2.2. Momentum Terms for a Differential Element of Wick

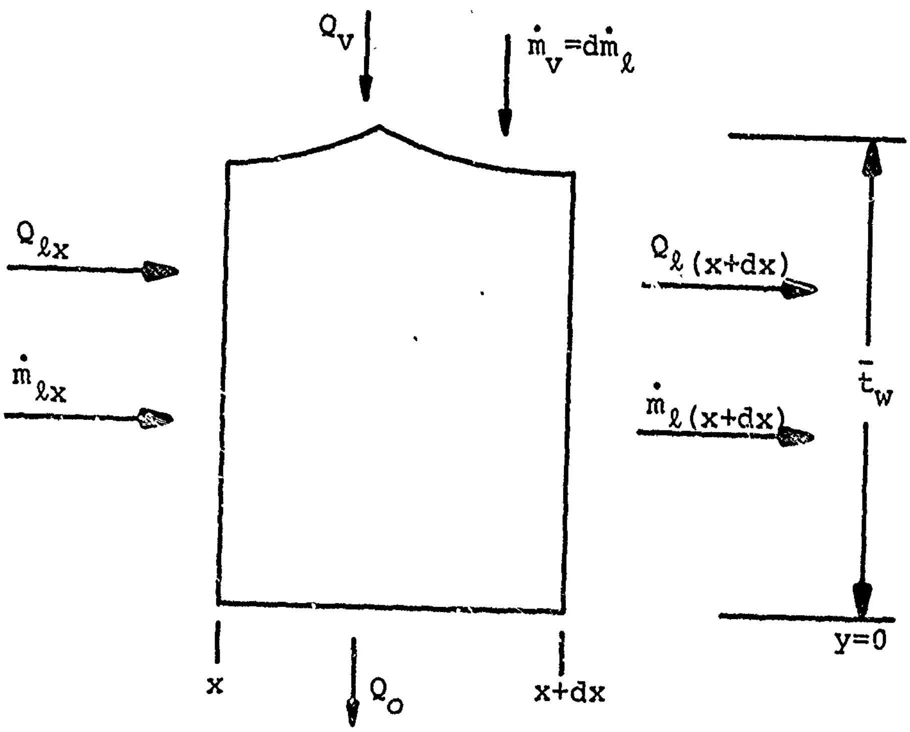

Figure 2.3. Energy Terms for a Differential Element of Wick

Application of conservation of momentum in the x direction to the element of Figure 2.2 yields

$$\Sigma F_x = M_{x+dx} - M_x \tag{2.6}$$

where the momentum terms are

$$M_x = \frac{\rho_\ell}{g_c} u_\ell^2 \, e \, \bar{t}_w Z_w \tag{2.7}$$

$$M_{x+dx} = \frac{\rho_\ell}{g_c} u_\ell^2 \, e \, \bar{t}_w Z_w + \frac{\rho_\ell}{g_c} \frac{d(u_\ell^2)}{dx} dx \, \varepsilon \, \bar{t}_w Z_w \tag{2.8}$$

where no contribution is made to momentum in the x direction by the vapor as it enters the element as a result of assumption 9.

The force terms are composed of the capillary pressure forces as described by the Laplace-Young equation

$$\Delta p = \sigma \left(\frac{1}{R_1} + \frac{1}{R_2}\right) \tag{2.9}$$

By assumption 4, this equation reduces to

$$\Delta p = \frac{2\sigma}{R} \tag{2.10}$$

where Δp is the pressure drop across the liquid vapor interface at x. The pressure forces are

$$F_{p_x} = \left(p_v - \frac{2\sigma}{R}\right) e \, \bar{t}_w Z_w \tag{2.11}$$

$$F_{p_{x+dx}} = \left(p_v + dp_v - \frac{2\sigma}{R+dR}\right) e \, \bar{t}_w Z_w \tag{2.12}$$

For the heat pipe with an annular wick with large vapor passage, a low density vapor and low vapor flow rate, p_v is constant and dp_v is zero. The force on the element is found by the summation of Equations 2.11 and 2.12

$$F_{px} - F_{p(x+dx)} = - e\ \bar{t}_w Z_w\ 2\sigma \frac{dR}{R^2 + RdR} \qquad (2.13)$$

RdR will be neglected when compared to R^2.

Because of the low flow rates and velocities that occur in capillary wicks, the flow is free of inertial effects, is laminar, is described by Darcy's law

$$\frac{dp}{dx} = \frac{\dot{m}_\ell \mu_\ell}{K\rho_\ell A_w} \qquad (2.14)$$

and viscous forces on the element are given by

$$F_f = \frac{dp}{dx}\, dx\ [e(\bar{t}_w Z_w)] \qquad (2.15)$$

The net viscous force on the element is obtained by combining Equations 2.2, 2.14, and 2.15

$$F_f = \frac{e^2}{K}\ \bar{t}_w Z_w\ \mu_\ell u_\ell\ dx \qquad (2.16)$$

If the heat pipe operates in a gravitational field (or acceleration field), another force term must be added which is the weight component of the fluid element along the direction of flow

$$F_g = \frac{g}{g_c}\ \rho_\ell\ e\ \bar{t}_w Z_w\ \cos\phi\ dx \qquad (2.17)$$

The gravity component force may be plus or minus depending on the orientation of the heat pipe. In this analysis, as shown in Figure 2.1, the heat pipe is oriented so that the evaporator is above the condenser and the gravity force opposes the liquid flow. The summation of forces on the element is

$$\Sigma F_x = F_{p(x)} - F_{p(x+dx)} - F_f - F_g \tag{2.18}$$

Combining Equations 2.6, 2.7, 2.8, 2.13, 2.16, 2.17, and 2.18, we obtain the differential momentum equation for the fluid element

$$- 2\sigma \frac{dR}{R^2} - \frac{e}{K} \mu_\ell \, u_\ell \, dx - \frac{g}{g_c} \rho_\ell \cos\phi \, dx = \frac{\rho_\ell}{g_c} \frac{d(u_\ell)^2}{dx} dx \tag{2.19}$$

Conservation of energy must also be satisfied. Referring to Figure 2.3, neglecting kinetic energy effects the energy terms are

<u>Energy in</u>

$$Q_v = \dot{m}_v h_v$$

$$Q_\ell = \dot{m}_\ell h_\ell - k_\ell (t_w Z_w) \frac{dT_\ell}{dx}$$

<u>Energy out</u>

$$Q_{\ell(x+dx)} = \dot{m}_\ell h_\ell + \frac{d(\dot{m}_\ell h_\ell)}{dx} dx - k_\ell (\bar{t}_w Z_w) \left[\frac{dT_\ell}{dx} + \frac{d^2 T_\ell}{dx^2} dx\right]$$

Q_o (heat removed externally)

W_g (work against gravity)

(2.20)

From assumption 5, the conduction terms are negligible and the energy equation becomes,

$$Q_v + Q_\ell = Q_{\ell(x+dx)} + Q_o - W_g \tag{2.21}$$

replacing $\dot{m}$ with Equation 2.4

$$Q_v = h_v \rho_\ell \frac{du_\ell}{dx} dx \; e \bar{t}_w Z_w \tag{2.22}$$

combining Equations 2.21 and 2.22,

$$h_v \rho_\ell \frac{du_\ell}{dx} + \frac{d(\dot{m}_\ell h_\ell)}{dx} - \frac{Q_o}{e\bar{t}_w Z_w dx} + \frac{W_g}{e\bar{t}_w Z_w dx} = 0 \tag{2.23}$$

and simplifying the derivative

$$h_v \rho_\ell \frac{du_\ell}{dx} - h_\ell \rho_\ell \frac{du_\ell}{dx} - u_\ell \rho_\ell \frac{dh_\ell}{dx} - \frac{Q_o}{dx \; e\bar{t}_w Z_w} + \frac{W_g}{e\bar{t}_w Z_w \; dx} = 0 \tag{2.24}$$

From assumption 5, axial temperature gradients are negligible and assuming axial pressure gradients are small for the water heat pipe

$$\frac{dh_\ell}{dx} \approx 0 \tag{2.25}$$

Combining Equations 2.24 and 2.25

$$\rho_\ell (h_v - h_\ell) \frac{du_\ell}{dx} - \frac{Q_o}{e\bar{t}_w Z_w \; dx} + \frac{W_g}{e\bar{t}_w Z_w \; dx} = 0 \tag{2.26}$$

where

$$W_g = + \frac{\rho_\ell u_\ell}{J} \frac{g}{g_c} \cos\phi \; e\bar{t}_w Z_w \; dx \tag{2.27}$$

$$Q_o = + q \; dx \; Z_w \tag{2.28}$$

$$h_v - h_\ell = h_{fg} \tag{2.29}$$

Combining Equations 2.26, 2.27, and 2.28

$$\rho_\ell \, h_{fg} \frac{du_\ell}{dx} - \frac{q}{e\bar{t}_w} + \frac{\rho_\ell u_\ell}{J} \frac{g}{g_c} \cos\phi = 0 \tag{2.30}$$

and simplifying

$$\frac{du_\ell}{dx} = \frac{q}{e\bar{t}_w \rho_\ell h_{fg}} - \frac{g}{g_c} \frac{\cos\phi}{J h_{fg}} u_\ell \tag{2.31}$$

Solving for the average velocity and integrating over the length of the condenser, the energy equation becomes

$$u_\ell = \frac{q}{h_{fg} e\bar{t}_w \rho_\ell} x - \frac{g}{g_c} \frac{\cos\phi}{J h_{fg}} \int_0^x u_\ell \, dx \tag{2.32}$$

Integrating to a position x along the condenser and rearranging terms

$$\frac{q x}{u_\ell h_{fg} e\bar{t}_w \rho_\ell} = \left(1 + \frac{g}{2g_c} \frac{x}{J h_{fg}}\right) \tag{2.33}$$

The gravity term inside the bracket is much smaller than 1 and can be neglected, resulting in the following simplified form of the energy equation

$$u_\ell = \frac{q}{h_{fg} e\bar{t}_w \rho_\ell} x \tag{2.34}$$

Combining Equations 2.34 and 2.19 to form the energy-continuity-momentum integral equation

$$-\int_{R_x=0}^{R_{x=x_{max}}} 2\sigma \frac{dR}{R^2} - \int_0^x \frac{1}{K} \frac{q}{h_{fg}\bar{t}_w} \frac{u_\ell}{\rho_\ell} x dx - \int_0^x \frac{g}{g_c} \rho_\ell \cos\phi \, dx$$

$$= \int_0^x \frac{2q^2}{g_c h_{fg}^2 \rho_\ell \varepsilon^2 \bar{t}_w^2} x dx \tag{2.35}$$

(at $x = 0$ $R \to \infty$, at $x = x_{max}$ $R \to R_{min} = r$)

The mass flow distribution resulting from the assumption of uniform heat flux in the evaporator and condenser is shown in Figure 2.4.

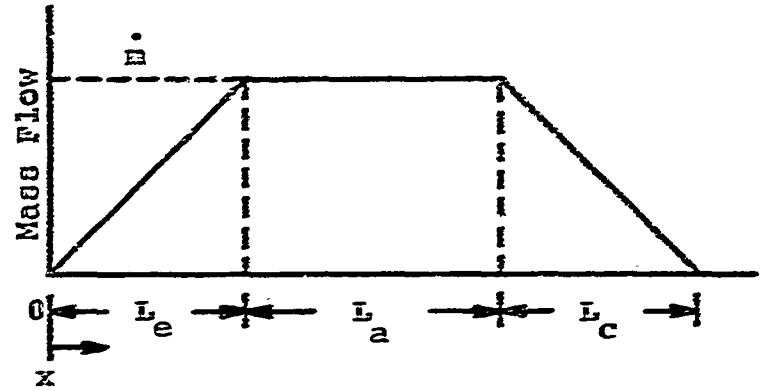

Figure 2.4. Mass Flow Distribution

Equation 2.35 is valid for the condenser region only and now a relation in the evaporator region is needed. To link the energy and momentum analysis between the condenser and evaporator, we will use the following boundary conditions

$$u_{max_c} = \frac{q_c L_c}{h_{fg} \bar{t}_w e \rho_\ell} = u_{max_e} = \frac{q_e L_e}{h_{fg} \bar{t}_w e \rho_\ell} \tag{2.36}$$

$$u_{\ell_e} = \frac{q_c L_c}{h_{fg} \bar{t}_w e \rho_\ell} - (L_e - x) \frac{q_e}{h_{fg} \bar{t}_w e \rho_\ell} \qquad 0<x<L_e \tag{2.37}$$

$$q_e = \frac{q_c L_c}{L_e} \tag{2.38}$$

$$u_{\ell_e} = \frac{q_c L_c}{h_{fg} \bar{t} e \rho_\ell} \left(1 + \frac{(x - L_e)}{L_e} \right) \tag{2.39}$$

Equation 2.39 is the link between the evaporator and condenser velocities and can be combined with Equation 2.35, resulting in the energy-continuity-momentum integral equation for the evaporator. The same but more simplified analysis may be applied to the adiabatic section since there the heat flux term is zero and the only forces entering into the equation are fluid friction and capillary pressure rise. Addition of the three momentum-continuity-energy equations yields

$$Q_{max} = \frac{\rho_\ell h_{fg} \sigma}{\mu_\ell} \left(\frac{K Z_w \bar{\xi}_w}{\frac{L_e}{2} + L_a + \frac{L_c}{2}} \right) \left(\frac{2}{r_e} - \frac{\rho_\ell g}{g_c} \frac{(L_e + L_a + L_a)}{\sigma} \cos\phi \right) \quad (2.40)$$

$$Q_{max} = \frac{\rho_\ell h_{fg} \sigma}{\mu_\ell} \left(\frac{KA}{L'} \right) \left(\frac{2}{r_e} - \frac{\rho_\ell g}{\sigma g_c} H \right) \quad (2.41)$$

Equation 2.41 is the basic deterministic maximum heat transfer rate equation for the heat pipe considered in this work. The term ($\rho h \sigma / \mu$) is commonly referred to as the liquid transport factor, which is a group of fluid properties. The term (KA/L') is a group of wick properties where L' is the effective flow length or average flow length of a given liquid particle in the wick. L' is obtained from the integration of Darcy's law, Equation 2.14, according to the mass flow distribution of Figure 2.4. The mass flow equations for the heat pipe considered in this work are given by

$$\dot{m}_e(x) = \dot{m} \frac{x}{L_e} \quad (0 \le x \le L_e)$$

$$\dot{m}_a(x) = \dot{m} \quad (L_e \le x \le L_e + L_a)$$

$$\dot{m}_c(x) = \dot{m} \left(1 - \frac{(x - L_e - L_a)}{L_c} \right) \quad (L_e + L_a < x < L) \quad (2.42)$$

The mechanics of the integration of Darcy's law are shown in Equation 2.43 resulting in the expression for L'.

$$\int_0^L dp = \frac{\mu}{KA\rho}\left[\int_0^{L_e} \dot{m}_e(x)\, dx + \int_{L_e}^{L_e+L_a} \dot{m}_a(x)\, dx + \int_{L_e+L_a}^{L} \dot{m}_c(x)\, dx\right] \tag{2.43}$$

$$\Delta p_w = \frac{\mu_\ell \dot{m} L'}{\rho_\ell K A} \tag{2.44}$$

$$L' = \frac{L_e}{2} + L_a + \frac{L_c}{2} \quad \text{(for fully saturated wick)} \tag{2.45}$$

Equation 2.45 appears as part of Equation 2.40 as a result of the combination and integration of the momentum-energy-continuity equation. The reason for the reiteration of the derivation of Equation 2.45 is that we will modify this integration step to obtain the design equation for the partially saturated wick condition.

2.2 Deterministic Model of Heat Pipe Operation with Partially Saturated Wick

One of the major assumptions in the preceding analysis was assumption 2 which stated that the heat pipe wick was fully saturated. Many times this is not the case. The liquid-vapor interface may recede into the wick resulting in performance different from that predicted by Equation 2.40. An attempt to modify Equation 2.40 for the partially saturated wick condition follows.

Modifying assumptions for a partially saturated wick analysis are:

1. Capillary force properties are non-uniform across the wick as the result of the variation of critical capillary radius in the wick. Critical radius will be a function of $\bar{t}$; therefore, critical radius will decrease in the direction towards the heat pipe wall.
2. Permeability is assumed uniform across the wick.
3. Uniform heat flux in the evaporator and condenser is maintained during the partially saturated (desaturated) mode of operation.
4. The effect of the desaturation is to increase viscous liquid flow losses in the wick due to higher liquid velocities in the desaturated wick. The higher liquid velocities are required to maintain the mass flow in a smaller area.
5. A heat pipe functioning at non-equilibrium during the desaturation or recession process will reestablish equilibrium only if the receding liquid vapor interface encounters a smaller pore size resulting in sufficient additional capillary force.

Figure 2.5 graphically illustrates the assumptions of the recession or desaturation mode of heat pipe operation. Figure 2.5(a) shows the mass flow distribution for the saturated and partially saturated mode of operation. The shape of the distribution is a result of the assumption that the

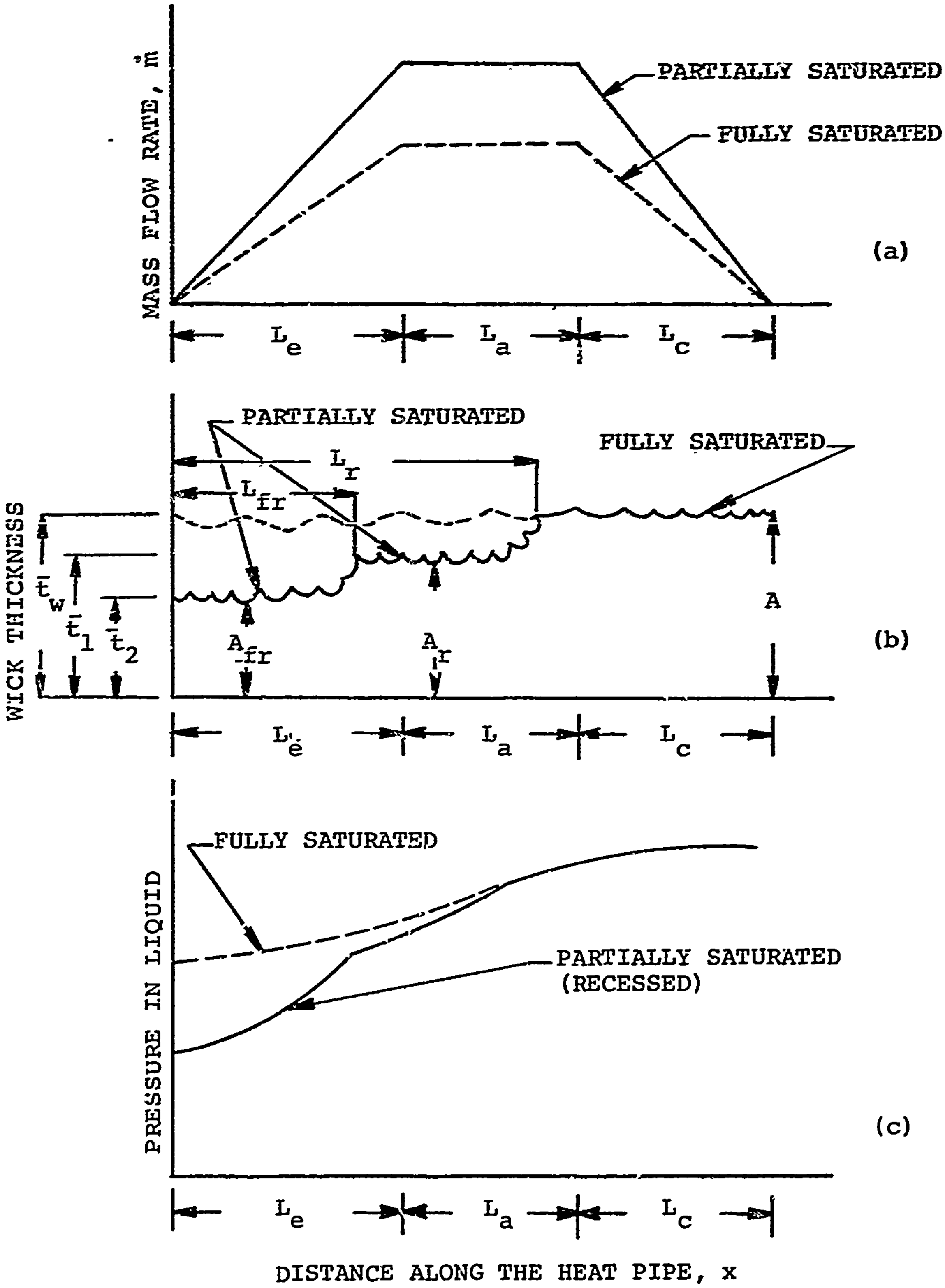

Figure 2.5. Mass Flow Rate, Liquid Recession Distribution, and Liquid Pressure Distribution for Fully Saturated and Partially Saturated Wicks

heat flux in the condenser and evaporator are uniform. Figure 2.5(b) shows the liquid-vapor interface for the fully saturated and partially saturated modes of operation. The fully saturated condition of Figure 2.5(b) indicates that there is sufficient capillary force at the upper $\bar{t}_w$ level in the wick to sustain the frictional and gravitational losses of the system. If this balance cannot be maintained by the capillary forces, liquid will be depleted due to evaporation in the evaporator more quickly than it can be restored by the capillary forces at the given liquid-vapor interface. The result is a non-equilibrium condition in which the liquid-vapor interface recedes into the wick. Now that the fluid is receding, there are two possible outcomes:

1. The fluid will recede until it encounters a stronger capillary force which will reestablish an equilibrium condition.
2. The fluid will recede until it encounters the heat pipe wall resulting in the dryout and failure of the heat pipe.

For the analysis of recession, we will assume that the liquid-vapor interface will reestablish an equilibrium condition at some level in the wick. Returning to Figure 2.5(b), we see a hypothetical liquid-vapor interface distribution for a partially saturated wick. The $\bar{t}_2$ level in the wick is assumed to have the highest capillary force capability and, therefore, the smallest critical radius. The $\bar{t}_1$ level has a higher capillary force capability than the $\bar{t}_w$ level but a smaller capability than the $\bar{t}_2$ level.

Referring to Figure 2.5(b and c), the mechanics of the recession will be described. Starting at the condenser end of the heat pipe, we observe the liquid pressure and liquid level (position of vapor-liquid interface). Moving from right to left in the condenser region, the liquid pressure begines to decrease due to gravity and viscous forces. This pressure loss can still be maintained, however, by the capillary pressure at the $\bar{t}_w$ level in the wick. Moving into the adiabatic region, the pressure loss in the liquid has exceeded the capillary pressure capability of the $\bar{t}_w$ level pores and the fluid recedes. The $\bar{t}_1$ level pores have sufficient capillary force to maintain the liquid pressure loss and the liquid level remains at $\bar{t}_1$. Moving into the evaporator region with ever increasing liquid pressure loss, it is observed that the $\bar{t}_1$ level pores cannot sustain any more pressure loss and the liquid level recedes to the next level, $\bar{t}_2$. At the $\bar{t}_2$ level, capillary forces are sufficient to maintain the viscous and gravitational losses of the system. The $\bar{t}_2$ level has the highest capillary pressure capability and any additional recession will result in burnout. The difficulty in this analysis is the determination of the capillary properties at different levels if such a situation exists. In this work, the above theory is applied to wire mesh wicks whose capillary properties can be determined at the various levels. This may be a difficult matter for powder metal or other types of wicks.

The preceding analysis indicated that the liquid-vapor interface recedes into the wick, resulting in a decreased flow area and increased liquid pressure loss. The only difference this introduces into the combined energy-continuity-momentum equation, 2.35, is the thickness of the liquid element. All other terms of Equation 2.35 must be maintained at their present values, consistent with Figure 2.5(a), except the liquid pressure loss term given by Equation 2.14, Darcy's law, which will be used to form the integral equation for the pressure loss in the liquid. For the recessed liquid-vapor interface, Equation 2.45 does not apply because the liquid flow area is not constant with length. This is shown in Figure 2.6

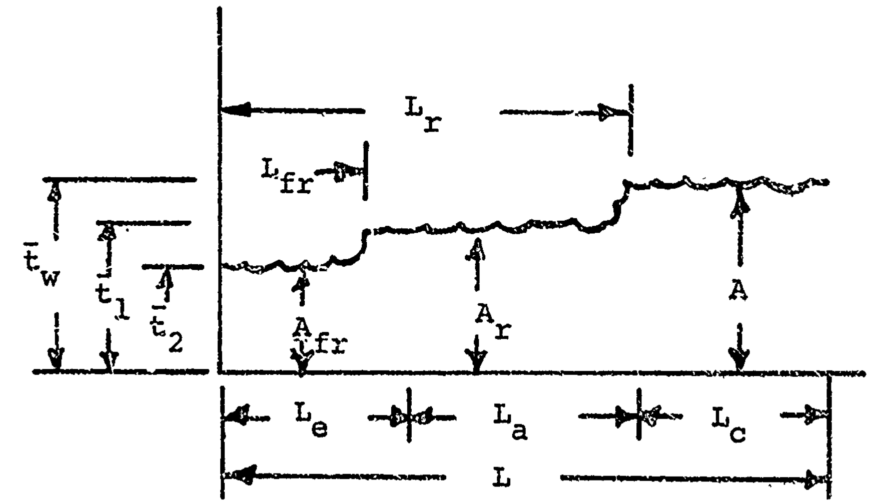

Figure 2.6. Liquid-Vapor Interface Distribution

Figure 2.6 is a redrawing of Figure 2.4(b) and will be used to determine the total liquid pressure loss for the recessed liquid level condition. Application of Equations 2.14 and 2.42 to Figure 2.6 the total pressure loss is

$$\int_{o}^{L} dp_r = \frac{\mu_\ell}{K\rho_\ell}\left[\int_{o}^{L_{fr}} \frac{\dot{m}_e(x)\,dx}{A_{fr}} + \int_{L_{fr}}^{L_e} \frac{\dot{m}_e(x)\,dx}{A_r}\right.$$

$$\left. + \int_{L_e}^{L_r} \frac{\dot{m}_a(x)\,dx}{A_r} + \int_{L_r}^{L_e+L_a} \frac{\dot{m}_a(x)\,dx}{A} + \int_{L_e+L_a}^{L} \frac{\dot{m}_c(x)\,dx}{A}\right] \tag{2.46}$$

Simplifying, we obtain

$$\Delta p_r = \frac{\mu \dot{m} L'(A)_r}{\rho_\ell K} \tag{2.47}$$

where

$$L'(A)_r = \left(\frac{L_{fr}}{2A_{fr}} + \frac{(L_e - L_{fr})}{2A_r} + \frac{(L_r - L_e)}{A_r} + \frac{(L_a + L_e - L_r)}{A} + \frac{L_c}{2A}\right) \tag{2.48}$$

and the resulting model for heat pipe operation in the desaturated or recessed wick condition is

$$Q_{max} = \frac{\rho_\ell h_{fg}\sigma}{\mu_\ell}\left(\frac{K}{L'(A)_r}\right)\left(\frac{2}{r_{fr}} - \frac{\rho_\ell g H}{\sigma g_c}\right) \tag{2.49}$$

The only difference between Equation 2.49 and 2.41 is the $L'(A)_r$ term (Darcy flow length) and the critical radius, r_c. In Equation 2.49, we use the $L'(A)_r$ to account for the additional pressure loss due to the recession and r_{fr} to account for the increased capillary force at the fully recessed level, therefore, level $\bar{t}_2$ in Figure 2.5. Figure 2.6 may be interpreted as a general case of fluid recession and does not imply that there are always three distinct levels of constant pore size,

r. The integration of Equation 2.46 may be applied to any amount of recession "steps" as long as one integrates between the discontinuities. The discontinuities of Figure 2.6 are at L_{fr}, L_e, L_r, and $L_e + L_a$.

In the design of heat pipes operating under the desaturated wick condition, the recession lengths, therefore, L_{fr} and L_r of Figure 2.6, must be determined to insert into Equation 2.48. Also, one must know the variation of r_c as a function of the t dimension of Figure 2.6. The r_c variation may be theoretically hypothesized or experimentally determined. In this work, r_c as a function of $\bar{t}$ is determined experimentally. Given that the r_c variation is known, one can calculate the recession lengths by plotting the pressure distribution along the wick and observing where the liquid pressure loss exceeds the capillary pressure rise of a given pore. The pressure loss in the wick is a combination of viscous and gravity effects and is given by

$$\frac{dp}{dx} = - \frac{\dot{m}(x)\mu_\ell}{KA(x)\rho_\ell} - \frac{\rho_\ell g}{g_c}\frac{H}{L} \qquad (2.50)$$

Integration of Equation 2.50 results in the pressure distribution along the wick of a heat pipe shown in Figure 2.7.

$$p_{(x)} - p_{(o)} = - \frac{\mu_\ell}{K\rho_\ell}\int_o^x \frac{\dot{m}(x)\,xdx}{A(x)} - \frac{\rho_\ell g}{g_o}\frac{Hx}{L} + H_o \qquad (2.51)$$

If one has no excess liquid in a pipe and neglects the effect of the diameter of the pipe, Equation 2.51 becomes

$$p_x - p_o = \frac{\mu_\ell}{K\rho_\ell} \int_o^x \frac{\dot{m}(x)\,x\,dx}{A(x)} - \frac{\rho_\ell g}{g_o} \cos\phi \qquad (2.52)$$

where $\dot{m}(x)$ is defined by Equation 2.42.

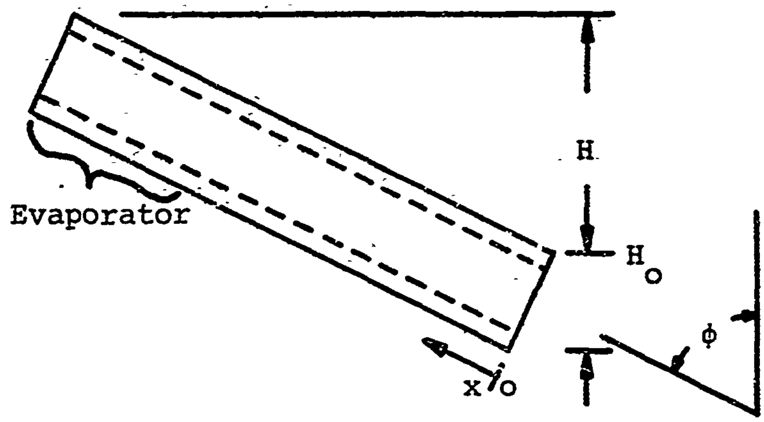

Figure 2.7. Heat Pipe Configuration

Equation 2.52 is difficult to solve in closed form because the area term is a function of x. A trial and error solution is proposed using Equations 2.49, 2.50, 2.52, and 2.53.

$$Q_{max} = \dot{m}_{max}\, h_{fg} \qquad (2.53)$$

First, compute Q_{max} using Equation 2.49, initially setting $L'(A)_r$ equal to L'/A. Second, compute $\dot{m}$ using Equation 2.53. Then, using Equation 2.52, start plotting p_x, beginning at the condenser end at x equal o. Increment, using small x until the term $(p_x - p_o)$ exceeds the capillary pressure rise of the pores at the inside diameter of the wick. At this point, set A(x) equal to the new and smaller recessed area as a result of the fluid recession and record the x position. Referring to Figure 2.6, the new area will be A_r. Continue to plot pressure along the entire length of the pipe in like manner, always observing the mass flow distribution of Figure 2.5(a). From this pressure plot, one can calculate the recessed lengths of the wick and, therefore, calculate $L'(A)_r$. The new $L'(A)_r$ from Equation 2.48 is inserted into Equation 2.49 and the procedure is repeated until the Q_{max} value converges, which usually takes about four iterations. A computer program was written to perform this computation and is discussed in Chapter 6.

2.3 The Probabilistic Model of Heat Pipe Operation

Many of the design parameters of Equation 2.49 are extremely variable. Experiments show that the wicking properties, K, A, and r_c may vary plus or minus 30% of the absolute mean value. The reasons for the variability or uncertainty in the determination of these variables result from variability of materials, variability of manufacturing, and, to some extent, experimental measurement variability. Generally, the uncertainty in these design variables is too large to be neglected. The probabilistic model of heat pipe operation incorporates the variability of the design parameters so that the variability of the design result, Q_{max}, can be determined.

Given that the design variables of a particular system are described by a distribution of values rather than a single deterministic point, we may be able to fit certain functions to data to describe the variability of design variables. These functions are called probability distributions. The permeability, K, may be described by a certain probability distribution while the critical radius, r_c, may be described by another.

The first step in the analysis of the probabilistic model will be the following assumptions:

1. Q, K, r_e, H, $L'(A)_r$, and A are assumed to be independent random variables described by a continuous probability distribution.

2. The continuous probability distributions will be described by two parameters, the mean and standard deviation.

3. All other variables will be considered deterministic since their variabilities are comparatively small.

The notation for a given random variable using these assumptions will be (μ_{zz}, σ_{zz}) where zz is the random variable, μ is the mean and σ_{zz} is the standard deviation. The permeability variate pair being (μ_K, σ_K).

The probabilistic design equation is the deterministic design equation with the random variate pairs inserted. The probabilistic design equation is

$$(\mu_Q,\sigma_Q) = (\frac{\rho_\ell \sigma_\ell h_{fg}}{\mu_\ell}) (\frac{(\mu_r,\sigma_r)}{(\mu_{L'(A)_r}, \sigma_{L'(A)_r})}) (\frac{2}{(\mu_{fr},\sigma_{fr})} - \frac{\rho_\ell g}{g_o} \frac{(\mu_H,\sigma_H)}{\sigma}) \qquad (2.54)$$

Equation 2.54 represents the functional relationship between the random variates of the probabilistic design model.

Many times, the distribution parameters (the mean and standard deviation in this analysis) must be estimated from experimental data. The consistent and unbiased estimator for the mean of a random variable, x, is defined by Miller and Freund[17] as

$$\bar{x} = \sum_{i=1}^{n} \frac{x_i}{n} \qquad (2.55)$$

where n is the number of readings and the estimator for the standard deviation is

$$S_x = \sqrt{\sum_{i=1}^{n} \frac{(x_i - \bar{x})^2}{n-1}} \qquad (2.56)$$

Since all the random variates will be determined using experimental data, their parameter will be estimated and Equation 2.54 for the case of partially saturated wick becomes

$$(\bar{Q}, S_Q) = \left(\frac{\rho_\ell \sigma_o h_{fg}}{\mu_\ell}\right)\left(\frac{(\bar{K}, S_K)}{(\bar{L}'_{(A)_r}, S_{L'(A)_r})}\right)\left(\frac{2}{(\bar{r}_{fr}, S_{r_{fr}})} - \frac{\rho_\ell g}{g_o \sigma_\ell}(\bar{H}, S_H)\right) \qquad (2.57)$$

The solution of Equation 2.57 is the random variate $(\bar{Q}, S_Q)$, which may be translated into a probability distribution function such as the normal distribution. Figure 2.8 shows a hypothetical distribution of maximum heat transfer rate for a given heat pipe design. The designer may determine the variability of the design and decide if it meets or exceeds the specified minimum value, Q_s. The area to the right of Q_s indicates the probability that a heat pipe, with the given variable properties, will exceed Q_s. The design engineer can adjust the Q_{max} distribution by changing the distribution of the heat pipe properties so that a very small portion of the distribution lies below Q_s in the failure region.

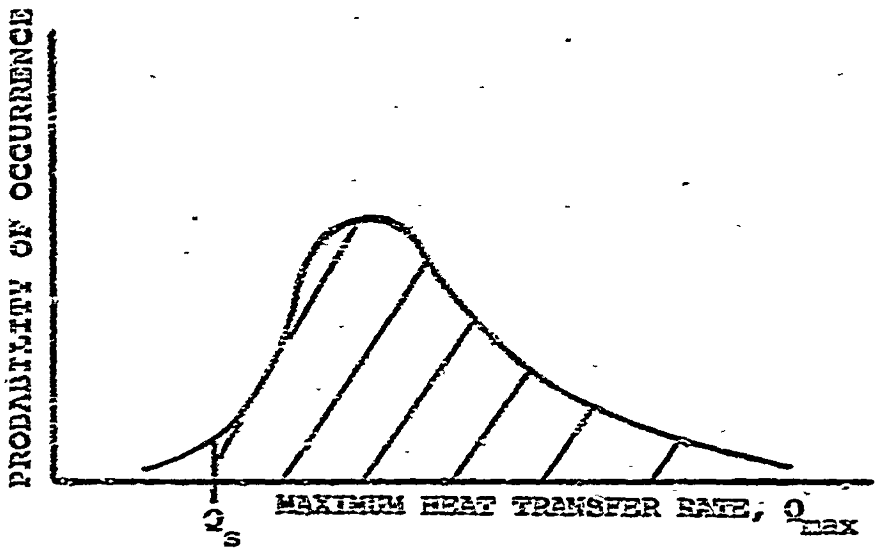

Figure 2.8. Distribution of Heat Flow Capability of a Heat Pipe Whose Design Parameters Are Assumed Random

Solution techniques will be discussed in depth in Chapter 6 for Equation 2.57.

The basic argument behind the probabilistic design approach is that we can obtain a quantitative measure of the uncertainty of the system performing as required. Many times we may obtain a set of measurements that, when inserted into the deterministic equation (Equation 2.49, or any equation for that matter), give a vastly different result from reality. The conclusion may be that the particular deterministic equation is poor, but this may not be a proper conclusion. One must look at the distribution of functional solution variables to determine the validity of the model. It may be highly possible to obtain a calculated result relatively far from the observed mean result yet still lie in the range of the distribution.

Chapters 6 and 7 will analyze the probabilistic design methodology in depth and comparisons will be made with actual test data. In Chapter 3, the details of experimental techniques for the measurement of our design variables, K, A, L', $\bar{r}_e$, and H, are presented.

CHAPTER 3

APPARATUS

The heat pipe design used as a basis for obtaining data on a typical wire mesh wick heat pipe is shown in Figure 3.1. The material used in the construction of the wicks and pipe was 304 stainless steel. The dimensions shown in Figure 3.1 were chosen as typical for a wire mesh heat pipe of this design with an annular wick. The active length of the heat pipe was 22 inches and the evaporator was 13.5 inches. The evaporator was chosen to be large (a significant portion of the pipe) to insure low radial heat transfer and therefore little chance of vapor blockage in the wick as a result of high radial heat fluxes. The inside diameter of the heat pipe was .743 inches and the outside diameter was 13/16 inches. Thermocouples were placed along the outside surface of the heat pipe to monitor axial temperature loss. The end caps on the heat pipe were removable to facilitate the testing of many different wicks without the additional labor and expense of constructing a new heat pipe for each wick. Vapor thermocouples were attached to the removable end caps to monitor vapor temperature. Four different sizes of wire mesh were used to obtain four variations in the design equation.

Figure 3.2 shows the stainless steel heat pipe with end caps. The thermocouple wiring harness was attached and bonding cement was applied to the thermocouple junctions. Figure 3.3 shows the same heat pipe of Figure 3.2 after insulation, heater wire, and calorimeter have been installed. Excessive insulation was added to the evaporator to maximize the input heater effectiveness. Figure 3.4 shows the experimental heat pipe mounted and ready for testing. The heat pipe is tested with the evaporator higher than the condenser so that the wick limited condition can be reached without excessive heat flux. The apparatus used to measure the gravity effect is shown in Figure 3.5. A sliding probe two feet in length is inserted into the heat pipe until electrical contact is made with the excess working fluid in the bottom of the pipe. Contact is indicated by a reading on a microammeter. The length of the probe, L_p, is measured and the pressure drop due to gravity, $\Delta p_{\ell g}$, is calculated using Equation 3.1. Figure 3.6 shows the wire mesh wick being inserted into a heat pipe. The wicks were manufactured to fit as tight as possible and were inserted through the condenser end and pressed tightly into the evaporator. Figure 3.7 shows the heat pipe under test. Figure 3.24 is a simplified drawing of the heat pipe operating at steady

$$\Delta p_{\ell g} = L_{p_i} \sin\theta + r_{pi} \quad (3.1)$$

state and temperature recorder monitoring temperature distributions along the pipe and the calorimeter temperature rise.

Figure 3.9 shows the technique used to experimentally determine wick permeability. A balloon approximately two feet in length was inserted into the vapor cavity of the heat pipe and pressurized to 50 psi. This pressure was chosen to ensure a sufficient force to press the balloon against the wick as shown in Figure 3.26. The objective of the measurement is to force fluid through the wick in a manner similar to the actual operation of the heat pipe. Figure 3.26 shows the small error that will result in the permeability test due to the inability of the balloon to seal off a small area near the seam. This error is considered insignificant since that seam void carries a small amount of fluid by the meniscus shown in Figure 3.27. A pressure head of six inches of water was used to drive the fluid through the wick. The liquid flow velocity resulting from this driving pressure was approximately .015 ft/sec (.015 ft/sec was calculated to be the maximum flow encountered during operation of these heat pipes and is in the Darcy flow regime) and the pressure loss was taken across the wick structure only. Permeability was calculated using Equation 2.14. Figure 3.11 shows the preparation for a permeability test with the balloon ready to be pressurized.

$$\frac{2\sigma}{r_e} = \frac{\rho g}{g_o} H \qquad (3.2)$$

The apparatus used in the determination of capillary critical radius is shown in Figure 3.14. Wick samples were pressed between two O-rings and submerged in a reservoir of working fluid. The sample covered a 2.25 inch hole which was attached to a 2.25 inch plastic tube. The tube acted as a fluid container so that the liquid head could be supported by the capillary forces of the wick sample structure. The fluid level was then lowered until the wick sample could no longer support the fluid inside the plastic cylinder by surface tension forces. At that instant the capillary rise height was measured. Critical radius, r_e, was determined using Equation 3.2. Figure 3.12 shows the capillary rise height apparatus broken down and in the testing configuration. Figure 3.13 shows the measurement of wire mesh thickness after the capillary rise test. The wire mesh thickness data will be used in Chapter 5 to determine liquid recession depths.

Figure 3.15 shows the apparatus used to manufacture the wire mesh wicks. The wrapping mandrel twenty-five inches in length is mounted between spring loaded jaws which press against the wire mesh as it is wrapped. Figure 3.16 shows the initial phase of manufacture. A piece of wire mesh is cut to size and a retainer rod is spot welded at the edge. The wire mesh is inserted into the mandrel and placed into the apparatus. The wire mesh is then wrapped on the mandrel with the spring loaded jaws pressing against the wire mesh to produce a tight fit as shown in Figure 3.17. Figures 3.18 through 3.23 reiterate this sequence in detail. Figure 3.25 shows the final result of the wick manufacture. The 1/4 inch overlap at the edge of the wick is necessary to insure strong spot welds. The resultant structure is quite strong and incompressible which gave accurate and repeatable readings in the permeability test.

The procedure for testing is given in the appendix. Chapter 4 will deal with properties of heat pipe wicks measured using the apparatus just described.

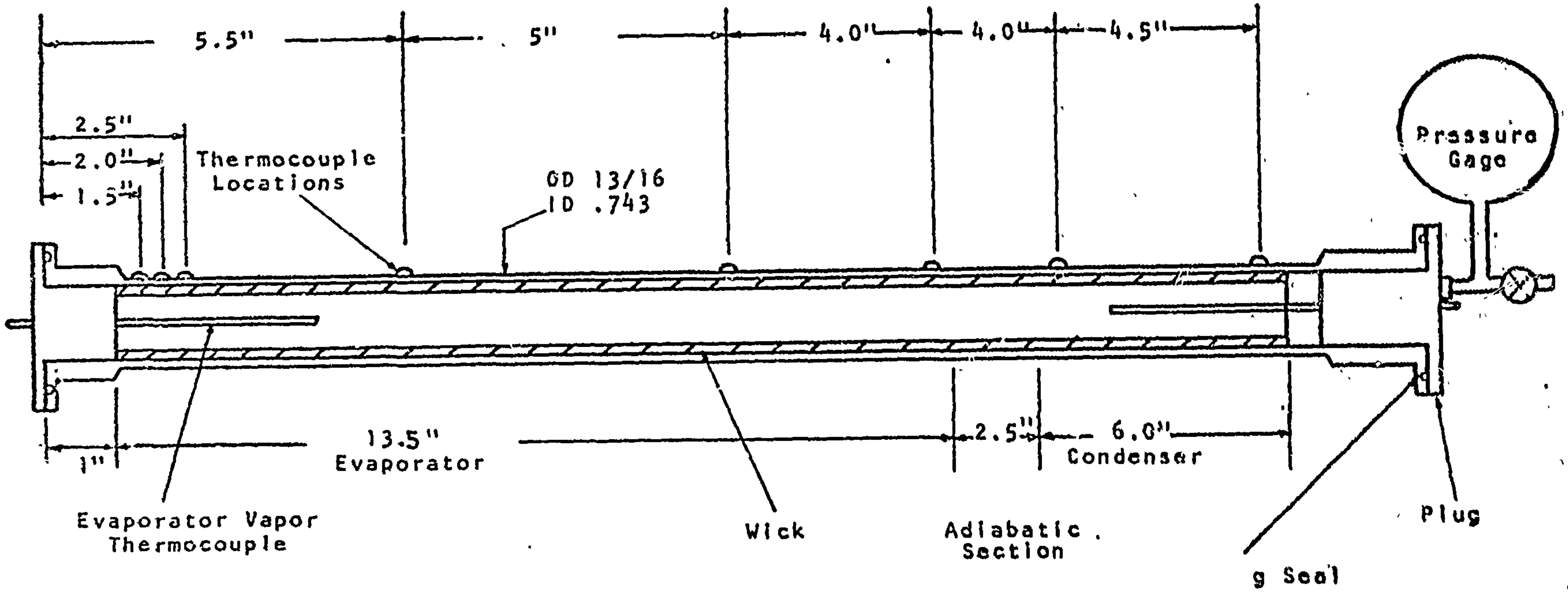

Figure 3.1. Experimental Heat Pipe Apparatus

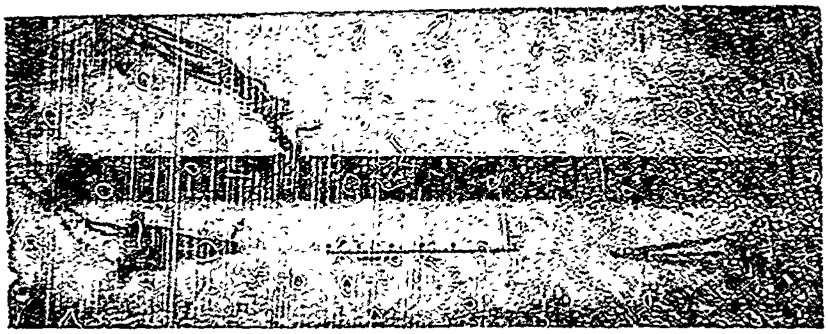

Figure 3.2. Stainless Steel Heat Pipe and Vapor Probes

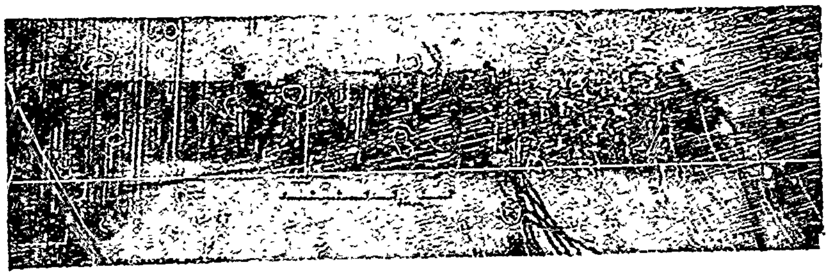

Figure 3.3. Evaporator Section (insulated) and Condenser Installed

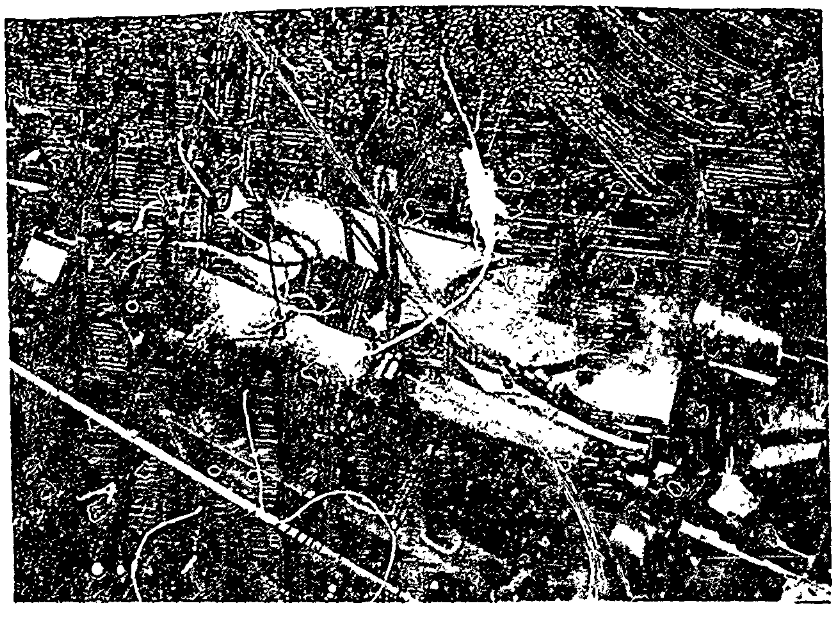

Figure 3.4. Testing Configuration

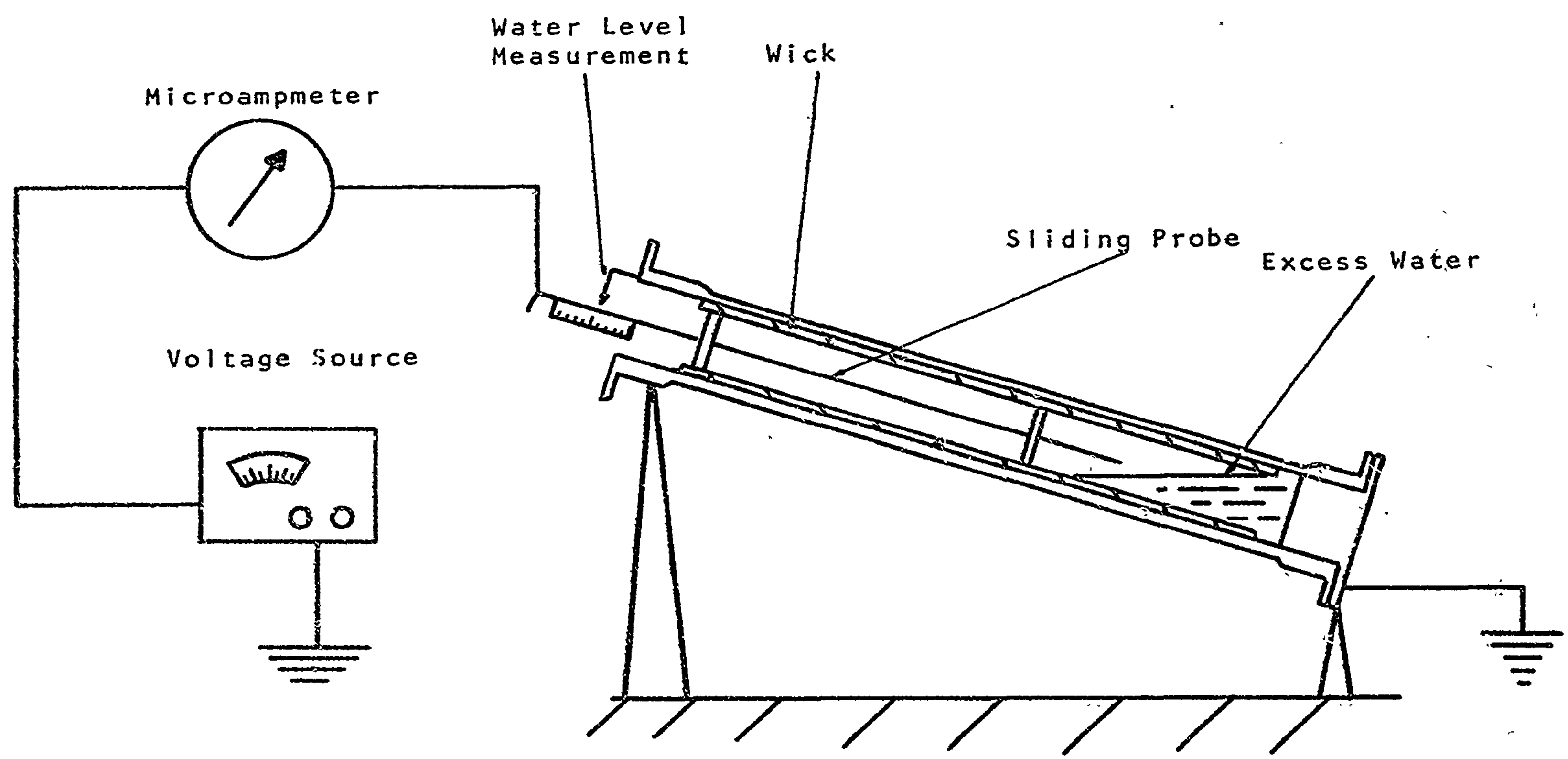

Figure 3.5. Apparatus Used to Determine the Gravity Head at a Particular Inclination

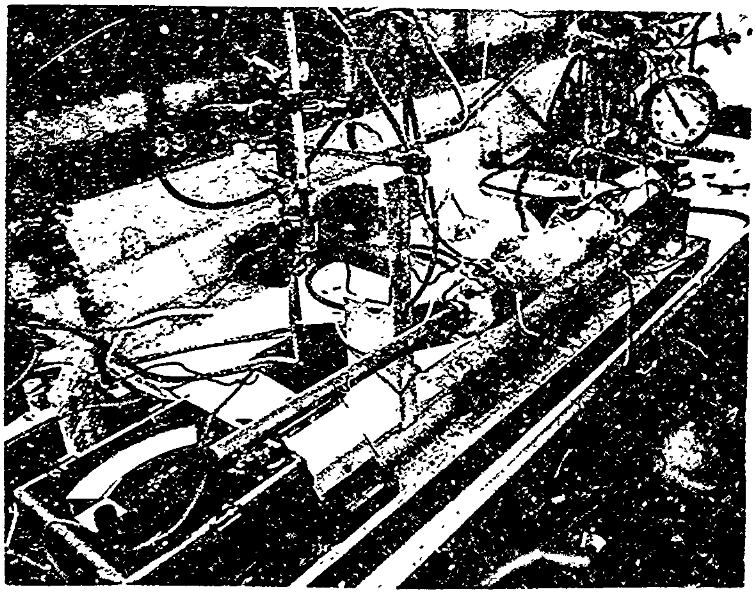

Figure 3.6.
Inserting Wire
Mesh Wick into
Heat Pipe

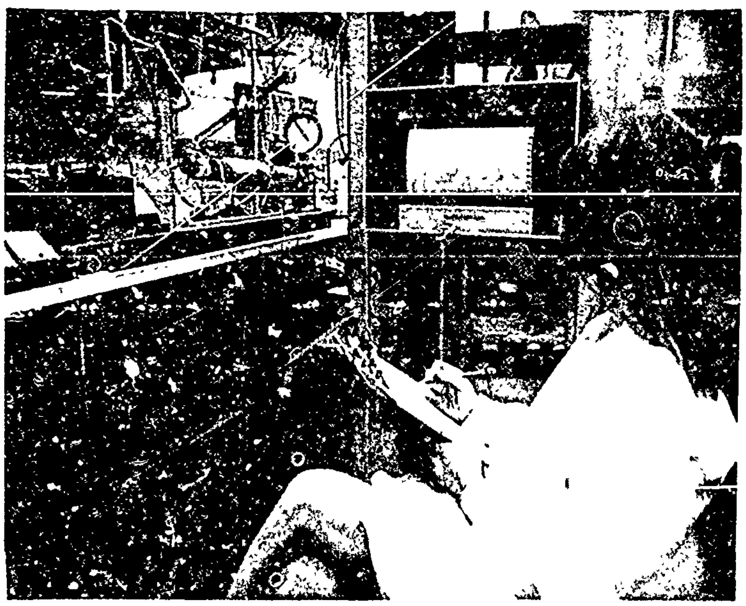

Figure 3.7.
Testing Maximum
Heat Transfer
Rate

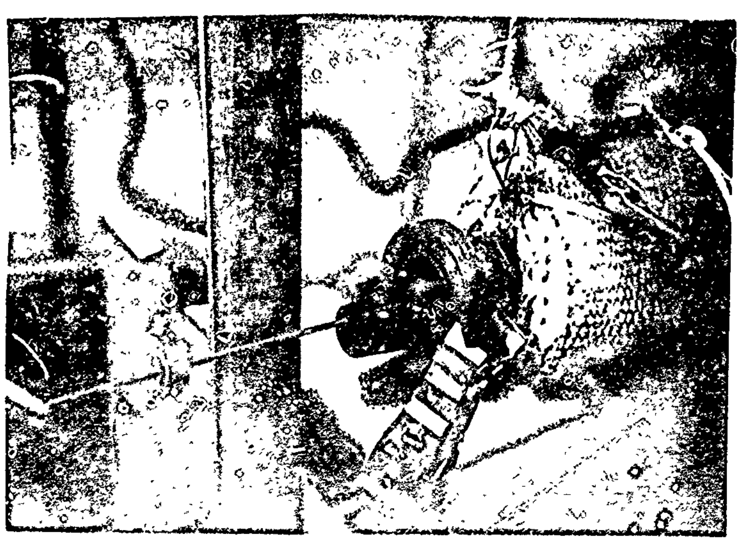

Figure 3.8.
Determination of
Liquid Heat Loss
Due to Gravity

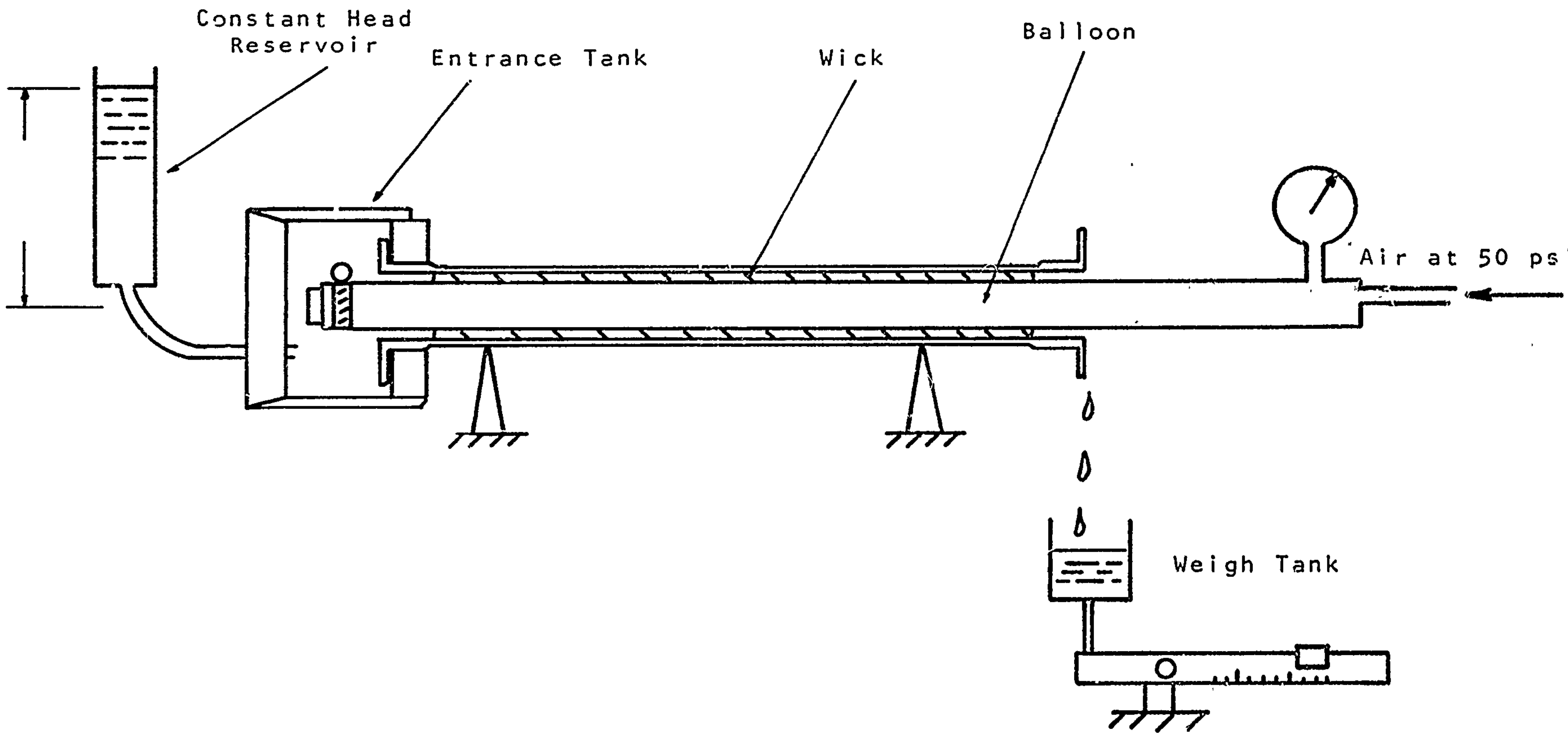

Figure 3.9. Apparatus for the Determination of Wick Permeability

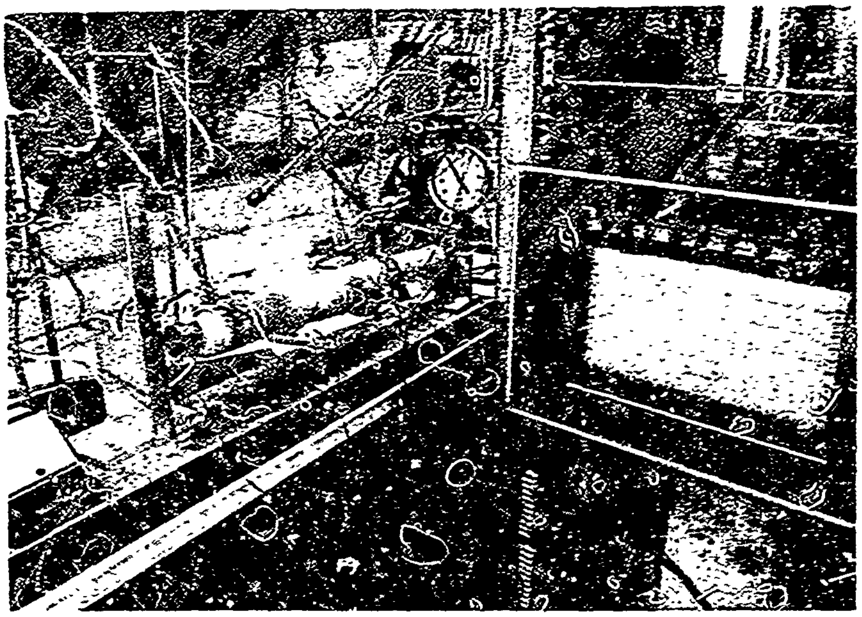

Figure 3.10. Heat pipe configuration for wick limiting test

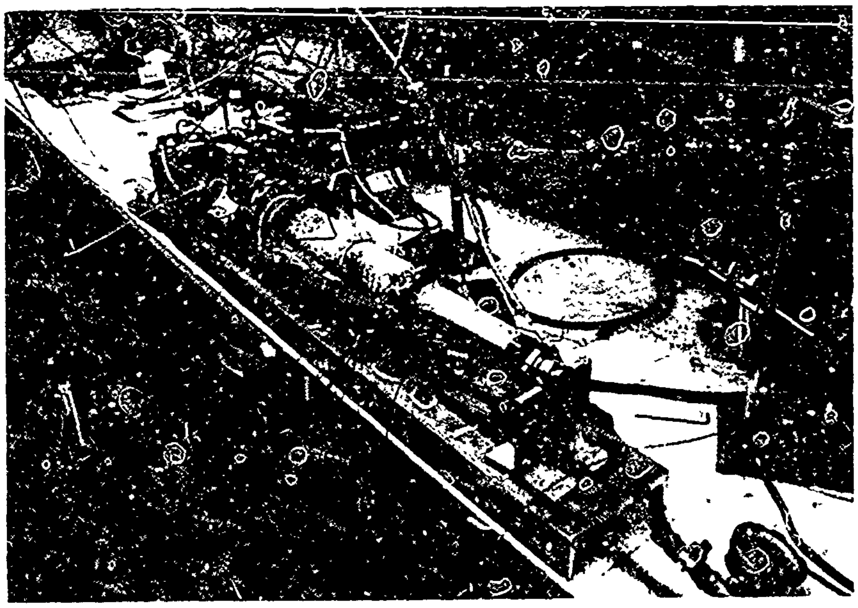

Figure 3.11. Permeability test

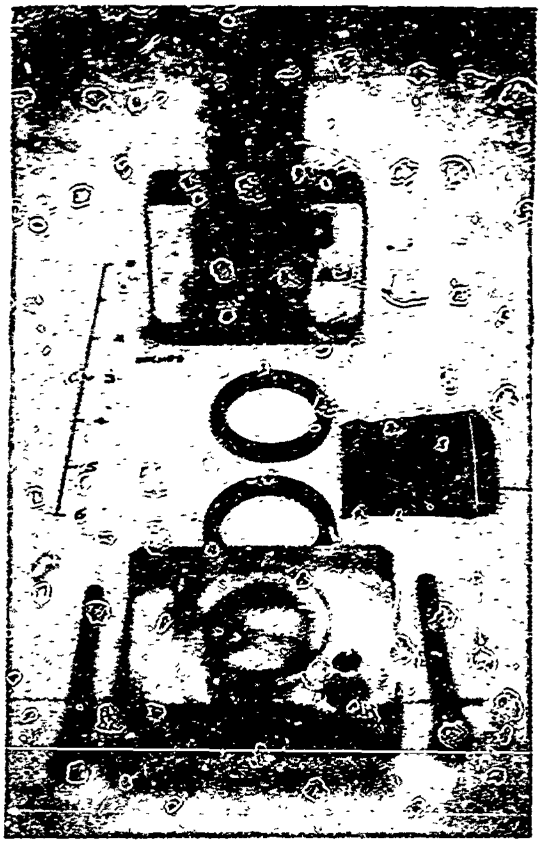

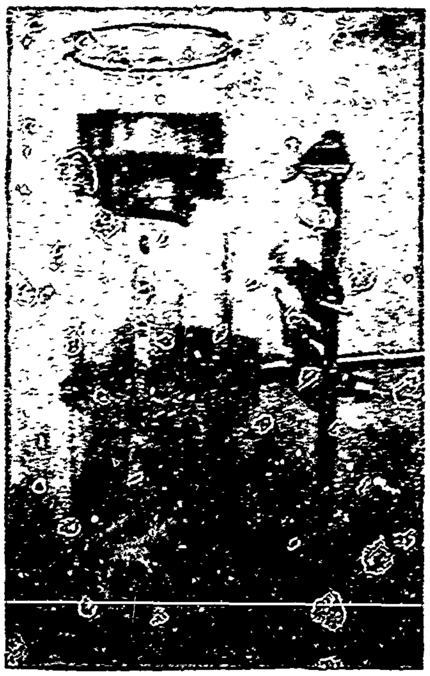

Figure 3.12. Capillary Rise Capability Test Apparatus

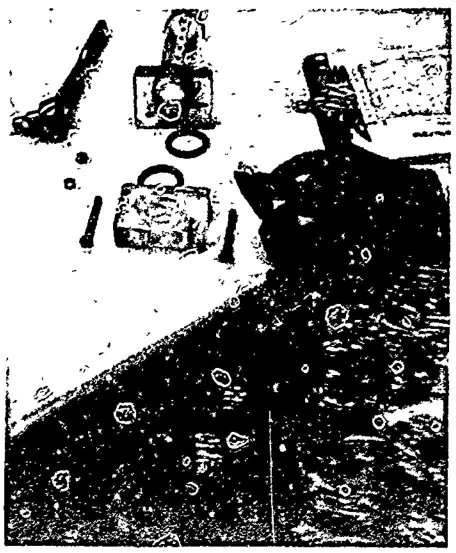

Figure 3.13 Checking Wire Mesh Thickness after Capillary Rise Test

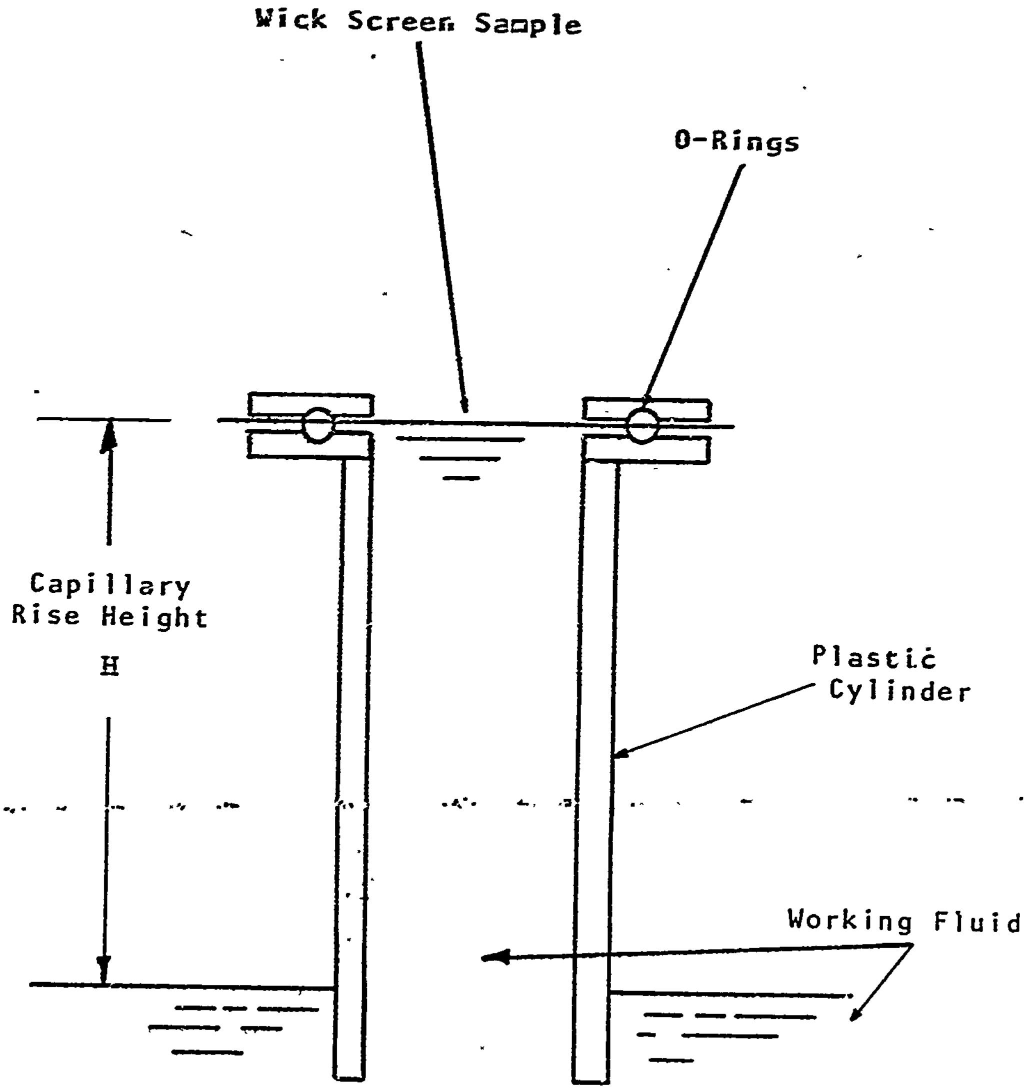

Figure 3.14. Capillary Rise Height Apparatus

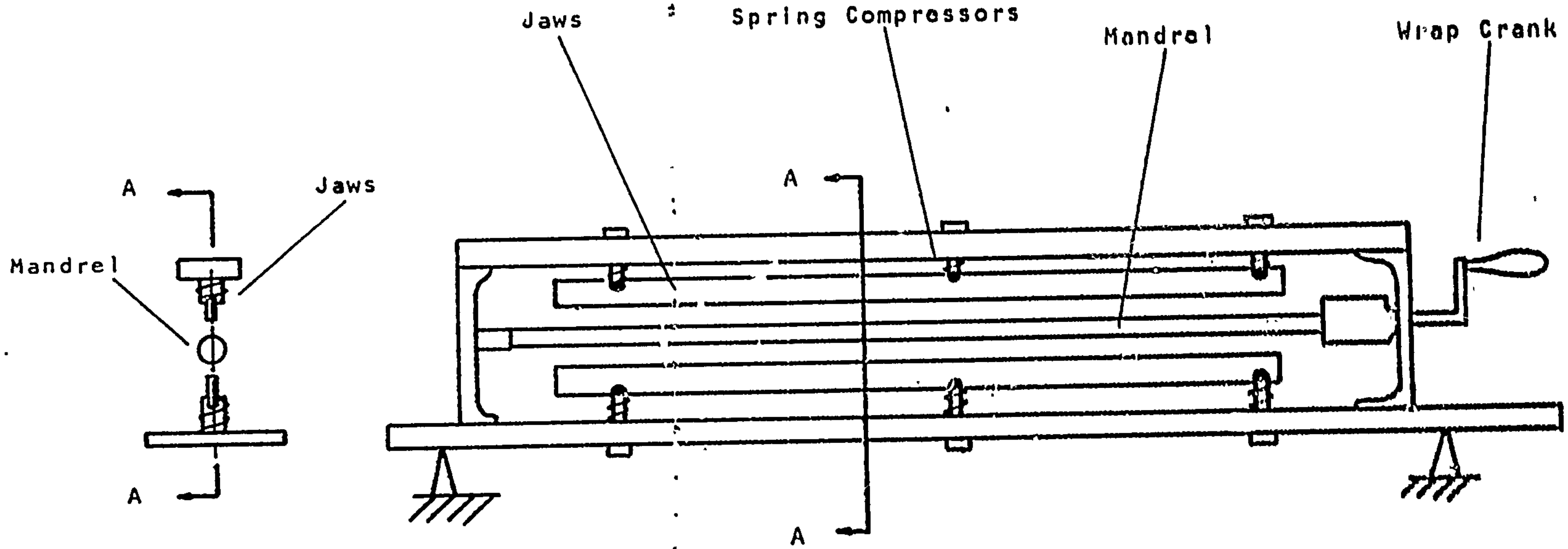

Figure 3.15. Basic Wick Wrapping Apparatus Structure

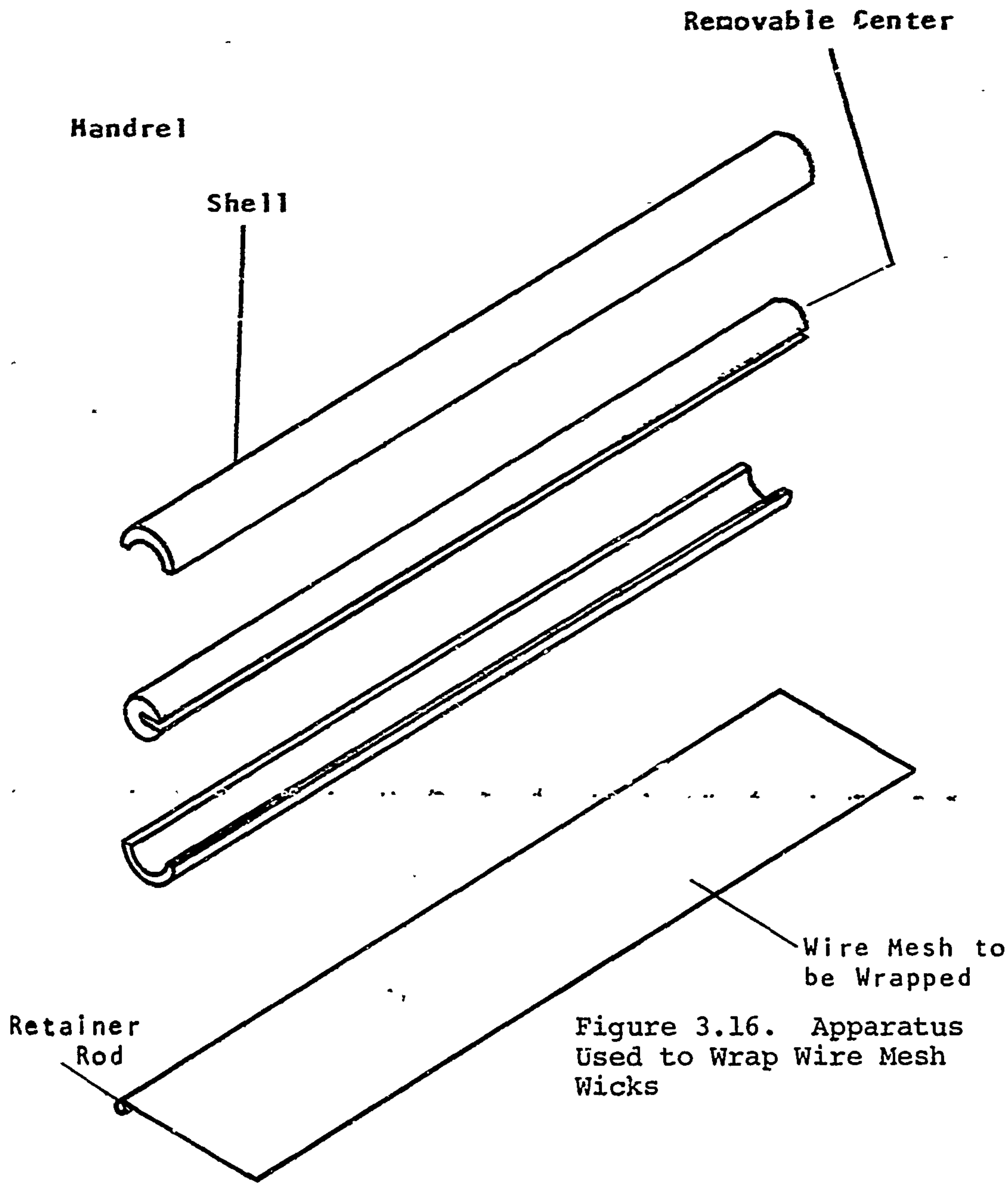

Figure 3.16. Apparatus Used to Wrap Wire Mesh Wicks

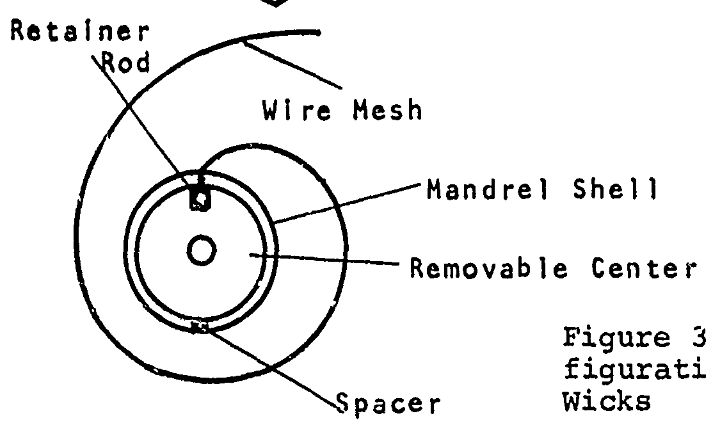

Figure 3.17. Wrapping Configuration for Wire Mesh Wicks

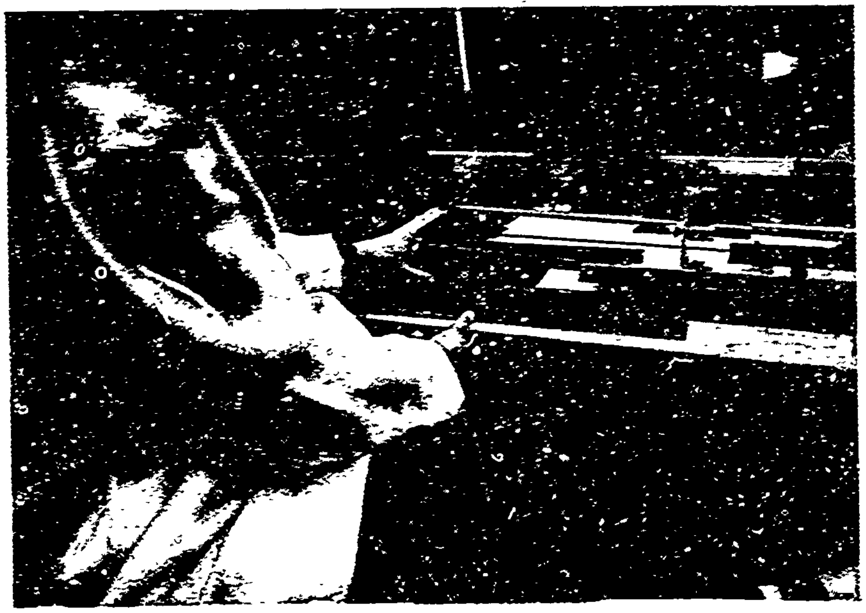

Figure 3.18. Initial Phase of Wire Mesh Wick Manufacture

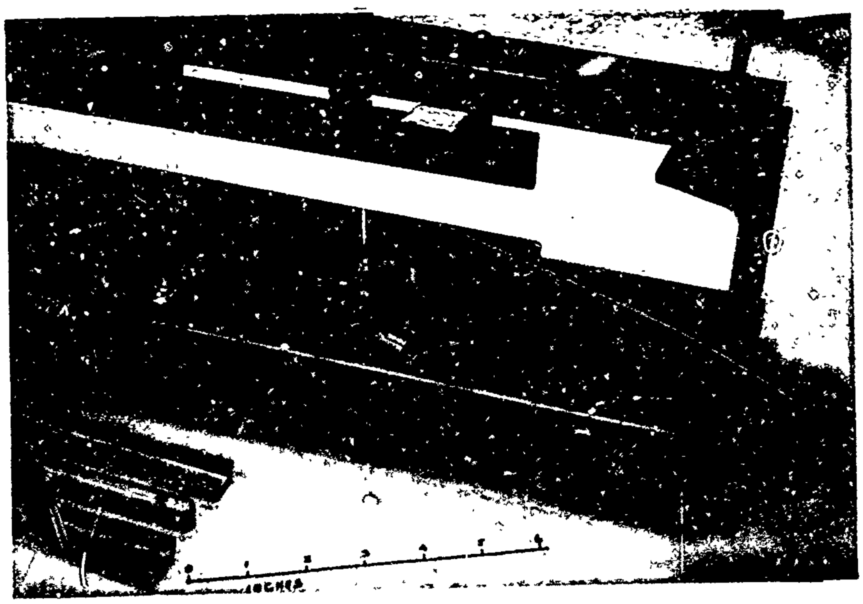

Figure 3.19. Apparatus Ready for Wrapping

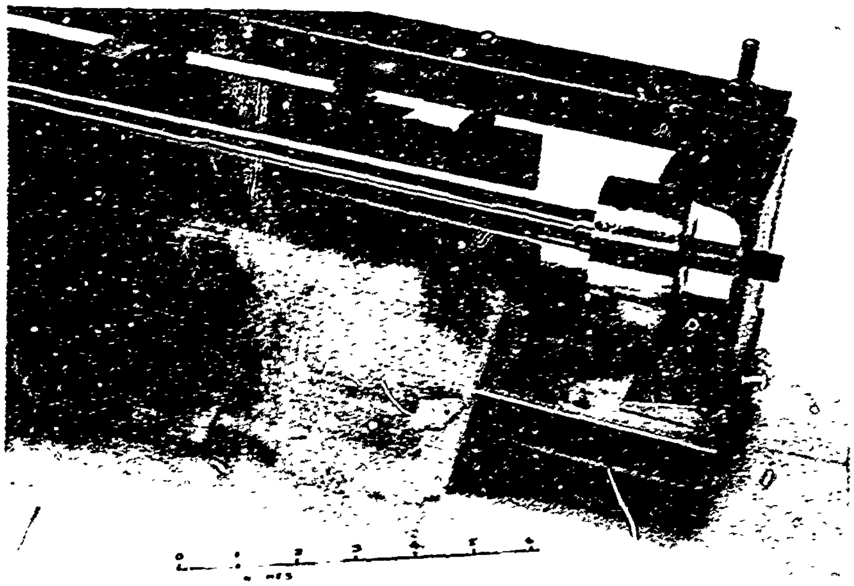

Figure 3.20. Mandrel and Wire Mesh Are Inserted into the Apparatus

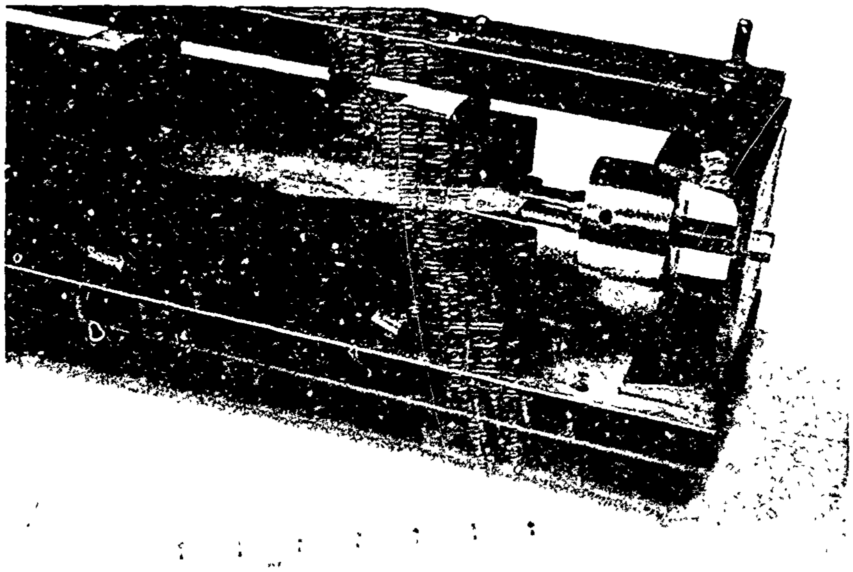

Figure 3.21. The Wrapping Is Initiated by Turning the Collet and Lowering the Compression Jaws

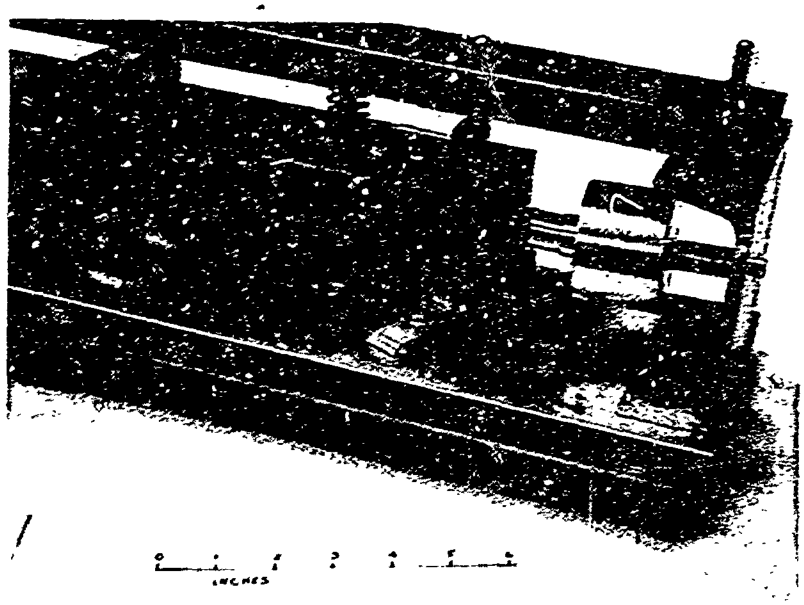

Figure 3.22. Wick Seam Is Spot Welded and Excess Material Removed

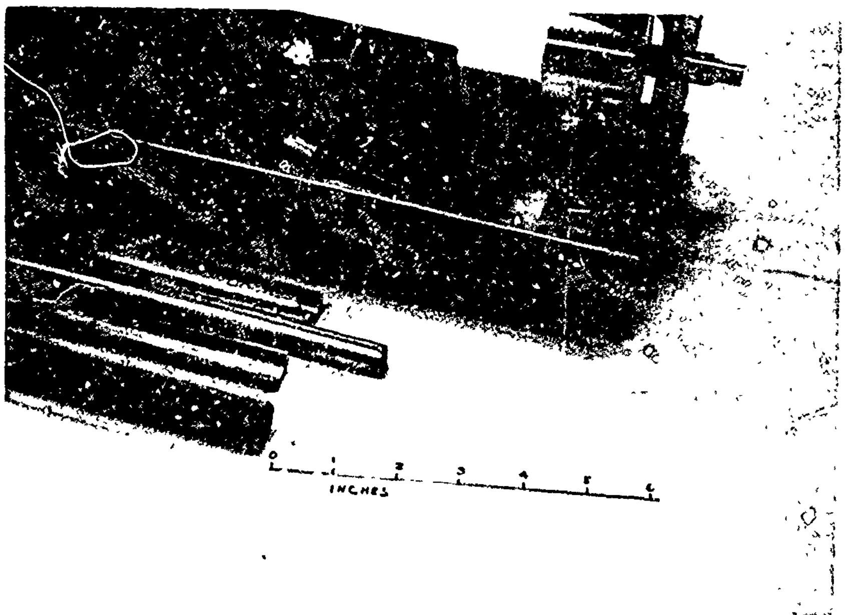

Figure 3.23. Mandrel Is Removed and Wick Is Extracted by Removing Center

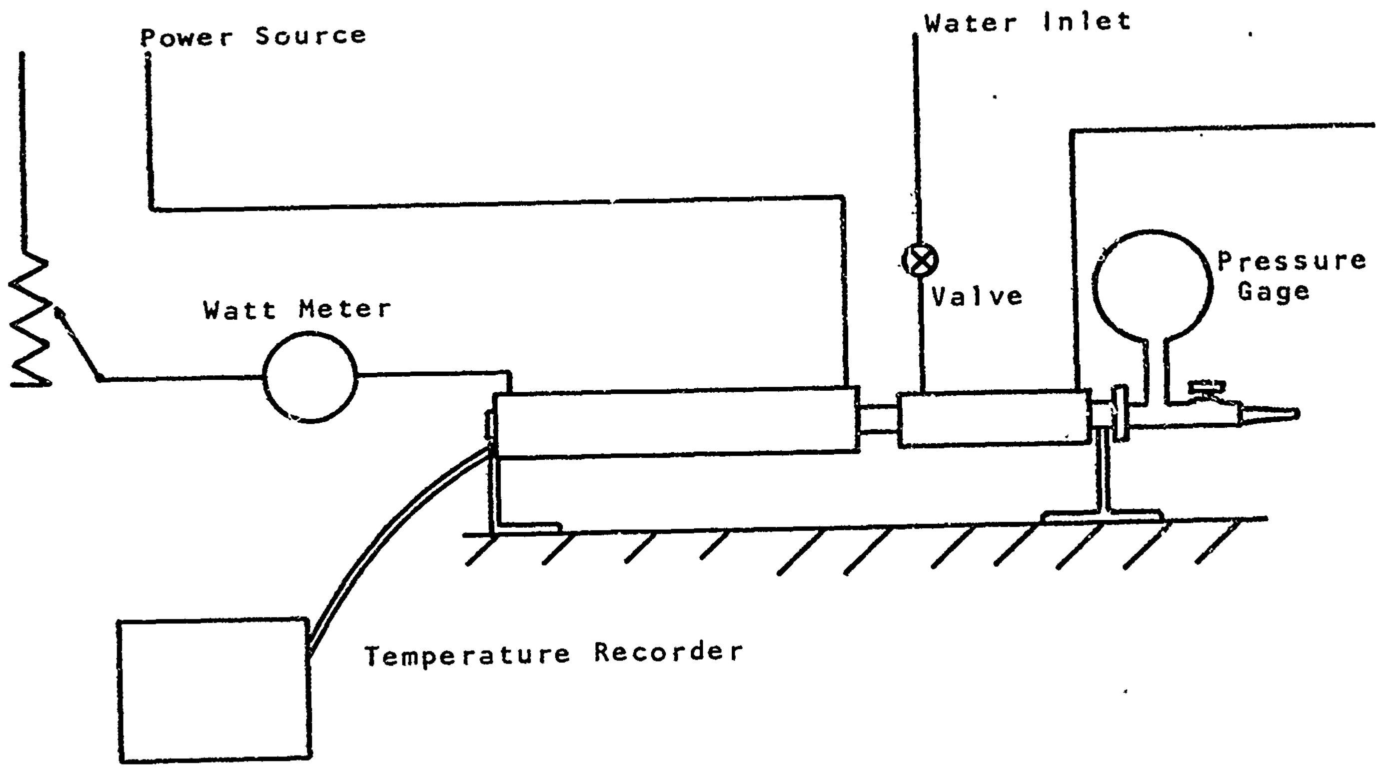

Figure 3.24. Heat Pipe Performance Test System

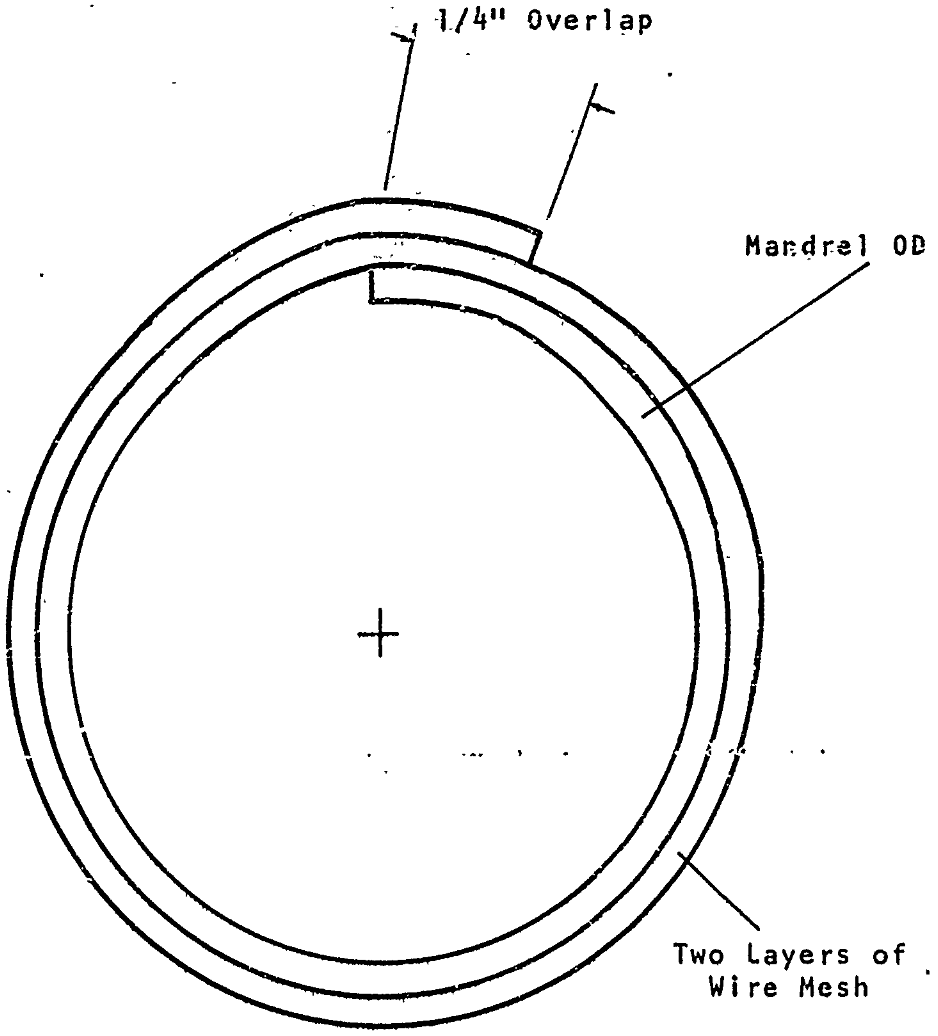

Figure 3.25. Wire Mesh Wick Cross Section of Typical Two Layer Wick

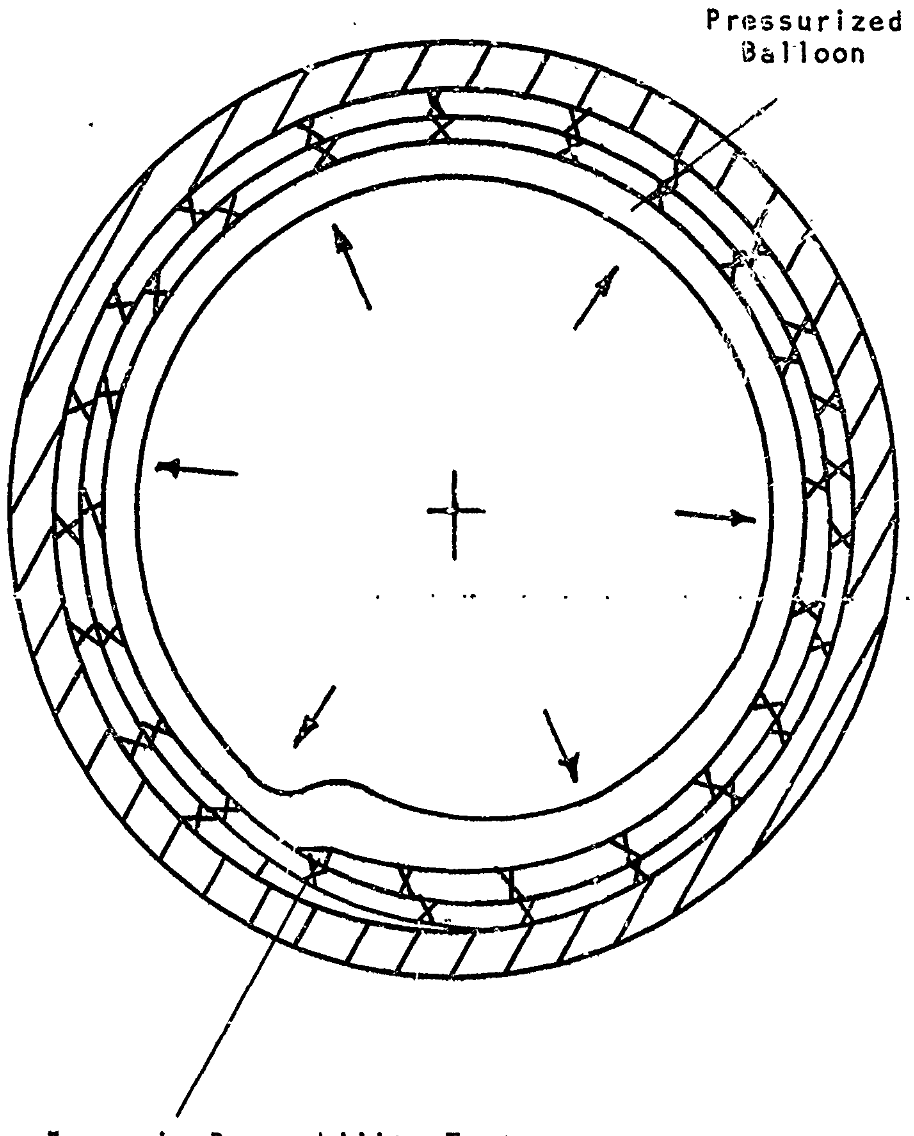

Figure 3.26. Illustration of the Permeability Error in Using Flexible Balloon

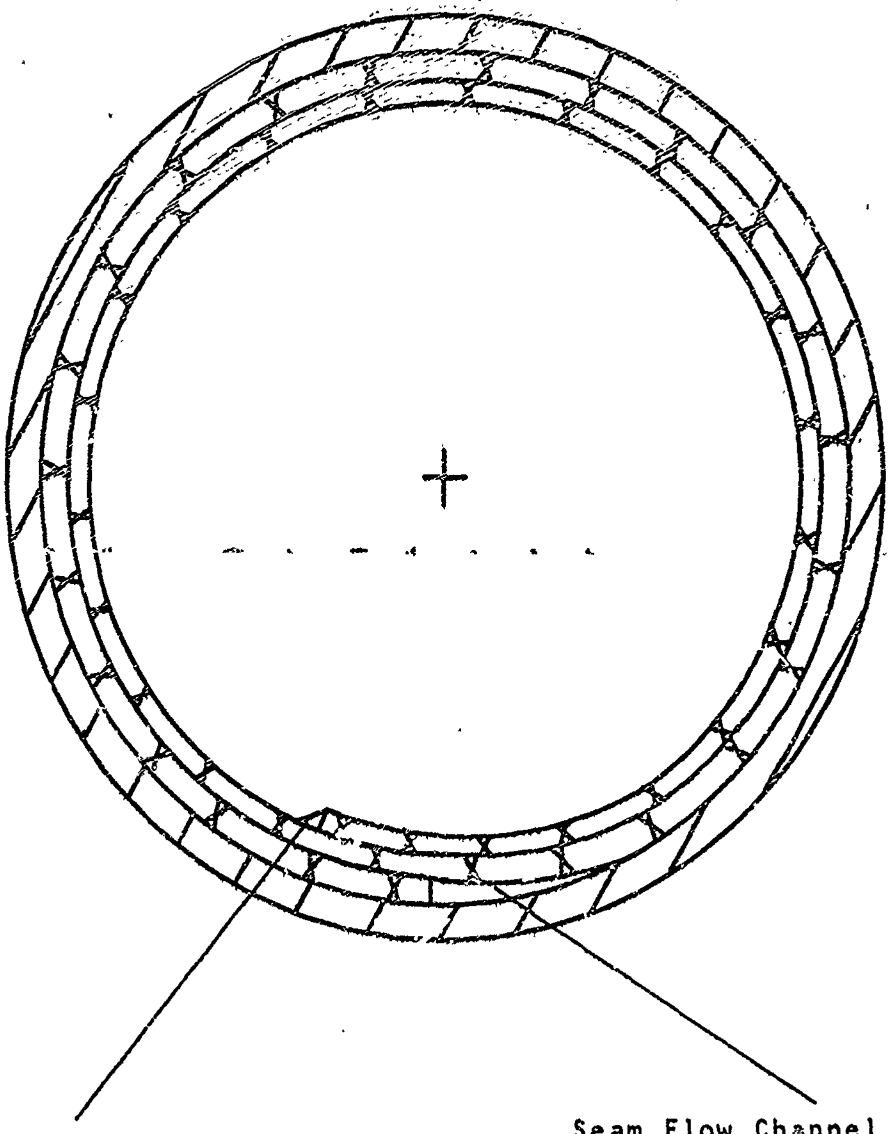

Figure 3.27. Additional Liquid Flow Paths in Wire Mesh Heat Pipes

CHAPTER 4

HEAT PIPE WICK PROPERTIES

The properties of heat pipe wicking materials are extremely variable. Wick properties such as porosity, critical radius, wetting angles, and cross sectional area are not identical for the same type of wicks manufactured from the same materials under carefully controlled uniform conditions. In order to measure the extent of such variability a total of 50 square weave wire mesh wicks were tested in the following categories

Type of Wick	Number of Wicks Tested
100 Mesh 304 Stainless Steel (tight wrap)	5
100 Mesh 304 Stainless Steel (moderately tight wrap)	30
200 Mesh 304 Stainless Steel	5
50 Mesh 304 Stainless Steel	5
100 Mesh Copper	5

Five properties were measured for each wick. These properties were permeability (K), critical radius (r_e), wick cross sectional area (A), porosity (e), and tortuosity (b).

In this chapter tabular values of the experimental data used to determine the heat pipe wick properties are presented. The reason for presentation of this data is to show the extreme variability of the readings and to show how one incorporates these readings into estimates of the random variates used in design.

4.1 Permeability

Permeability measurements for each of the 50 wire mesh wicks tested are shown in Figures 4.1 through 4.5. Each mean value and standard deviation was generated using Equations 2.55 and 2.56 using the number of replicated points which is designated as the sample size. The individual means and standard deviations result from experimental error in observing the data. The overall mean is the mean of all the individual means and the overall standard deviation is calculated using Equation 2.56 for all the data points in the data set. (Note: Each data set is data for a specific type of wick.) The overall mean and overall standard deviation are used as the parameters of the random variate pair to describe variability of the manufacturing process. According to Data Set 1, the permeability variate, $(\bar{K}, S_k)$, for the 100 mesh stainless steel wicks, is $(5.243 \times 10^{-9}, 1.096 \times 10^{-9})$. Now that the distribution parameter estimates are known, it is helpful to assume a probability distribution for the given random variable. Since these data are repeated readings, one generally chooses the normal distribution to model variability of the design variable. All of the data were tested for normality and did not reject the Kolomogorov-Smirnov Significance Test[17] at the 99% significance level; thus, the data are considered normally distributed.

Factors contributing to the uncertainty in prediction of the permeability are:

1. Variability of wire diameter in the mesh and between mesh lots

2. Weave manufacture variability

3. Wrapping manufacture variability

   a) Weights of wire mesh wicks are not identical indicating more wire mesh on certain wicks.

   b) Wrap compression is not completely consistent due to change alignment of the two screen layers.

   c) Tightness of wick fit in the pipe may vary resulting in a variable seam channel flow path.

One may notice the significant difference between the permeability in data sets 1 and 2 shown in Tables 4.1 and 4.2 Although each of the wicks had identical mesh sizes, the wicks of data set 1 were wrapped to fit very tightly in the heat pipe. This tight fit compressed the screen structure which resulted in a low permeability. This demonstrates the sensitivity of the permeability measurement to compression of the wick layers against the pipe wall.

The uncertainty in the prediction of heat flow capability for a heat pipe with the above permeability characteristic is directly proportional to the variability of the permeability.

4.2 Critical Radius

Capillary critical radius readings are affected by

1. Wetting angle

2. Width of wire mesh openings

3. Compression of the two or multiple layers of wire mesh

The data of Table 4.6 shows the uncertainty in the measurement of capillary pressure capability of one and two layers of wire mesh. Here capillary pressure capability is the pressure rise measurement using the apparatus of Figure 3.14.

The data of Table 4.6 are taken from data set 1 and 2* since 100 mesh stainless steel screen was used in both sets. The equality of standard deviations between the two layer and one layer data indicates the consistency of the capillary pressure measuring device. All of the single layer capillary pressure measurements proved to be statistically different from the two layer measurements according to a hypothesis test.[17]

It should be pointed out that the difference between the one and two layer capillary pressure capabilities may vary depending on the degree of compression and distortion of the two layers. If the two layers of wire mesh were compressed tightly together, a rather large difference in capillary pressure capability would be expected between the compressed two layer structure and the single layer of wire mesh due to the smaller capillary pores formed between the two layers. If the two layer structure was loose, very little difference would be expected. The wick structures mentioned in Chapter 3 are compressed sufficiently to cause intermeshing of the multiple layers of wire mesh.

The difference in capillary pressure capability of one and two layers of the same wire mesh is an important factor in the recession theory analysis of these types of wicks. During the two layer capillary pressure tests, the liquid receded into the two layer structure and encountered higher capillary force resulting in the difference between one and

*Reference Appendix A

two layer readings. This will be discussed in detail in Chapter 5.

Table 4.7 shows small samples of data from other tests and in every case the one and two layer capillary pressure capabilities proved to be different, statistically.

Tables 4.8, 4.9, 4.10, 4.11, and 4.12 show the critical radius values, r_{fr}, for all the data.

Uncertainty of the widths of wire mesh openings (due to the manufacturing) are considered the prime variabilities in the measurement of this property. Wetting angle was assumed constant throughout the structure since the wicks were cleaned uniformly.

4.3 Wick Cross Sectional Area

The wick cross sectional area distributions proved to be very consistent with low standard deviations. Tables 4.13, 4.14, 4.15, 4.16, and 4.17 show cross sectional area data for all of the area tests. The low standard deviations indicate a consistent intermeshing of the multiple layers of wire mesh. Uncertainties in the measurement of this property arise from

a) Differences in wire mesh lots

b) Measurement variations for the wick inside diameter (one must avoid additional compression of the wick structure while making the measurement)

4.4 Porosity and Tortuosity

Porosity and tortuosity for all 50 wicks were calculated from measured values according to the following definitions

$$\text{porosity} \qquad e = \frac{\text{Void Vol}}{\text{Total Vol}} = 1 - \frac{\text{Weight of Wick}}{\rho_W \ (A) \ (L)} \qquad (4.1)$$

$$\text{tortuosity} \qquad b = \frac{e r_{fr}^2}{K} \qquad (4.2)$$

The porosity distributions proved to be almost identical from wick to wick. Tables 4.18, 4.19, 4.20, 4.21, and 4.22 show the porosity and tortuosity data. The tortuosity data were almost independent of wire mesh size except for data set 1 which had a very low permeability. One might expect higher tortuosity for these wicks but looking at the variables for the calculation of b we are able to see the opposite. The r_e used in the calculation was the value of the two layer wick, (r_{fr}), which was about 20% smaller than that for the single layer. The permeability for this wick design is higher than other designs because of the additional flow through the seam flow channel (see Figure 3.26). This tends to lower the tortuosity, b, somewhat as compared to other wire mesh structures since the permeability seems to have dominated the tortuosity calculation. The standard deviations for e and b were calculated from the input variabilities into the equations using the algebra of moments method.[7] The uncertainty in the calculation of b was rather high as a result of the high uncertainties of the input properties e, r_e, and K.

4.5 Summary of Wick Property Data

Table 4.23 summarizes the uncertainties in predicting properties of wire mesh wicks of this particular design. Many of the properties may vary considerably depending on the type of manufacture methods used. Since all of the data distributions are considered normal, one can quote the mean property value plus or minus three standard deviations and be assured that 99.7% of the property values will lie within these bounds.[7] (For small sample sizes, tolerances should be placed on this probability.) Figures 4.1 - 4.5 show discrete probability plots of the various design variables which were assumed normally distributed.

TABLE 4.1

PERMEABILITY DISTRIBUTION FROM

DATA SET 1

(100 mesh, stainless steel, 304 2 layer)

Mean K (ft^2)	Standard Deviation K (ft^2)	Sample Size
$3.584 x 10^{-9}$	$1.926 x 10^{-10}$	30
$5.244 x 10^{-9}$	$2.685 x 10^{-10}$	↓
$5.246 x 10^{-9}$	$2.874 x 10^{-10}$	↓
$5.407 x 10^{-9}$	$1.495 x 10^{-10}$	↓
$6.654 x 10^{-9}$	$42.158 x 10^{-10}$	↓

Overall Mean $5.243 x 10^{-9}$

Overall Standard Deviation $1.096 x 10^{-9}$

*Note: These standard deviations are a result of experimental error in the determination of each individual K reading. The sample sizes are the number of replications per K reading.

TABLE 4.2

PERMEABILITY DISTRIBUTION FROM

DATA SET 2

(100 mesh stainless steel, 304 2 layer wrap mandral .001" smaller diameter than Data Set 1)

Mean K (ft^2)	Standard Deviation K (ft^2)	Sample Size
$5.951 x 10^{-9}$	$4.467 x 10^{-10}$	10
$6.080 x 10^{-9}$	$3.364 x 10^{-10}$	↓
$6.081 x 10^{-9}$	$2.297 x 10^{-10}$	↓
$6.204 x 10^{-9}$	$2.575 x 10^{-10}$	↓

TABLE 4.2 continued

6.234×10^{-9}	2.833×10^{-10}
6.250×10^{-9}	4.356×10^{-10}
6.326×10^{-9}	2.176×10^{-10}
6.412×10^{-9}	1.968×10^{-10}
6.427×10^{-9}	3.795×10^{-10}
6.566×10^{-9}	3.085×10^{-10}
6.698×10^{-9}	3.641×10^{-10}
6.850×10^{-9}	3.748×10^{-10}
6.909×10^{-9}	4.862×10^{-10}
6.953×10^{-9}	3.122×10^{-10}
7.184×10^{-9}	3.601×10^{-10}
7.191×10^{-9}	3.192×10^{-10}
7.323×10^{-9}	2.834×10^{-10}
7.463×10^{-9}	1.381×10^{-10}
7.474×10^{-9}	5.334×10^{-10}
7.479×10^{-9}	2.634×10^{-10}
7.482×10^{-9}	4.464×10^{-10}
7.775×10^{-9}	3.342×10^{-10}
8.116×10^{-9}	4.518×10^{-10}
8.154×10^{-9}	2.877×10^{-10}
8.214×10^{-9}	4.302×10^{-10}
8.246×10^{-9}	2.674×10^{-10}
8.337×10^{-9}	3.730×10^{-10}
8.338×10^{-9}	2.142×10^{-10}
8.379×10^{-9}	5.015×10^{-10}
8.701×10^{-9}	3.439×10^{-10}

Overall Mean 7.193×10^{-9} sq. ft.

Overall Standard Deviation 0.841×10^{-9} sq. ft.

TABLE 4.3

PERMEABILITY DISTRIBUTION FROM

DATA SET 3

(200 mesh stainless steel, 316 3 layer)

Mean K (ft^2)	Standard Deviation K (ft^2)	Sample Size
2.584×10^{-9}	1.483×10^{-10}	10
2.798×10^{-9}	9.819×10^{-10}	
3.074×10^{-9}	2.845×10^{-10}	
3.171×10^{-9}	2.149×10^{-10}	
3.796×10^{-9}	6.949×10^{-10}	

Overall Mean 3.084×10^{-9} sq. ft.

Overall Standard Deviation 0.460×10^{-9} sq. ft.

TABLE 4.4

PERMEABILITY DISTRIBUTION FROM

DATA SET 4

(50 mesh stainless steel, 304 2 layer)

Mean K (ft^2)	Standard Deviation K (ft^2)	Sample Size
2.739×10^{-8}	1.339×10^{-9}	10
2.822×10^{-8}	8.494×10^{-9}	
3.209×10^{-8}	1.625×10^{-9}	
3.230×10^{-8}	9.071×10^{-9}	
3.290×10^{-8}	1.625×10^{-9}	

Overall Mean 3.056×10^{-8} sq. ft.

Overall Standard Deviation 0.260×10^{-8} sq. ft.

TABLE 4.5

PERMEABILITY DISTRIBUTION FROM

DATA SET 5

(100 mesh Cu 2 layer)

Mean K (ft^2)	Standard Deviation K (ft^2)	Sample Size
6.031×10^{-9}	4.131×10^{-10}	10
6.400×10^{-9}	3.475×10^{-10}	↓
6.421×10^{-9}	4.344×10^{-10}	↓
6.577×10^{-9}	3.111×10^{-10}	↓
6.737×10^{-9}	2.586×10^{-10}	↓

Overall Mean 6.433×10^{-9} sq. ft.

Overall Standard Deviation 0.263×10^{-9} sq. ft.

TABLE 4.6

CAPILLARY PRESSURE CAPABILITY OF ONE LAYER AND TWO LAYERS OF WIRE MESH
(100 mesh stainless steel 304, 35 readings taken from data set #1 and #2)

	One layer capillary pressure capability (inches H_2O), h_1	Two layer capillary pressure capability, h_2	Difference data $h_2 - h_1$
	5.000	5.625	0.625
	4.625	5.250	0.625
	5.250	5.875	0.625
	5.000	5.500	0.500
	4.625	5.000	0.375
	4.750	5.250	0.500
	4.625	5.500	0.875
	4.750	5.899	1.149
	4.750	5.750	1.000
	4.500	5.750	1.250
	5.250	6.250	1.000
	4.000	5.625	1.625
	4.750	5.350	0.600
	5.250	6.250	1.000
	5.500	6.000	0.500
	4.675	5.500	0.824
	4.500	5.250	0.750
	4.250	4.625	0.375
	4.125	5.364	1.239
	4.625	4.750	0.125
	5.000	5.625	0.625
	4.750	5.875	1.125
	5.364	5.750	0.385
	4.750	5.500	0.750
	5.250	5.875	0.625
	5.000	5.750	0.750
	4.875	5.500	0.625
	4.875	5.500	0.625
	4.362	5.625	1.262
	4.375	5.875	1.500
	4.500	5.364	0.864
	4.500	5.364	0.864
	5.000	5.500	0.500
	4.750	5.500	0.750
	4.500	5.364	0.864
Mean	4.761	5.552	0.790
Standard deviation (all distributions Normal)	0.349	0.350	0.332

TABLE 4.7

CAPILLARY PRESSURE CAPABILITY OF ONE LAYER AND TWO LAYERS OF WIRE MESH
(data taken from data sets 3,4,5)

One Layer capillary pressure capability (inches H_2O), h_1	Two layer capillary pressure capability h_2	Difference data $h_2 - h_1$
(Data set 3, 200 mesh stainless steel, 3 layer)	(note: for data set 3, this is 3 layer capability)	
8.000	9.750	1.750
7.000	9.500	2.500
7.500	9.000	1.500
9.250	10.250	1.000
7.350	8.750	1.400
7.819 (Overall Mean)	9.450	1.630
0.876 (Overall Standard Deviation)	0.597	0.556
(Data set 4, 50 mesh stainless steel, 2 layer)		
2.364	2.875	0.510
2.364	2.750	0.385
2.000	2.625	0.625
1.875	2.625	0.750

TABLE 4.7 (continued)

2.250	2.625	0.375
2.171 (Overall Mean)	2.700	0.529
0.223 (Overall Standard Deviation)	0.112	0.160
(Data set 5, 100 mesh Cu, 2 layer)		
5.250	5.875	0.625
5.250	5.875	0.625
5.164	5.750	0.585
5.250	5.875	0.625
5.250	5.875	0.625
5.233 (Overall Mean)	5.850	0.617
0.038 (Overall Standard Deviation)	0.056	0.018

TABLE 4.8

CRITICAL RADIUS DISTRIBUTION

FROM DATA SET 1

(100 mesh stainless steel, two layer)

Mean r_{fr} inches)	Standard Deviation r_{fr}(inches)	Sample Size
4.055×10^{-3}	1.000×10^{-4}	5
4.247×10^{-3}	↓	↓
4.337×10^{-3}	↓	↓
4.809×10^{-3}	↓	↓
4.906×10^{-3}	↓	↓

Overall Mean 4.470×10^{-3} inches

Overall Standard Deviation 0.369×10^{-3} inches

TABLE 4.9

CRITICAL RADIUS DISTRIBUTION

FROM DATA SET 2

(100 mesh stainless steel, two layer)

Mean r_{fr}(inches)	Standard Deviation r_{fr}(inches)	Sample Size
3.639×10^{-3}	1.000×10^{-4}	5
3.645×10^{-3}	↓	↓
3.786×10^{-3}	↓	↓
3.858×10^{-3}	↓	↓
3.870×10^{-3}	↓	↓
3.877×10^{-3}	↓	↓
3.878×10^{-3}	↓	↓
3.887×10^{-3}	↓	↓

TABLE 4.9 (continued)

3.958×10^{-3}		
3.961×10^{-3}		
3.969×10^{-3}		
3.969×10^{-3}		
5.051×10^{-3}		
5.051×10^{-3}		
5.053×10^{-3}		
4.139×10^{-3}		
5.140×10^{-3}		
4.140×10^{-3}		
4.140×10^{-3}		
4.140×10^{-3}		
4.140×10^{-3}		
4.141×10^{-3}		
4.143×10^{-3}		
4.245×10^{-3}		
4.257×10^{-3}		
4.257×10^{-3}		
4.265×10^{-3}		
4.337×10^{-3}		
4.337×10^{-3}		
4.539×10^{-3}		

Overall Mean 4.069×10^{-3} inches

Overall Standard Deviation 0.214×10^{-3} inches

Note: All r_{fr} readings are those of the multiple layers of screen.

TABLE 4.10

CRITICAL RADIUS DISTRIBUTION

FROM DATA SET 3

(200 mesh stainless steel, 3 layer)

Mean r_{fr} (inches)	Standard Deviation r_{fr} (inches)	Sample Size
2.162×10^{-3}	1.000×10^{-4}	5
2.336×10^{-3}		
2.396×10^{-3}		
3.575×10^{-3}		
2.603×10^{-3}		

Overall Mean 2.414×10^{-3} inches

Overall Standard Deviation 0.181×10^{-4} inches

TABLE 4.11

CRITICAL RADIUS DISTRIBUTION

FROM DATA SET 4

(50 mesh stainless steel, two layer)

Mean r_{fr} (inches)	Standard Deviation r_{fr} (inches)	Sample Size
7.921×10^{-3}	1.000×10^{-4}	5
8.278×10^{-3}		
8.278×10^{-3}		
8.278×10^{-3}		
8.675×10^{-3}		

Overall Mean 8.444×10^{-3} inches

Overall Standard Deviation 0.339×10^{-3} inches

TABLE 4.12

CRITICAL RADIUS DISTRIBUTION

FROM DATA SET 5

(100 mesh copper,
two layer)

Mean r_{fr} (inches)	Standard Deviation r_{fr} (inches)	Sample Size
3.888×10^{-3}	1.000×10^{-4}	5
$3,888 \times 10^{-3}$	↓	↓
3.888×10^{-3}	↓	↓
3.888×10^{-3}	↓	↓
3.971×10^{-3}	↓	↓

Overall Mean 3.904×10^{-3}

Overall Standard Deviation 1.000×10^{-4}

TABLE 4.13

WICK CROSS SECTIONAL AREA DISTRIBUTION

(Data from data set 1, 100 mess stainless steel, two layer)

Mean A(sq.ft.)	Standard Deviation A	Sample Size
2.285×10^{-4}	5.040×10^{-5}	16
2.354×10^{-4}	6.289×10^{-5}	
2.375×10^{-4}	5.250×10^{-5}	
2.445×10^{-4}	4.790×10^{-5}	
2.503×10^{-4}	1.104×10^{-5}	

Overall Mean 2.392×10^{-4} sq. ft..

Overall Standard Deviation 0.848×10^{-5} sq. ft.

TABLE 4.14

WICK CROSS SECTIONAL AREA DISTRIBUTION

(Data from data set 2, 100 mesh stainless steel, two layer)

Mean A(sq.ft.)	Standard Deviation A(sq.ft)	Sample Size
2.236×10^{-4}	6.790×10^{-6}	16
2.261×10^{-4}	7.510×10^{-6}	
2.270×10^{-4}	4.900×10^{-6}	
2.294×10^{-4}	2.294×10^{-6}	
2.324×10^{-4}	5.370×10^{-6}	
2.334×10^{-4}	6.270×10^{-6}	
2.336×10^{-4}	1.124×10^{-5}	
2.337×10^{-4}	6.280×10^{-6}	
2.353×10^{-4}	7.900×10^{-6}	
2.359×10^{-4}	7.890×10^{-6}	

2.363x10^{-4}	7.780x10^{-6}
2.373x10^{-4}	6.270x10^{-6}
2.382x10^{-4}	1.236x10^{-5}
2.387x10^{-4}	1.001x10^{-5}
2.387x10^{-4}	6.000 10^{-6}
2.392x10^{-4}	9.780 10^{-6}
2.392x10^{-4}	6.880x10^{-6}
2.401x10^{-4}	8.750x10^{-6}
2.402x10^{-4}	9.200x10^{-6}
2.416x10^{-4}	1.022x10^{-5}
2.416x10^{-4}	1.134x10^{-5}
2.421x10^{-4}	1.300x10^{-5}
2.426x10^{-4}	8.500x10^{-6}
2.426x10^{-4}	1.169x10^{-5}
2.441x10^{-4}	1.117x10^{-5}
2.469x10^{-4}	1.674x10^{-5}
2.475x10^{-4}	1.479x10^{-5}
2.555x10^{-4}	1.190x10^{-5}
2.558x10^{-4}	1.189x10^{-5}
2.584x10^{-4}	6.540x10^{-5}

Overall Mean 2.393x10^{-3} sq. ft.

Overall Standard Deviation 0.816x10^{-5} sq. ft.

TABLE 4.15

WICK CROSS SECTIONAL AREA DISTRIBUTION

(Data from data set 3, 200 mesh, stainless steel, 3 layer)

Mean A(sq. ft.)	Standard Deviation A	Sample Size
1.579×10^{-4}	5.390×10^{-6}	16
1.614×10^{-4}	1.294×10^{-5}	↓
1.677×10^{-4}	6.440×10^{-6}	↓
1.682×10^{-4}	7.860×10^{-6}	↓
1.688×10^{-4}	8.570×10^{-6}	↓

Overall Mean 1.648×10^{-4} sq. ft.

Overall Standard Deviation 0.487×10^{-5} sq. ft.

TABLE 4.16

WICK CROSS SECTIONAL AREA DISTRIBUTION

(Data from data set 4, 50 mesh stainless steel, 2 layer)

Mean S(sq. ft.)	Standard Deviation A	Sample Size
5.203×10^{-5}	2.091×10^{-6}	16
5.295×10^{-5}	1.100×10^{-5}	↓
5.314×10^{-5}	1.890×10^{-5}	↓
5.406×10^{-5}	1.860×10^{-6}	↓
5.438×10^{-5}	1.001×10^{-5}	↓

Overall Mean 5.331×10^{-4} sq. ft.

Overall Standard Deviation 0.936×10^{-5} sq. ft.

TABLE 4.17

WICK CROSS SECTIONAL AREA DISTRIBUTION

(Data from data set 5, 100 mesh Cu 2 layer)

Mean A(sq. ft.)	Standard Deviation A	Sample Size
2.759×10^{-4}	1.719×10^{-5}	16
2.836×10^{-4}	1.474×10^{-5}	↓
2.893×10^{-4}	1.037×10^{-5}	↓
2.939×10^{-4}	1.053×10^{-5}	↓
3.092×10^{-4}	9.650×10^{-6}	↓

Overall Mean 2.903×10^{-4} sq. ft.

Overall Standard Deviation 0.124×10^{-4} sq. ft.

TABLE 4.18

POROSITY AND TORTUOSITY DISTRIBUTIONS

(Data from data set 1, 100 mesh stainless steel, two layer)

Mean Porosity (dimensionless)	Standard Deviation Porosity	Mean Tortuosity Dimensionless)	Standard Devistion Tortuosity
0.582	0.0[illegible]24	18.553	3.244
0.577	0.113	18.944	2.827
0.591	0.0898	14.113	2.376
0.614	0.0180	19.561	1.403
0.602	0.0782	14.322	2.016
Overall Mean 0.593		16.098	
Overall Standard Deviation 0.0359		2.727	

TABLE 4.19

POROSITY AND TORTUOSITY DISTRIBUTIONS

(Data from data set 2, 100 mesh stainless steel, two layer)

Mean Porosity	Standard Deviation Porosity	Mean Tortuosity	Standard Deviation Tortuosity
0.596	0.0249	10.257	0.975
0.636	0.0107	8.472	0.557
0.611	0.0190	8.229	0.687
0.583	0.0210	8.794	0.740
0.619	0.0186	9.836	0.752
0.606	0.0273	8.927	0.888

TABLE 4.19 (continued)

	0.607	0.0189	8.157	0.663
	0.597	0.0166	10.688	0.772
	0.594	0.0148	9.721	0.652
	0.604	0.0151	8.757	0.661
	0.578	0.0168	10.323	0.690
	0.569	0.0132	9.984	0.610
	0.582	0.0233	10.519	0.984
	0.584	0.0186	9.106	0.742
	0.585	0.0168	11.644	0.833
	0.577	0.0137	9.136	0.645
	0.574	0.0154	9.618	0.710
	0.591	0.0206	9.300	0.707
	0.580	0.0226	9.225	0.795
	0.587	0.0203	10.312	0.866
	0.573	0.0158	10.303	0.708
	0.578	0.0130	7.924	0.525
	0.568	0.0114	8.116	0.473
	0.585	0.0184	10.375	0.863
	0.584	0.0122	9.885	0.685
	0.570	0.0157	1.704	0.551
	0.552	0.0143	10.841	0.670
	0.581	0.0127	8.314	0.572
	0.578	0.0116	9.219	0.511
	0.589	0.0179	9.482	0.670
Overall Mean	0.588		9.473	
Overall Standard Deviation	0.0170		0.937	

TABLE 4.20

POROSITY AND TORTUOSITY DISTRIBUTIONS

(Data set 3, 200 mesh stainless steel, three layer)

Mean Porosity	Standard Deviation Porosity	Mean Tortuosity	Standard Deviation Tortuosity
0.631	0.0142	10.074	0.600
0.622	0.00588	9.221	0.463
0.641	0.00553	10.186	0.562
0.645	0.00844	11.941	0.361
0.630	0.00950	10.184	0.287
Overall Mean	0.634	10.321	
Overall Standard Deviation	0.00933	0.992	

TABLE 4.21

POROSITY AND TORTUOSITY DISTRIBUTIONS

(Data set 4, 50 mesh stainless steel, two layer)

Mean P Porosity	Standard Deviation Porosity	Mean Tortuosity	Standard Deviation Tortuosity
0.617	0.0312	7.617	1.035
0.614	C.0145	9.468	0.985
0.656	0.0183	7.957	1.598
0.640	0.0149	7.428	2.701
0.653	0.0171	9.696	1.025
Overall Mean	0.636	8.433	
Overall Standard Deviation	0.0197	1.068	

TABLE 4.22

POROSITY AND TORTUOSITY DISTRIBUTIONS

(Data set 5, 100 mesh, Cu 2 layer)

Mean Porosity	Standard Deviation Porosity	Mean Tortuosity	Standard Deviation Tortuosity
0.648	0.0122	10.105	0.676
0.600	0.0256	10.450	1.000
0.634	0.0142	10.358	0.911
0.626	0.0202	10.277	0.837
0.623	0.0147	10.373	0.757
Overall Mean 0.626		10.313	
Overall Standard Deviation 0.0175		0.313	

TABLE 4.23 SUMMARY OF HEAT PIPE WICK PROPERTIES

	Data Set 1 (100 mesh ss, 2 layer)	Date Set 2 (100 mesh ss, 2 layer)	Data Set 3 (200 mesh ss, 3 layer)	Data Set 4 (50 mesh ss, 2 layer)	Data Set 4 (100 mesh cu, 2 layer)
Number of Wicks Tested	5	30	5	5	5
K, (Ft^2)	$5.243x10^{-9}$	$7.193x10^{-9}$	$3.084x10^{-9}$	$3.056x10^{-8}$	$6.433x10^{-9}$
Sk, (Ft^2)	$1.096x10^{-9}$	$0.841x10^{-9}$	$0.460x10^{-9}$	$0.260x10^{-8}$	$0.263x10^{-9}$
r_{fr}, (in)	$4.470x10^{-3}$	$4.069x10^{-3}$	$2.414x10^{-3}$	$8.444x10^{-3}$	$3.904x10^{-3}$
$S_{r_{fr}}$, (in)	$0.369x10^{-3}$	$0.214x10^{-3}$	$0.181x10^{-3}$	$0.339x10^{-3}$	$1.000x10^{-4}$
A, (Ft^2)	$2.392x10^{-4}$	$2.393x10^{-3}$	$1.648x10^{-4}$	$5.331x10^{-4}$	$2.903x10^{-4}$
Sa, (Ft^2)	$0.843x10^{-5}$	$0.816x10^{-5}$	$0.487x10^{-5}$	$0.936x10^{-5}$	$0.124x10^{-5}$
e	0.593	0.588	0.634	0.636	0.626
Se	0.0359	0.0170	0.00933	0.0197	0.0175
b	16.098	9.473	10.321	8.433	10.313
Sb	2.727	0.937	0.992	1.068	0.131

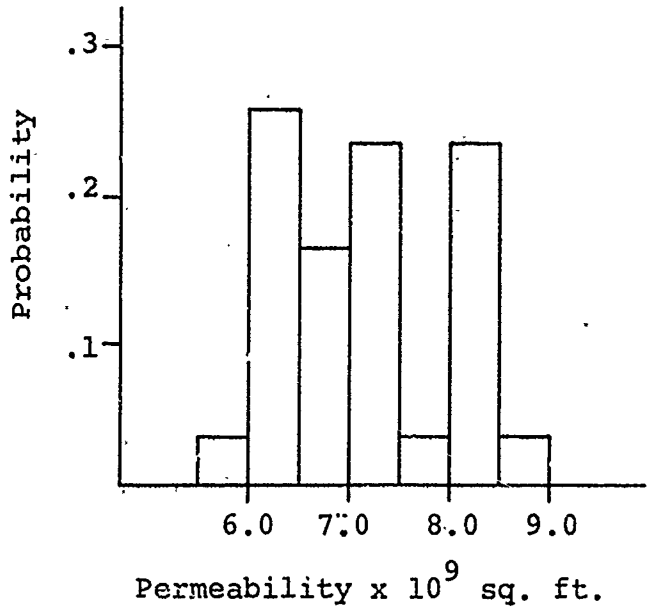

Figure 4.1. Permeability Distribution for Data Set 2

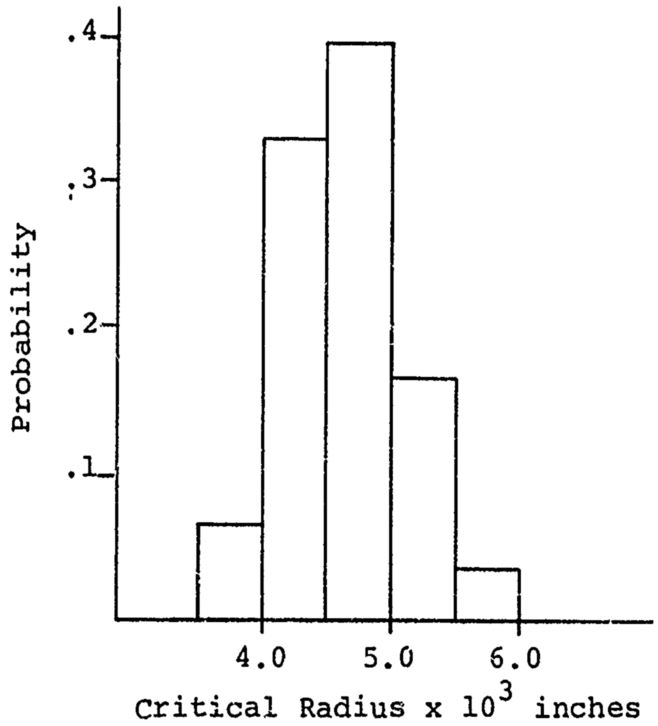

Figure 4.2. Critical Radius Distribution (two layer capability) for Data Set 2

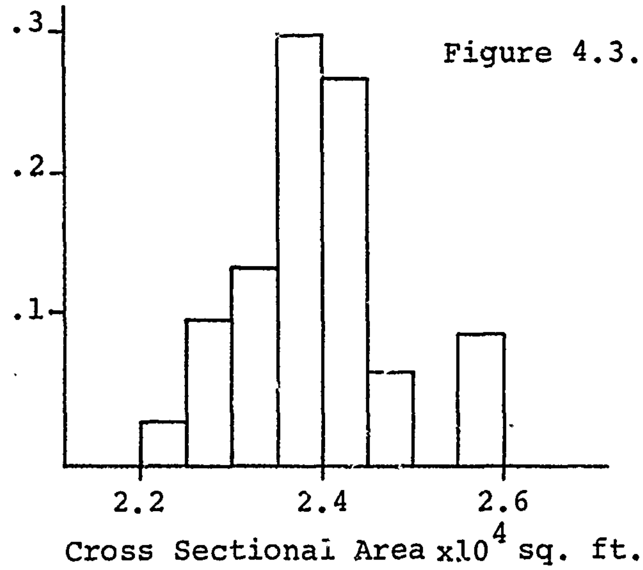

Figure 4.3. Cross Sectional Area Distribution for Data Set 2

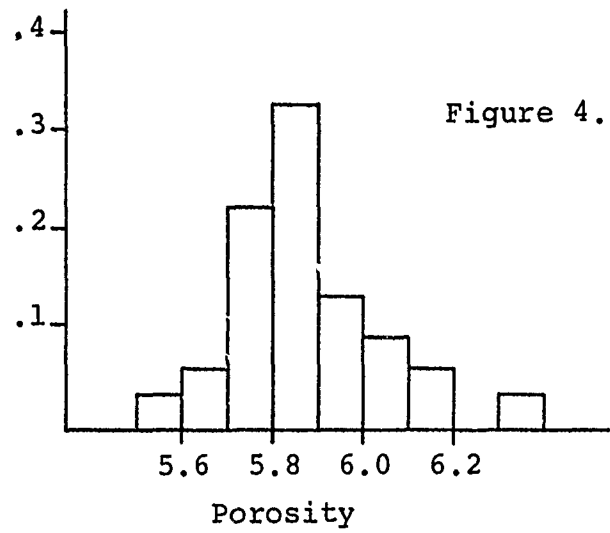

Figure 4.4. Porosity Distribution for Data Set 2

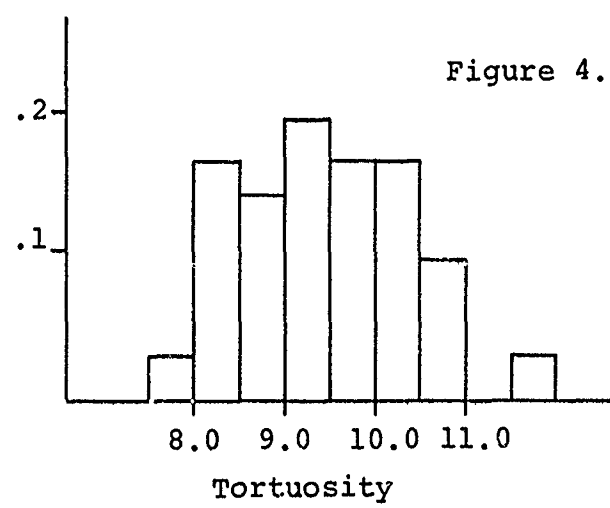

Figure 4.5. Tortuosity Distribution for Data Set 2

CHAPTER 5

RECESSION IN WIRE MESH WICKS

In Chapter 4 the basic determination of wire mesh wick properties was described. In this chapter the application of the recession theory of Chapter 4 to the wire mesh wicks will be presented. The wire mesh wicks to be analyzed will be the two layer square weave type wicks that were used in the experimental measurements.

Many descriptions[7] of wire mesh wick characteristics have modeled the surface tension phenomenon as shown in Figure 5.1. The screen layers are spaced one screen opening apart, and the radius is equal to one half the screen opening size. Liquid recession is shown in Figure 5.2(a). This desaturation process is unstable since the capillary forces have not increased due to the recession (Figures 5.2(a) and (b)). Using this physical model, the wick would dry out at relatively low heat transfer rate, yet experimentation shows this not to be the case. Many times fluid recession occurs down to the second layer and remains stable, and no dry out is observed at higher than expected heat transfer rates. Thus, a more accurate description of the wire mesh capillary structure is apparently required to help explain these observations.

Figure 5.3 shows a sketch of plain square weave wire cloth. Figure 5.4 shows a sketch of two layers of wire cloth compressed together as occurs in the construction of a heat pipe wick. Generally, when wicks are wrapped, the two layers do not align perfectly as suggested in Figure 5.1. Normally the wrapping results in the structure shown in Figure 5.5. The high points of the bottom layer of wire mesh tend to fit into openings of the top layer, resulting in a structure with a thickness less than the sums of the thicknesses of the individual layers. Figures 5.6, 5.7, and 5.8 show a cross section view, A-A, of the compressed doube layer of wire mesh previously shown in Figure 5.4.

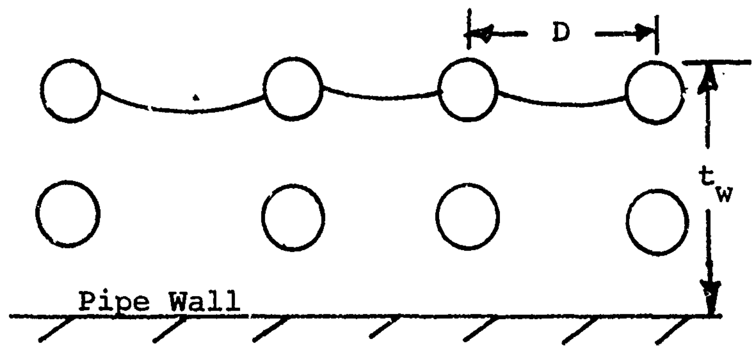

Figure 5.1. Classical Wire Mesh Capillary Model

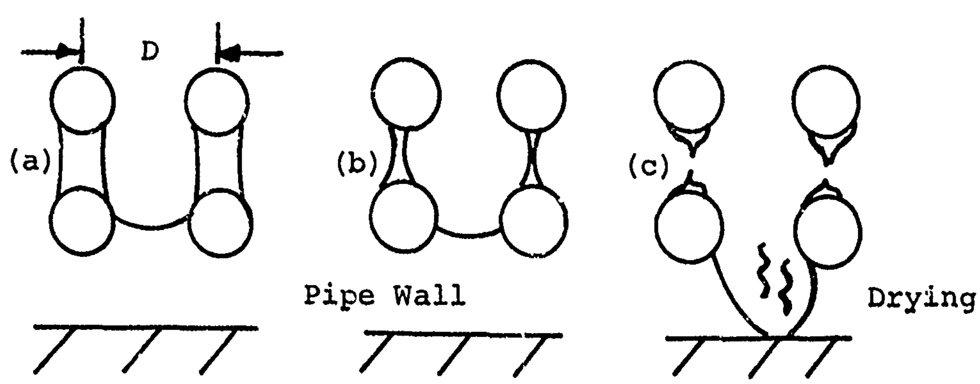

Figure 5.2. Recession and Dryout

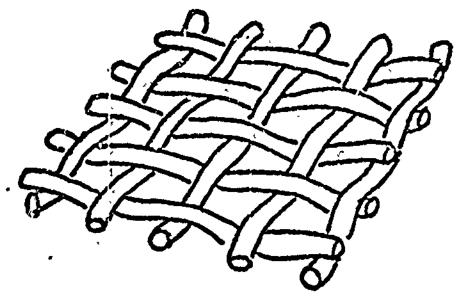

Figure 5.3. Single
Layer of Wire Mesh

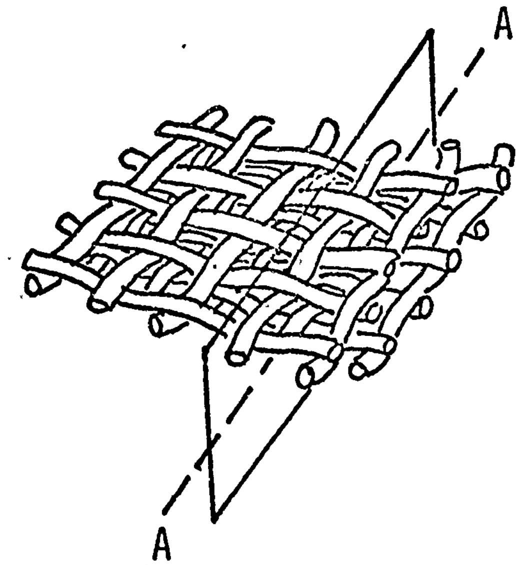

Figure 5.4. Compressed Double
Layer of Wire Mesh

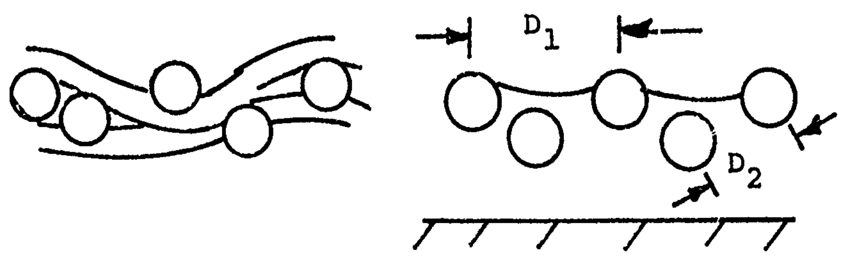

Figure 5.5. Proposed Wire Mesh Capillary Model

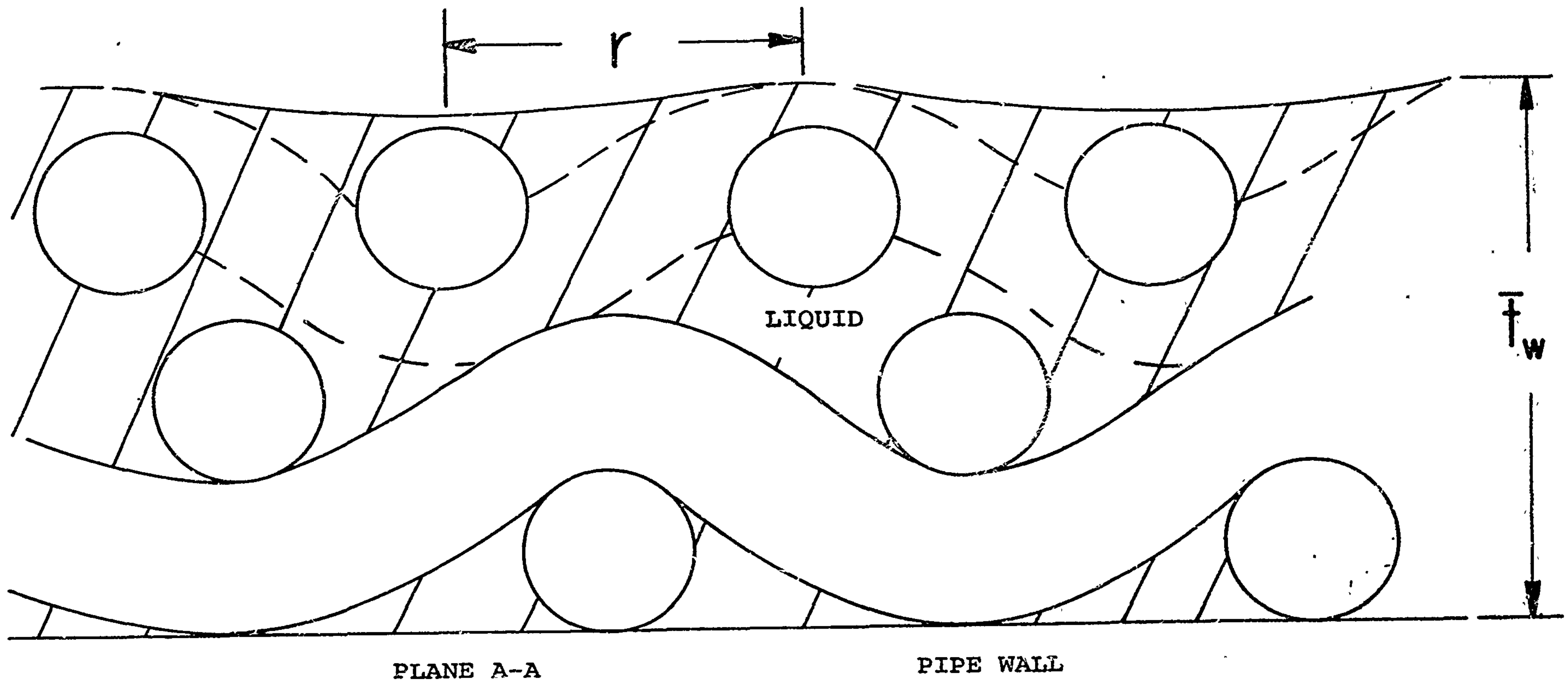

Figure 5.6. Two Layers of Screen Wick with Full Liquid Saturation

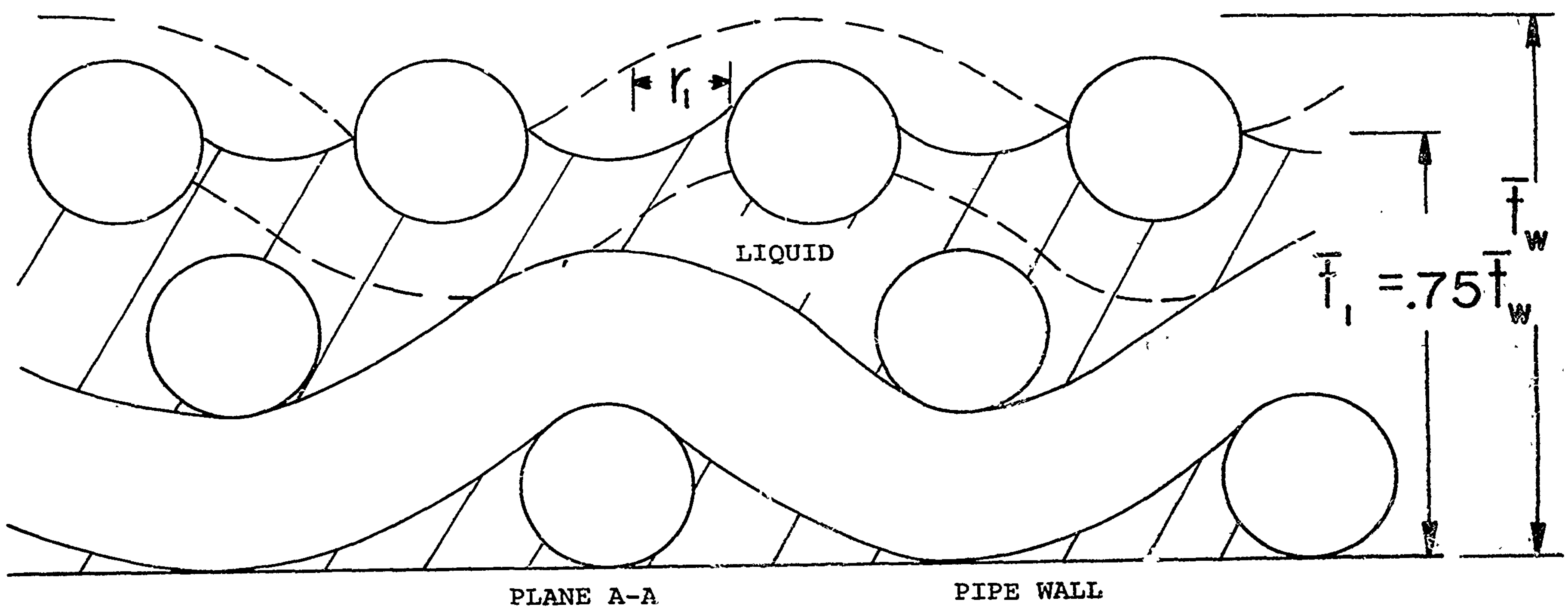

Figure 5.7. Two Layers of Screen Wick with Liquid Recessed to the First Layer

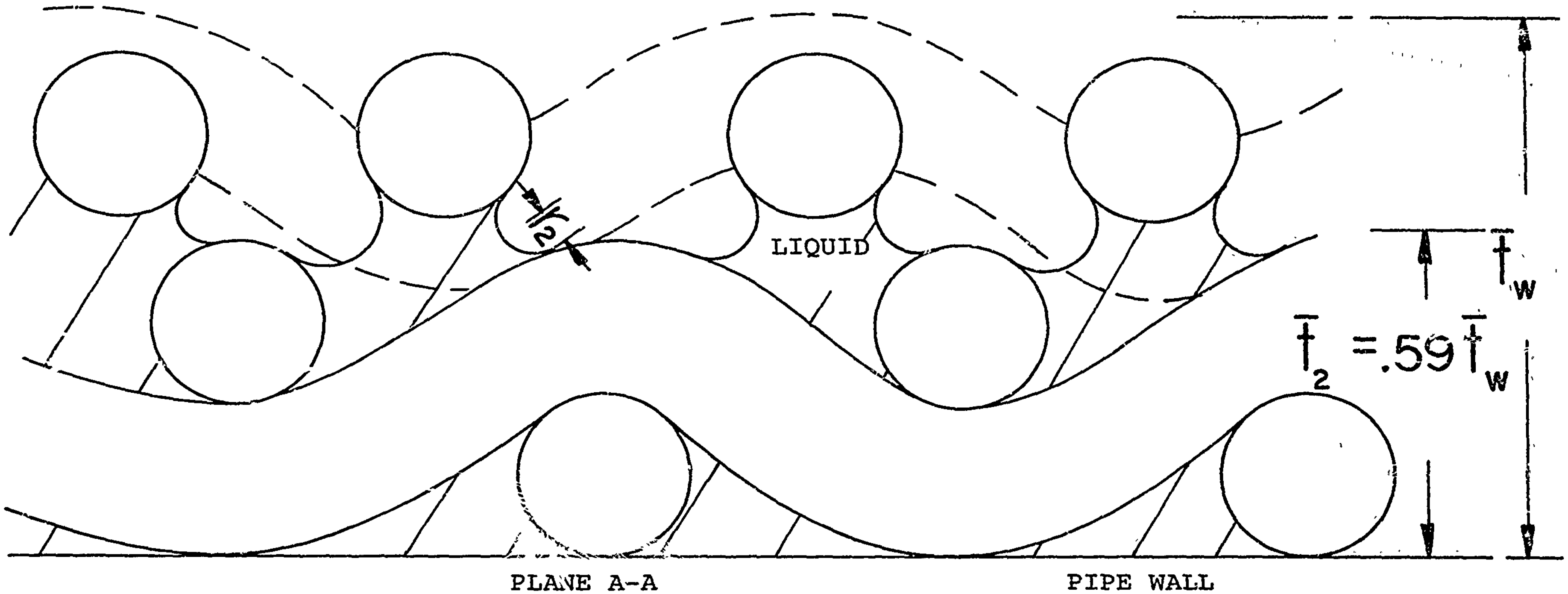

Figure 5.8. Two Layers of Screen Wick with Liquid Recessed to the Second Layer

In Figure 5.5, the simplified drawing of the intermeshing of the two layers shows that a smaller capillary radius exists at the interface of the two layers. Figures 5.6, 5.7, and 5.8 are detailed drawings of Figure 5.5. The mean thickness of a double layer of 100 mesh stainless steel was .0160 inches with a standard deviation of .00107 inches based on 72 readings. In Figure 5.6, the fully saturated wick is shown with a large capillary radius at the $\bar{t}_w$ level. In Figure 5.7, liquid is shown recessed to the first layer of wire mesh. This recessed level will be termed the first layer capillary pressure capability of the wick and, when the liquid-vapor interface recedes to that level, the fluid experiences a capillary force characteristic of the first layer. The distance from the wall of the first layer is called the recessed depth, $\bar{t}_1$, and is graphically determined from Figure 5.7. The graphical determination of $\bar{t}_1$ is performed by measuring the distance from the pipe wall to the hypothesized liquid level on a large cross sectional drawing of the wick. For the first layer, $\bar{t}_1$ is three fourths the thickness of the wick, $\bar{t}_w$, with the same standard deviation. Therefore, for a 100 mesh stainless steel wick, the liquid experiences a capillary force equivalent to the first layer capability at a distance .00120 inches from the wall with a standard deviation of .00107 inches. The first layer capillary pressure capability was determined experimentally and is tabulated in Tables 4.6 and 4.7 of Chapter 4.

If additional capillary force is required of the wick, the liquid level will receed to the configuration shown in Figure 5.8. The liquid-vapor interface has now encountered a smaller capillary radius, r_2. This configuration is termed the two layer capillary pressure capability, the data for this liquid level tabulated in Tables 4.6 and 4.7. The recessed depth of this level of recession, t_2, is again determined graphically and averages 59% of the wick thickness with the standard deviation of the wick thickness. For the 100 mesh stainless steel wick the liquid level will encounter a capillary pressure equal to the two layer capillary pressure capability .0094 inches from the wall of the heat pipe with a standard deviation of 00107 inches. If additional capillary force is required of the wick, no smaller r_e will be encountered during the recession and the wick will dry out.

To add to the information presented in Figures 4.7 and 4.8 we will refer to Figures 5.9 and 5.10 which are photographs of the wick structures tested in this work. The photograph of the 100 mesh two layer wick (12.5x) of Figure 5.9 shows the intermeshing of the two layers of wire mesh consistent with Figures 5.6 and 5.7. Figure 5.12 shows a top view of the intermeshing and illustrates how the high points of the lower layer tend to fill the openings of the top layer of wire mesh. Figure 5.11 is a sequential recession of fluid in a 100 mesh stainless steel two layer wick. High intensity lamps were used to observe the liquid vapor interface as it recedes. The liquid receded to a location between the two

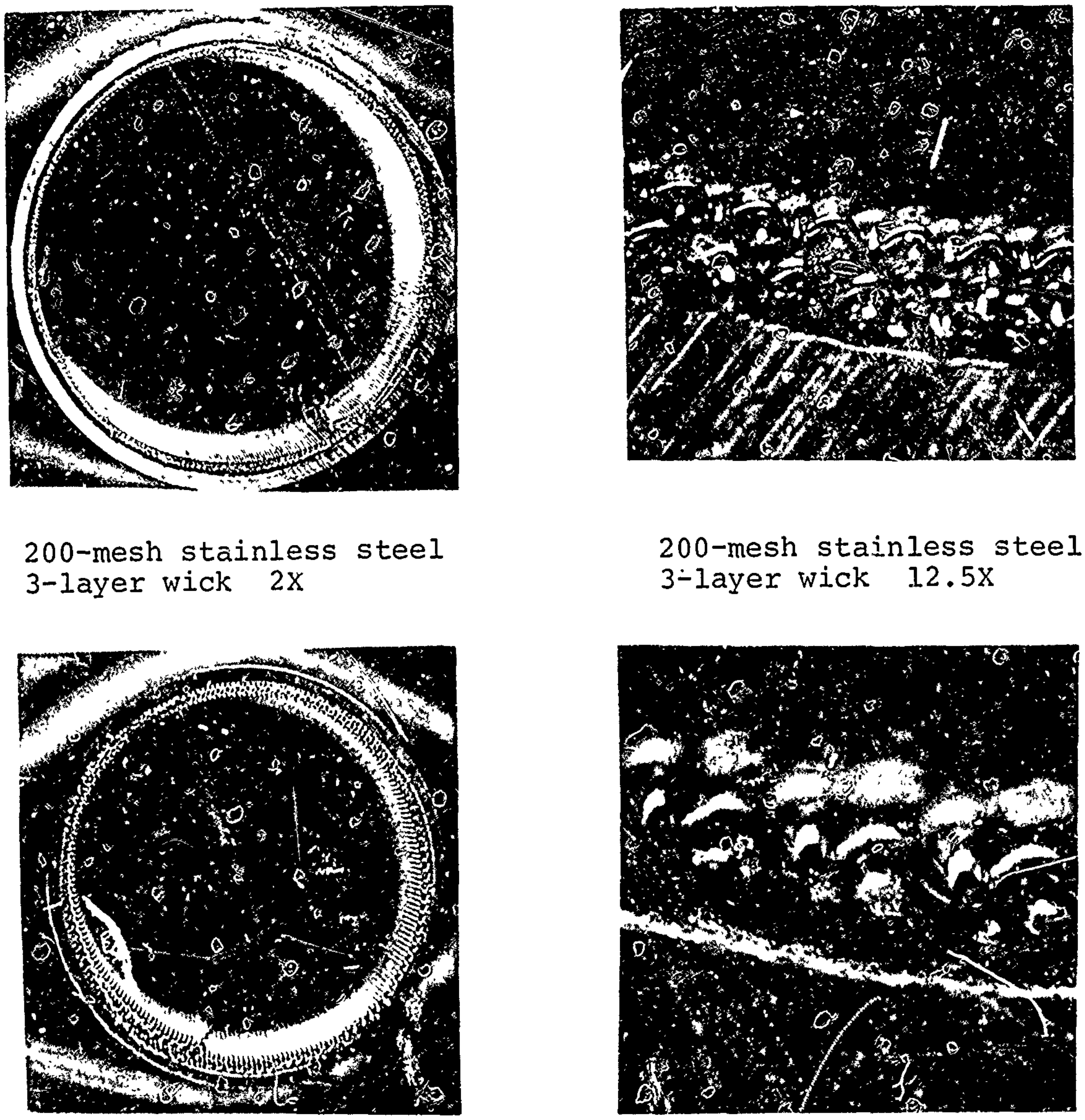

200-mesh stainless steel
3-layer wick 2X

200-mesh stainless steel
3-layer wick 12.5X

100-mesh stainless steel
2-layer wick 2X

100-mesh stainless steel
2-layer wick 12.5X

Figure 5.9. Wire mesh structures for 200- and 100-mesh stainless steel wicks

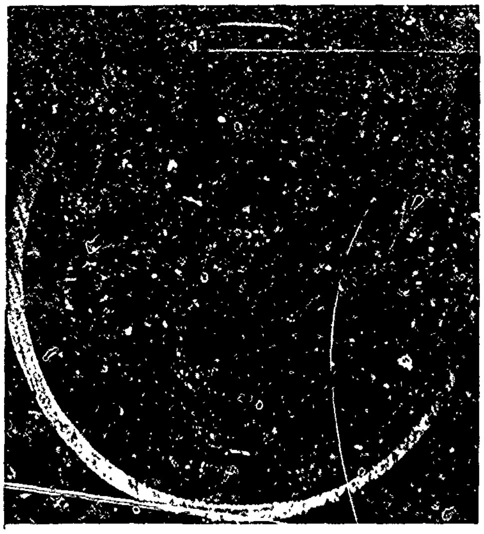

50-mesh stainless steel
2-layer wick 2X

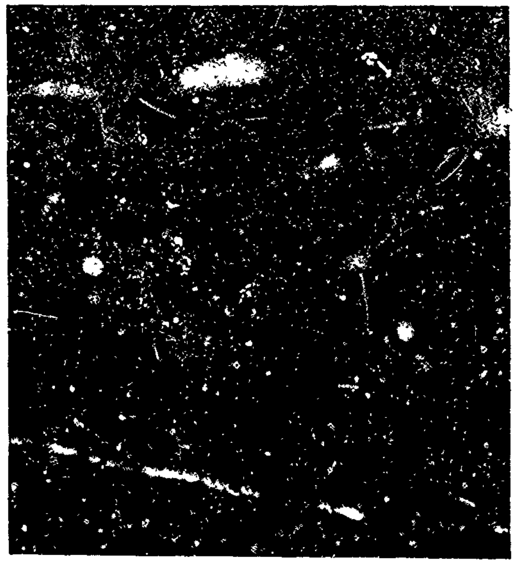

50-mesh stainless steel
2-layer wick 12.5X

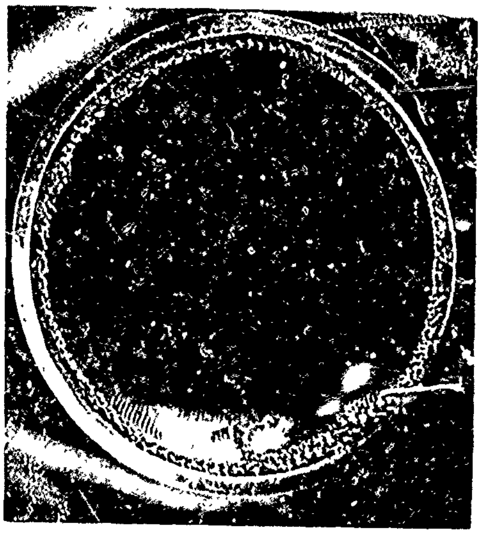

100-mesh copper
2-layer wick 2X

Figure 5.10. Wire mesh structures for 50-mesh stainless steel and 100-mesh copper wicks

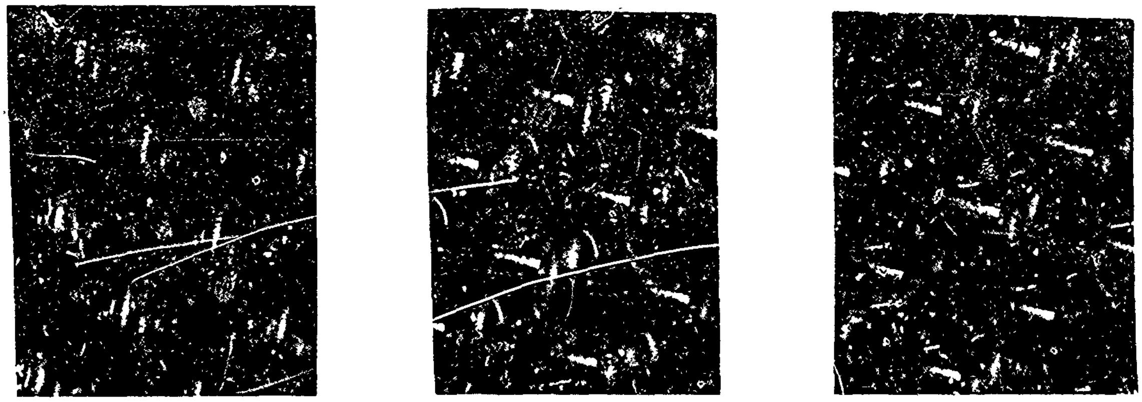

Fully saturated wick at low wattage

Wattage increased, recession begins

Recession Increases

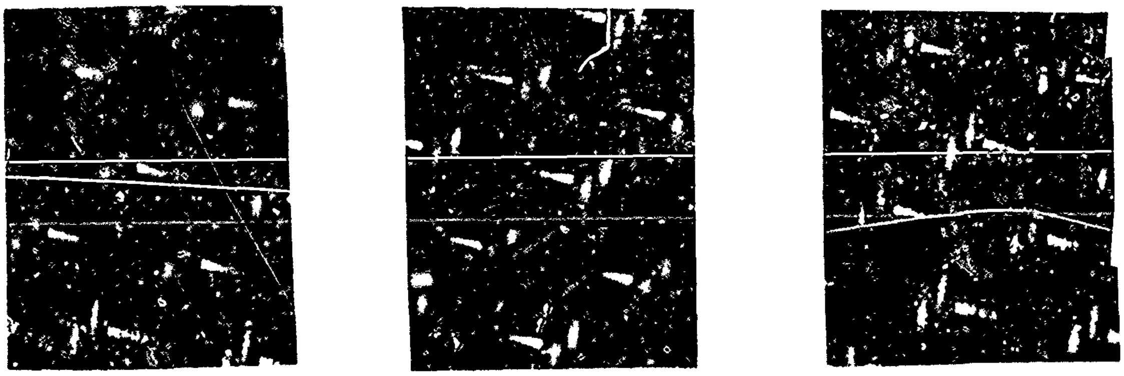

Liquid has recessed to minimum capillary radius

Burnout begins randomly

Wick function terminated at complete burnout

Figure 5.11. Sequential observation of liquid recession and final burnout for 100-mesh stainless steel 2-layer wick

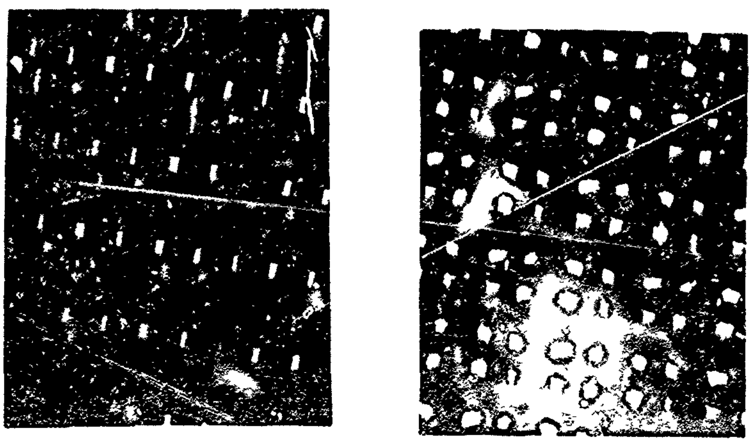

Figure 5.12. Comparison of Randon Intermeshing of Two Layers of 100-Mesh Stainless Steel Screen Compressed Together

layers where maximum capillary forces were encountered. When the heat transfer rate was increased further, the liquid-vapor interface receded to dry out. Maximum capillary forces were encountered at the interface of the two screen layers which is illustrated in Figure 5.8. Tables 4.6 and 4.7 of Chapter 4 indicate a significant capillary force difference between one and two layers of wire mesh.

Figure 5.14 shows the three possible configurations of the liquid-vapor interface that will be observed in this analysis. Figure 5.14 (a) shows the fully saturated wick with large capillary radii at the $\bar{t}_w$ level. The capillary pressure capability of this level is small and will be neglected. This configuration of the liquid vapor interface is assumed for the condenser and adiabatic sections of the heat pipe considered here.

The partially recessed configuration of Figure 5.14 (b), where the wick is saturated at a level where $\bar{t}_1 = .75\bar{t}_w$ is assumed to exist from $x = L_{fr}$ to $x = L_e$. The configuration of Figure 5.14 where the liquid is fully recessed to the level where $\bar{t}_2 = .59\bar{t}_w$ is assumed to exist from $x = 0$ to $x = L_{fr}$. The reason for this detailed analysis is to determine the actual saturation distribution as shown in Figure 5.13 (b), of the wick so that $L'(A)_r$ may be calculated. Now that the values of r_e at various levels are specified, we can calculate $L'(A)_r$ using Equation 2.52. Applying Equation 2.14 to the evaporator section of our heat pipe we obtain the expression for liquid pressure loss and

$$\Delta p_\ell = \frac{\mu_\ell}{K\rho_\ell} \int_0^{L_e} \frac{\dot{m}(x)}{A(x)} dx + \frac{\mu \dot{m}}{\rho K A} \left(L_a + \frac{L_c}{2} \right)$$

$$\begin{aligned} A_{fr} &= .59A && 0 \leq x \leq L_{fr} \\ A_r &= 3/4A && L_{fr} < x \leq L_e \qquad (5.1) \\ A &= A && L_e < x \leq L \end{aligned}$$

$$\dot{m}(x) = \dot{m} \frac{x}{L_e} \qquad 0 < x \leq L_e$$

$$\Delta p_r = \frac{\mu_\ell \dot{m}}{\rho_\ell} L'(A)_r$$

$$L'(A)_r = \left[\frac{2}{3} L_e + \frac{L_{fr}^2}{5.25 L_e} + La + \frac{L_c}{2} \right] \frac{1}{A} \qquad (5.2)$$

$L'(A)_r$ is the expression that accounts for the reduction of flow area due to recession. Equation 5.2 can now be used in conjunction with Equations 2.49, 2.53, and 5.1 in the iterative solution discussed in Chapter 2.

This concludes discussion of the deterministic recession model. Chapter 6 will outline computation techniques for the solution of Equation 2.52 using probabilistic techniques. The analysis presented in this chapter is considered valid for any size square weave wire mesh wrapped according to the procedure shown in Chapter 3. Although this particular analysis was done with two layer wicks, the effects of multiple layers (greater than two) could be incorporated into this analysis. For instance, this analysis was used successfully on a three layer 200 mesh wick assuming no recession into the third layer.

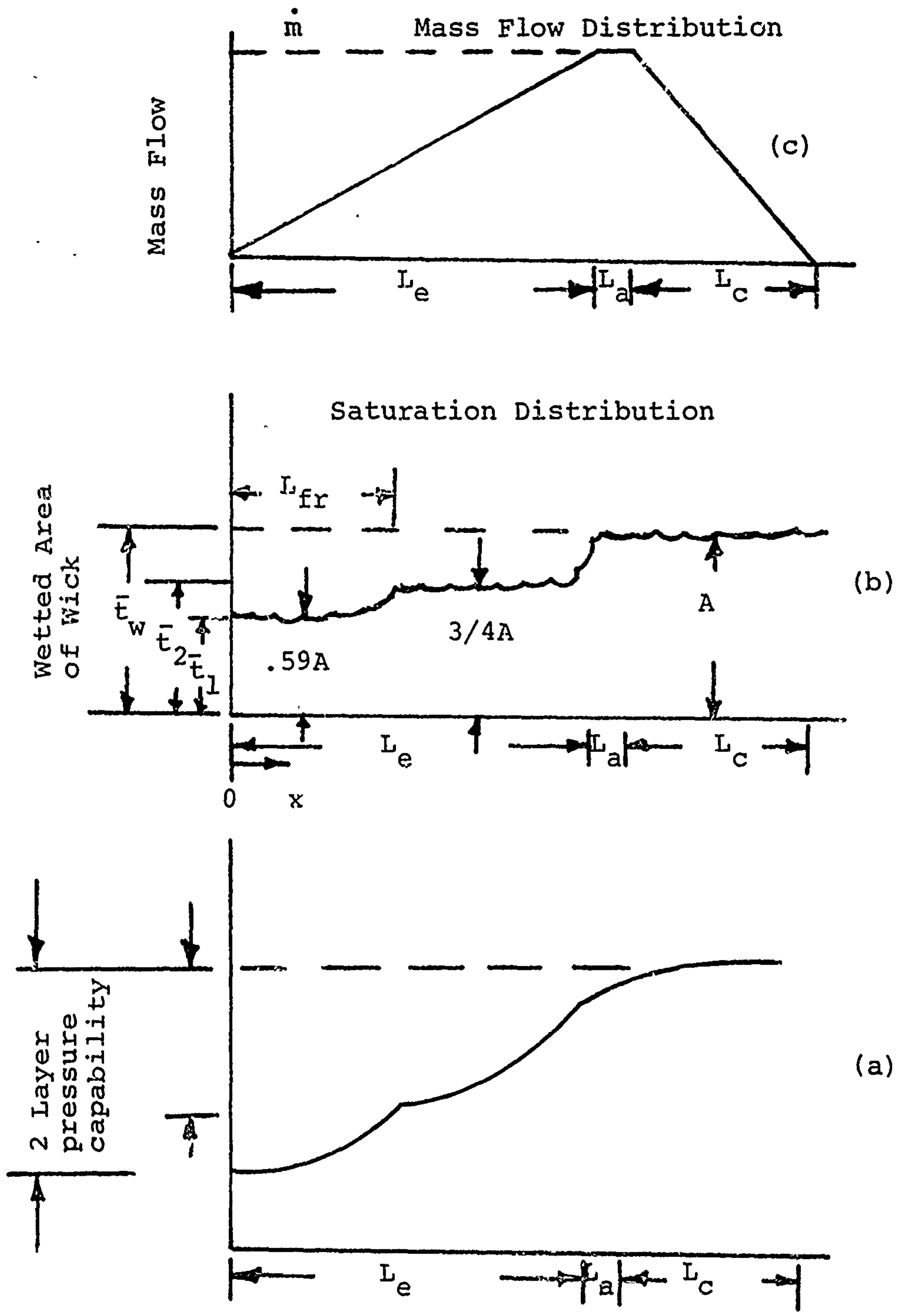

Figure 5.13. Hypothesized Recession Model for Two Layer Square Weave Wire Mesh Wicks

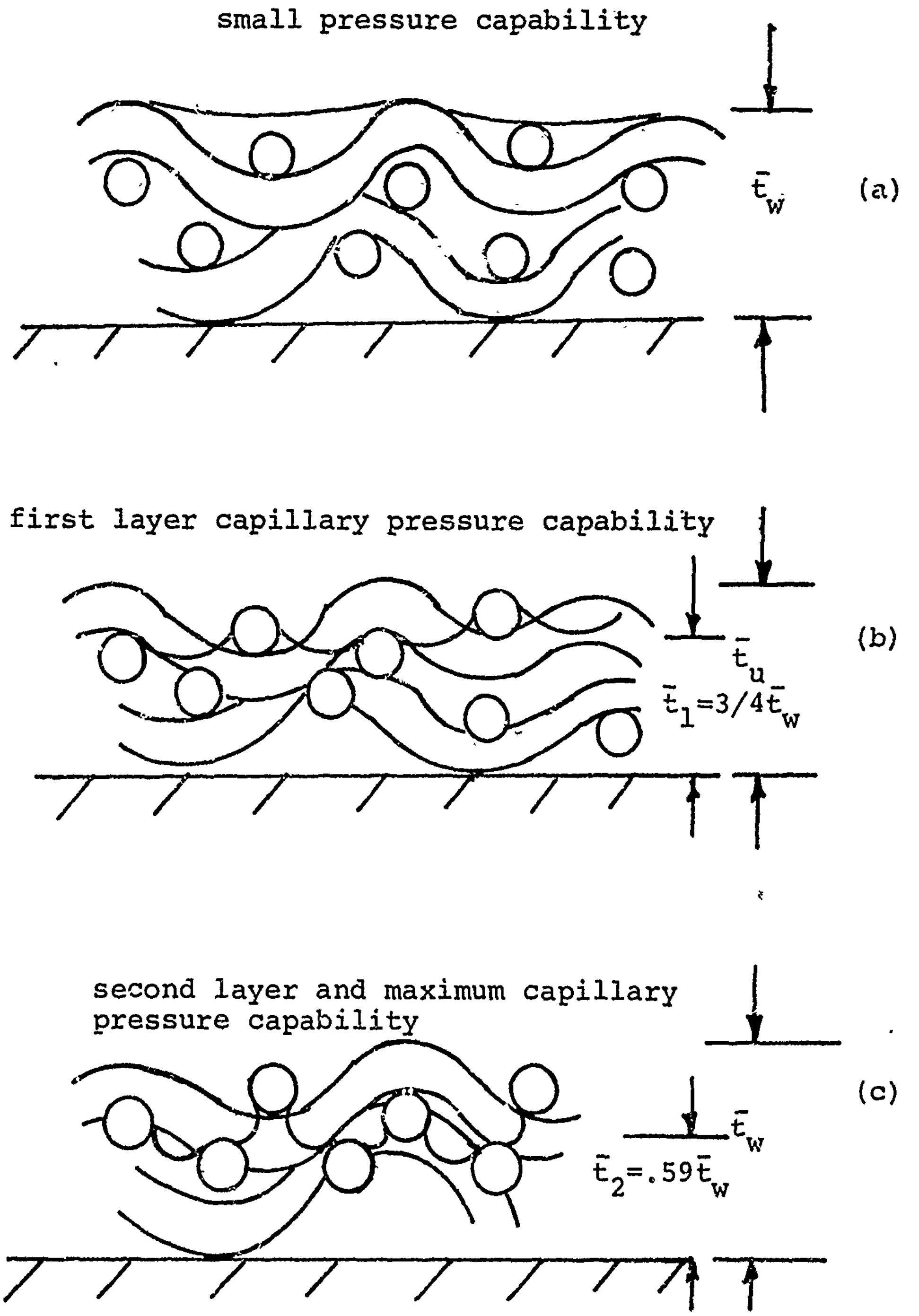

Figure 5.14. The Three Possible Configurations of the Liquid Vapor Interface in 100-Mesh Square Weave Wire Cloth

CHAPTER 6

COMPUTATIONAL METHODOLOGY

6.1 Methodology

In this chapter the foundation is developed for the solution of Equation 2.57, the probabilistic model of heat pipe operation. Simple deterministic equations are used as examples of the formulation of a probabilistic design model. The probabilistic model uses the basic equation structure of the deterministic model. Probabilistic methodology is applied to account for the variability in the deterministic model.

To illustrate the solution to the probabilistic design equation, simple mathematical models will be used.

Many physical phenomena may be described by mathematical models. A simple example is shown below.

$$Q_3 = Q_1 + Q_2 \tag{6.1}$$

Q = Flow Rate

Assuming that this deterministic model describes the physical phenomena adequately, we may form a probabilistic model by transforming the deterministic variables into random variables which are governed by some statistical distribution

$$(Q_3P_1, Q_3P_2, \ldots Q_3P_n) = (Q_1P_1, Q_1P_2, \ldots Q_1P_n) + (Q_2P_1, Q_2P_2, \ldots Q_2P_n)$$

Q_1, Q_2, Q_3 = Random variables

QP = Random variable distribution parameters

Q_1, Q_2 = Independent (6.2)

For our particular analysis, virtually all distributions of physical properties are two parameter. Therefore, the distribution is determined solely by the mean and standard deviation. We may now transform our general probabilistic model to that of simple two-parameter distributions and obtain

$$(\bar{Q}_3, S_{Q_3}) = (\bar{Q}_1, S_{Q_1}) + (Q_2, S_{Q_2}) \qquad (6.3)$$

where $(\bar{Q}, S_Q)$ is a random variate pair.

The reason for changing the deterministic variable to a random variable is that most physical variables may not be known precisely. If there is uncertainty in describing these input variables, there will be uncertainty in the functional result. Describing the uncertainty of the functional result may be the best way to describe the natural phenomenon.

There are three techniques for finding functional variability and they are discussed as follows:

a) Simulation: We will use the flow rate example to illustrate the procedure. We are given the following

$$Q_3 = Q_1 + Q_2 \qquad \begin{array}{l} Q_1 = \text{Flow Rate} \sim ZZ_1^*(\bar{Q}_1, S_{Q1}) \\ Q_2 = \text{Flow Rate} \sim ZZ_2(\bar{Q}_2(\bar{Q}_2, S_{Q2}) \end{array} \qquad (6.4)$$

This solution technique uses a random number generator to supply a ZZ_1 distributed flow rate, Q_1, and a ZZ_2 distributed flow rate, Q_2. These individual random numbers are inserted into the above equation and the random result, Q_3, is recorded. This procedure is repeated many times, and the Q_3 parameters and distribution can be determined using Equations 2.55 and 2.56 and a significance test.

* ZZ_1 designates a particular two parameter distribution such as the normal distribution.

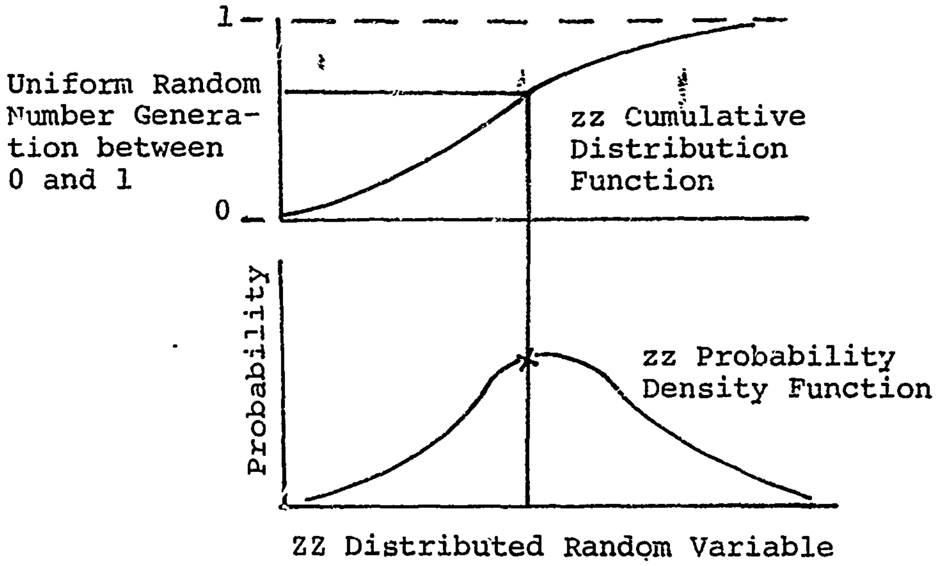

Figure 6.1. Simulation of Functional Variability

The simulation algorithm is as follows

Do down to and including 5, n times

Call ZZ_1 Distributed Random Q_1

Call ZZ_2 Distributed Random Q_2

Random Q_3 = Random Q_1 + Random Q_2

Store Random Q_3

5 Continue

Call Subroutine Parameter Estimation

Call Significance Test

End

From this technique we can determine the functional mean, variability (standard deviation) and distribution.

b) Partial Derivative Method: This method uses a Taylor approximation of functional variability and is derived in most elementary statistical texts. To find functional variability using this method we proceed as follows:

Given

$$F = f(x_1, x_2 \ldots x_n) \quad (6.5)$$

$$E(F) = \bar{F} = f(E(x_1), E(x_2) \ldots E(x_n)) \quad (6.6)$$

All X Independent

$$\bar{F} = f(\bar{x}_1, \bar{x}_2 \ldots \bar{x}_n) \quad (6.7)$$

(the mean function result is the computation of all the variables means in the given equation)

The functional variability (standard deviation) is derived from the Taylor approximation as,

$$S^2_F = \left(\frac{\partial F}{\partial x_1}\right)^2 \left(S_{x_1}\right)^2 + \left(\frac{\partial F}{\partial x_2}\right)^2 \left(S_{x_2}\right)^2 \ldots + \left(\frac{\partial F}{\partial x_n}\right)^2 \left(S_{x_n}\right)^2 \quad (6.8)$$

and for our example

$$\bar{Q}_3 = \bar{Q}_1 = \bar{Q}_2$$

$$SQ_3 = (S_{Q_1}^{\ 2} + S_{Q_2}^{\ 2})^{1/2}$$

Note that this method yields a good approximation of the functional mean and standard deviation but indicates nothing of the functional distribution.

c) Algebra of moments: This method uses the algebra of moments or expectations to determine functional variability exactly. Unfortunately, algebra of expectations becomes difficult when functions contain many random variables and powers of random variables. Because of this difficulty this method is used only on simple functions and these results are shown in Table 6.1.

TABLE 6.1

MEANS AND STANDARD DEVIATIONS FOR
SIMPLE FUNCTIONS USING ALGEBRA OF EXPECTATIONS

Function	Mean	Standard Deviation
$a=b+c$	$\bar{a}=\bar{b}+\bar{c}$	$S_a=(S_b{}^2+S_c{}^2)^{1/2}$
$a=b-c$	$\bar{a}=\bar{b}-\bar{c}$	$S_a=(S_b{}^2+S_c{}^2)^{1/2}$
$a=bc$	$\bar{a}=\bar{b}\bar{c}$	$S_a=(\bar{b}^2S_c{}^2+\bar{c}^2S_b{}^2+S_b{}^2S_c{}^2)^{1/2}$
$a=b/c$	$\bar{a}=\bar{b}/\bar{c}$	$S_a=\left[\frac{\bar{c}^2S_b{}^2+\bar{b}^2S_c{}^2}{\bar{c}^4}\right]^{1/2}$
$a=b^2$	$\bar{a}=\bar{b}^2$	$S_a=(4\bar{b}^2S_b{}^2+2S_b{}^4)^{1/2}$

b,c independent

The algebra of expections gives the functional mean and the standard deviation but does not indicate the functional distribution. For example, the algebra of expectations gives the following exact result which is incidentally the same as the partial derivative result.

$$\bar{Q}_3 = \bar{Q}_1 + \bar{Q}_2$$

$$S_{Q_3} = \left(S_{Q_1}{}^2 + S_{Q_2}{}^2\right)^{1/2}$$

Examples of Functional Uncertainty

The three sample functions we will investigate are*

1) $Q_3 = Q_1 + Q_2$

2) $A = B - C$

3) $V = Q/A$

The first function, $Q_1 + Q_2$, appears in Table 6.2. The standard deviation of the function was calculated using simulation, partial derivative and exact techniques at various standard deviations and sample sizes. Looking at the range of input variable standard deviations, one can conclude that this function is well behaved. The functional standard deviations are actually smaller, percentage wise, than the input variable standard deviations. Even at large input standard deviations this holds true and all techniques give the same resultant standard deviation.

The second function, $A = B - C$, is not so well behaved. Table 6.3 shows what can happen if the input variables, B & C, are nearly the same in magnitude with high standard deviations. This is the classic numerical problem of subtracting two numbers of almost equal magnitude. Notice that at moderate input standard deviations (say 9% of the input variable mean) the functional standard deviation grows to 225% of the functional result. The simulation mean becomes unstable at these high standard deviations as one might expect.

---

* The reason for choosing these simple functions is that they appear in many engineering applications and also form the basic structure of Equation 2.57.

TABLE 6.2

COMPARISON OF THE MEAN AND STANDARD DEVIATION OF THE FUNCTION XX* USING SIMULATION, PARTIAL DERIVATIVE AND ALGEBRA OF MOMENTS METHOD

Random Variable Standard Deviation (in % of Mean)	Simulation Mean	Simulation Stdv.	Sample Size	Partial Derviative & Algebra of Moments Method** Mean	Partial Derviative & Algebra of Moments Method** Stdv.
1	15.01294	0.133798	10	15.0000	0.118032
21	15.31819	2.133224	10	"	2.347870
41	14.96837	3.337952	10	"	4.583938
1	14.97922	0.110570	110	"	0.118032
21	14.95654	2.465327	110	"	2.347870
41	15.39133	4.378109	110	"	4.583938
1	15.00402	0.103209	160	"	0.118032
21	14.91508	2.317058	160	"	2.347870
41	14.86921	4.404308	160	"	4.583938

*($XX = Q_3 = Q_1 + Q_2$, $Q_1 \sim N(10, S_{Q_1})$ and $Q_2 \sim N(5, S_{Q_2})$)

**In this case the partial derivative and algebra of moments method are identical.

TABLE 6.3

STANDARD DEVIATION GROWTH OF THE FUNCTION YY* USING SIMULATION, PARTIAL DERIVATIVE AND ALGEBRA OF MOMENTS METHOD

Random Variable Standard Deviation (in % of mean)	Simulation			Partial Derivative & Algebra of Moments Method**	
	Mean	Stdv.	Sample Size	Mean	Stdv.
.1	50.0098	1.3278	300	50.00	1.3793
1	48.6319	15.3096	300	50.00	15.1724
2	51.6134	28.9453	300	50.00	28.9655
3	48.6156	43.4557	300	50.00	42.7586
4	47.0834	53.3973	300	50.00	56.5571
5	48.5659	70.2449	300	50.00	70.3448
6	53.0261	83.8806	300	50.00	70.9831
7	44.2171	99.3238	300	50.00	97.9310
8	51.4417	107.2407	300	50.00	111.7231
9	53.8297	131.5490	300	50.00	125.5173

*($YY = A = B - C$, $B \sim N(1000, S_b)$, $C \sim N(950, S_c)$)

** In this case the partial derivative and algebra of moments method are identical.

TABLE 6.4

COMPARISON OF THE MEAN AND STANDARD DEVIATION OF THE FUNCTION ZZ*
USING SIMULATION, PARTIAL DERIVATIVE AND ALGEBRA OF MOMENTS METHOD

Random Variable Standard Deviation (in % of Mean)	Simulation		Sample Size	Partial Derivative & Algebra of Moments Method**	
	Mean	Stdv.		Mean	Stdv.
1	2.0213	0.02155	10	2.00	0.028284
21	1.9888	0.53969	10	2.00	0.593695
41	2.4993	1.04819	10	2.00	1.159654
1	2.0034	0.02727	60	2.00	0.028284
21	2.0314	0.0218	60	2.00	0.593695
41	2.3744	1.48769	60	2.00	1.159654
1	1.9977	0.03412	110	2.00	0.028284
21	2.1942	0.80706	110	2.00	0.593695
41	2.4625	5.12479	110	2.00	1.159654

*(ZZ = Q/A, where $Q \sim N(10, S_q)$ and $A \sim N(5, S_a)$)

**In this case the partial derivative and algebra of moments method are identical.

The third function, $V = Q/A$, presents a problem when denominator random variables approach zero. Table 6.4 shows the standard deviation growth of this function. Notice that in this case the partial derivative and exact method diverge from the simulation method. The simulation is affected considerably by random choices of A near zero while the other techniques are not. This divergence may be a good indicator of numerical problems in this function.

The purpose of these examples is to point out the numerical problems associated with the computation of the functional standard deviation. Caution must be observed in this calculation since the physical phenomenon variability may differ, significantly, from the calculation.

6.2 Application to Heat Pipe Design

In the next several pages the three techniques are presented for finding functional variability as applied to Equation 2.57.

a) Simulation

The simulation technique is the most useful because the distribution of the heat transfer rate can be determined as well as the mean and variability. The mean heat transfer rate is

$$\bar{Q} = \sum_{i=1}^{n} \frac{q_i}{n} \quad \text{(estimate of mean heat transfer rate)} \qquad (6.9)$$

where

$$q_i = N_\ell \frac{(K_i)}{L'(A)_{r_i}} \left(\frac{2}{r_{fr_i}} - \frac{\rho_\ell g(\bar{H}_i)}{g_c \sigma} \right) \qquad (6.10)$$

$$N_\ell = \frac{\rho_\ell \sigma h_{fg}}{\mu_\ell}$$

The q_i values are obtained by randomly choosing a value for each of the random variables $(r_{fr}, H, K, A, L'(A)_r)$. The random values $(K_i, r_{fr_i}, H_i, A_i, L'(A)_{r_i})$ are chosen by entering the cumulative distribution functions of each of these parameters using a random number generation technique. The procedure for generating a random variable from a particular distribution is shown in Figure 6.1. The cumulative distribution functions are determined from experimental data using Equations 2.55 and 2.56. The estimate of the heat transfer rate standard deviation is obtained from Equation 2.56 and is rewritten in Equation 6.11.

$$S_Q = \sum_{i=1}^{n} \frac{(q_i - \bar{Q})^2}{n-1} \quad \text{estimate of variability (standard deviation)} \qquad (6.11)$$

The parent distribution of q_i is hypothesized using a goodness of fit test. This technique becomes accurate for large and moderate coefficients of variation.

b) Partial Derivative Method

The mean heat transfer rate is determined by introducing the means of the random variables into the deterministic design equation and solving for $\bar{Q}$.

$$\bar{Q} = N_\ell \frac{\bar{K}}{\bar{L}'(A)_{\bar{r}}} \left(\frac{2}{\bar{r}_{fr}} - \frac{\rho_\ell g(\bar{H})}{g_c \sigma}\right) \quad (6.12)$$

The standard deviation is given by an approximation using a Taylor expansion

$$F = Fx_1, X_2, \ldots x_n)$$

$$S_F = \left(\frac{\partial f}{\partial x_1}\right)^2 \left(S_{x_1}\right)^2 + \left(\frac{\partial f}{\partial x_2}\right)^2 \left(S_{x_2}\right)^2 \cdots \left(\frac{\partial f}{\partial x_n}\right)^2 \left(S_{x_n}\right)^2 \quad (6.13)$$

and in our case

$$S_q = \left(\frac{\partial \bar{Q}}{\partial \bar{K}}\right)^2 S_k{}^2 + \left(\frac{\partial \bar{Q}}{\partial r_{fr}}\right)^2 \left(S_{r_{fr}}\right)^2 + \left(\frac{\partial \bar{Q}}{\partial \bar{H}}\right)^2 \left(S_H\right)^2 + \left(\frac{\partial \bar{Q}}{\partial \bar{L}'(A)_r}\right)^2 \left(S_{L'(A)_r}\right)^2 \quad (6.14)$$

The distribution of Q cannot be determined through significance tests and must be assumed or calculated in closed form.

c) Algebra of Moments

This technique, introduced by Haugen,[1] is an exact technique for determining $\bar{Q}, S_q$. The mean is calculated as in the partial derivative method

$$\bar{Q} = N_\ell \frac{\bar{K}}{\bar{L}'(A)_r} \left(\frac{2}{\bar{r}_{fr}} - \frac{\rho_\ell g(\bar{H})}{g_c \sigma}\right) \quad (6.15)$$

(all random variables are independent)

The standard deviation is formulated using algebra of the first and second moments. For the functions

$$Z_1 = XY$$

$$S_{Z_1} = \sqrt{\bar{X}^2 S_y + \bar{Y}^2 S_x^{\ 2} + S_x^{\ 2} S_y^{\ 2}}$$

$$Z_2 = X - Y$$

$$S_{Z_2} = \sqrt{S_x^{\ 2} + S_y^{\ 2}}$$

These formulae may be used in succession to obtain S_q. The distribution is determined in the same way as the partial derivative method.

The computer program block diagram is shown in Figure 6.1, and the actual listing appears in the appendix. The computer program is simply the iteration procedure mentioned in Chapter 2 using the three solution techniques of this chapter.

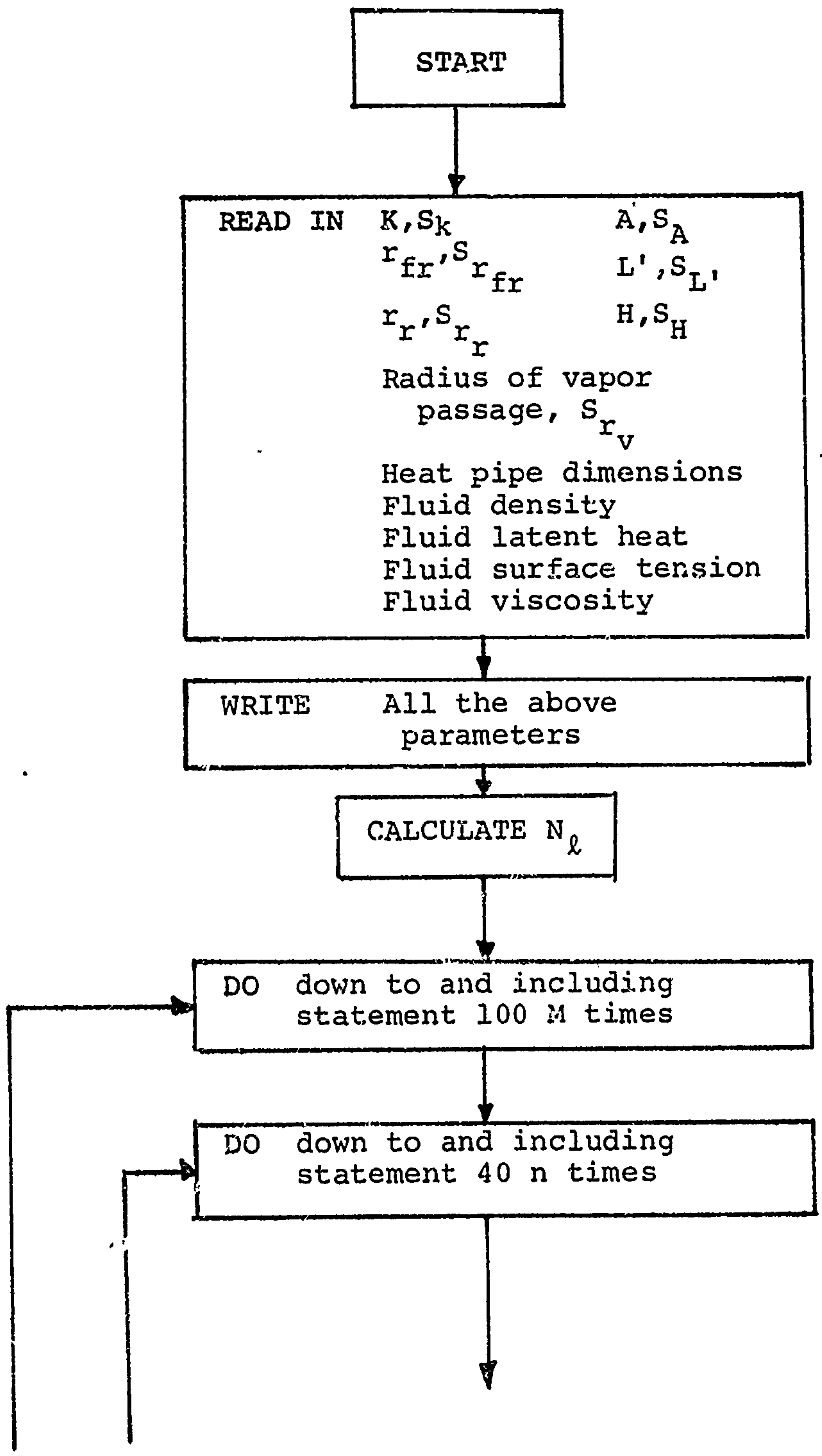

Figure 6.2. Computer Program Flow Diagram

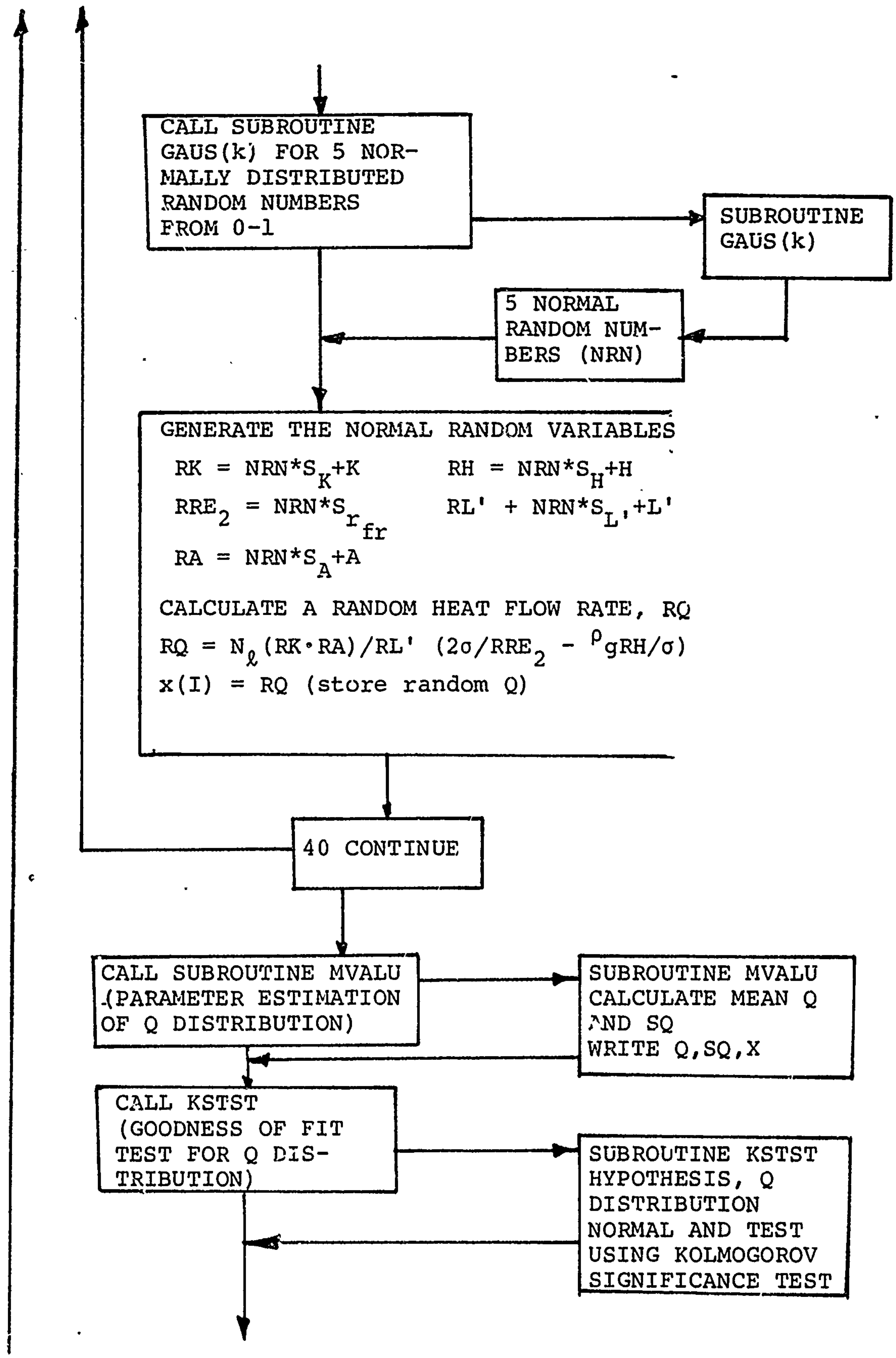

Figure 6.2. (continued)

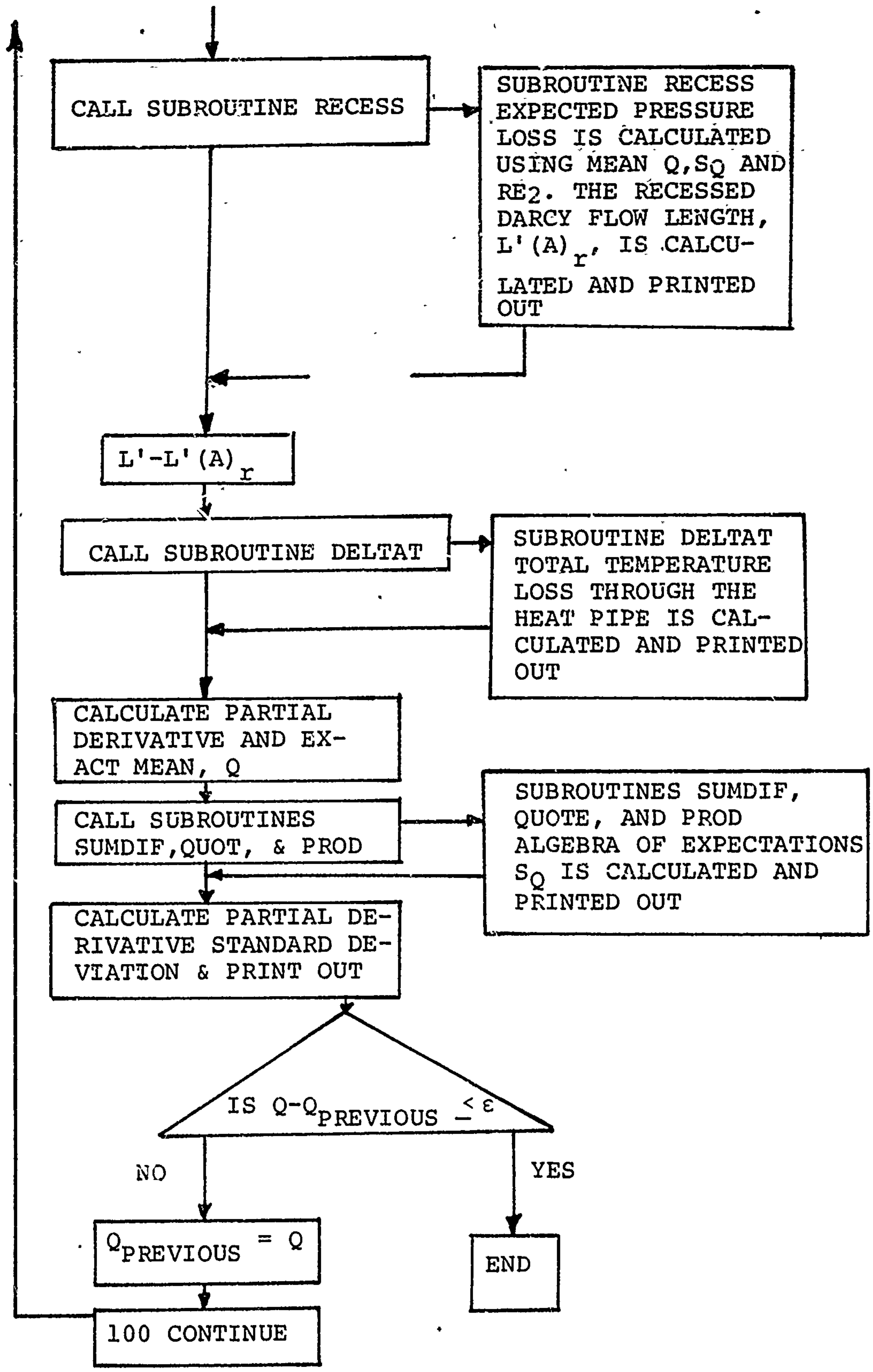

Figure 6.2. (continued)

CHAPTER 7

THE PROBABILISTIC DESIGN EQUATION

The probabilistic model was mentioned in Chapter 5 and is written below for the recessed condition

$$(\bar{A}S_Q) = N_\ell \frac{(\bar{K},S_k)}{(\bar{L}'(A)_r,S_{L'(A)_r})} \left(\frac{2}{(\bar{r}_{fr},S_{r_{fr}})} - \frac{\rho_\ell}{g_c} \frac{g(\bar{H},S_H)}{\sigma} \right) \tag{7.1}$$

The assumptions are the same as the deterministic equation with the addition of the following:

a) A, K, r_{fr}, $L'(A)_r$ and H are random variables and are described by simple two parameter continuous distributions.

b) Variabilities of all other parameters are considered small and are therefore deterministic

c) All random variables are independent

d) Coefficients of variation $(\bar{x}/s_x)$ are large (>7) for denominator random variables.

7.1 Comparison of Probabilistic Model with Experimental Data

To test the validity of the probabilistic model, fifty heat pipe wicks were manufactured, tested, and their properties recorded in the Appendix and analyzed in Chapter 5. The following analysis will examine data set 2 in detail since this data set is composed of thirty tests and carries the most significance. The analysis for the other data sets are identical and will be mentioned throughout the discussion. For each of the fifty heat pipe wicks tested, K, A, L', and r_{fr} were recorded. A steady state heat transfer rate was established and the evaporator section was raised until the wick began to dry out. The steady-state maximum heat transfer rate, Q_{ob}, was recorded along with the gravity effect, H, at dry out. The experimental values of K, A, L', r_{fr}, and H were inserted into the recession design equation, Equation 2.57, and Q_{ca} was calculated. The deviation of the observed experimental mean heat transfer rate from the calculated mean heat transfer rate, $Q_{co} - Q_{ob}$, was calculated for each test. Table 7.1 shows the mean and standard deviation of $Q_{ca} - Q_{ob}$. The mean difference, $Q_{ca} - Q_{ob}$, was small in all cases when compared to the standard deviation. We will test this hypothesis using the following Student's T Statistic,[17]

$$T_{calc.} = \frac{|\bar{D}|(n)^{1/2}}{S_{\bar{D}}} \sim T\ \alpha/2\ (n-1) \qquad (7.2)$$

$$\bar{D} = \sum_{i=1}^{n} \frac{Q_{ca_i} - Q_{ob_i}}{n}$$

If the calculated T value, Tcalc., is less than the critical T value at the $\alpha = .005$ significance level, we will accept the hypothesis that there is no significant difference between Q_{cz} and Q_{ob}. Table 7.1 shows the results of the hypothesis test. At every heat transfer rate, the mean observed heat transfer rate was not significantly different from the mean calculated heat transfer rate. This indicates that Equation 2.57 is a good predictor of the mean heat transfer rate. Figures 7.7 through 7.11 show plots of the data from Table 7.2 and a comparison of the mean maximum calculated heat transfer rate with experimental data for each of the data sets. Figures 7.1 through 7.3 show the distribution of $Q_{ca} - Q_{ob}$, which is called the difference distribution. Appendix A shows values of Q_{ca} and $S_{Q_{ca}}$ for all the heat pipes tested.

TABLE 7.1

COMPARISON OF OBSERVED AND CALCULATED DATA

Mean Wattage Level	Data Set	Mean $Q_{ca}-Q_{ob}$ (watts)	Stdv. $Q_{ca}-Q_{ob}$ (watts)	Sample Size	T Cal.	T(005) Crit.	Does $Q_{ca}=Q_{ob}$
49.199	1	- 3.399	6.269	5	1.21	4.604	yes
80.399	1	2.599	12.177	5	0.47	4.604	yes
110.399	1	10.199	19.524	5	1.15	4.604	yes
50.566	2	- 2.608	6.719	30	2.13	2.750	yes
81.333	2	4.833	14.459	30	1.83	2.750	yes
116.799	2	5.466	18.552	30	1.62	2.750	yes
25.799	3	- 1.000	4.183	5	0.54	4.604	yes
76.599	3	9.799	10.986	5	1.98	4.604	yes
55.000	4	-11.400	18.215	5	1.39	4.604	yes
121.22	4	0.399	23.319	5	0.39	4.604	yes
56.302	5	- 0.199	12.072	5	0.038	4.604	yes
102.700	5	- 3.000	14.159	5	0.48	4.604	yes

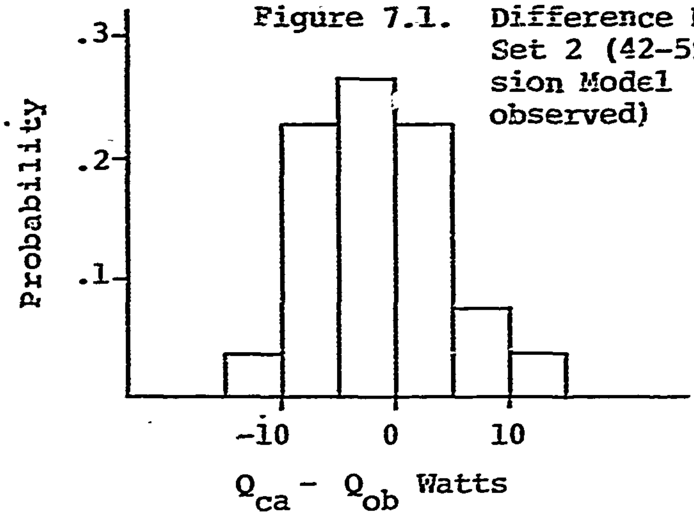

Figure 7.1. Difference Distribution for Data Set 2 (42-59 watts) Using Recession Model (Q calculated minus Q observed)

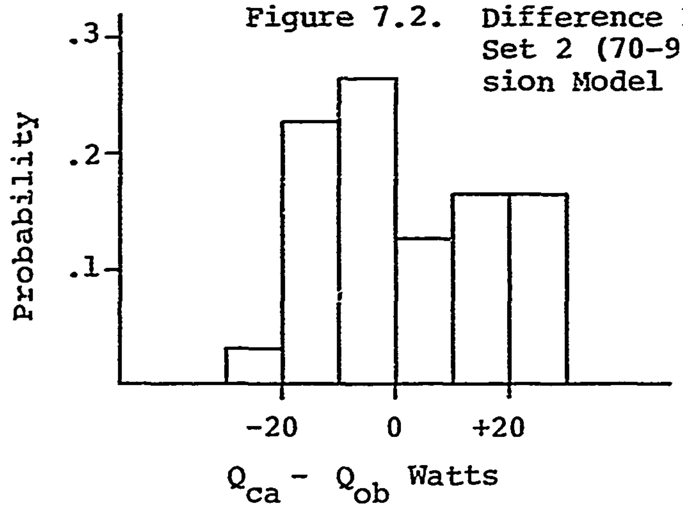

Figure 7.2. Difference Distribution for Data Set 2 (70-90 watts) Using Recession Model

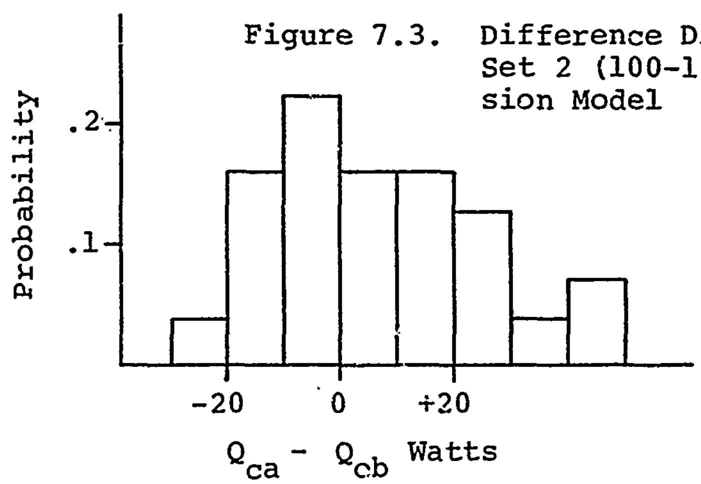

Figure 7.3. Difference Distribution for Data Set 2 (100-130 watts) Using Recession Model

These values were calculated from Equation 2.57 using the simulation technique. 200 random variables were calculated for each simulation and the resultant Q_{ca} distribution did not reject the Kolmogorov Smirnov significance test at 99% significance. The distribution of Q_{ca} was hypothesized as normal. The uncertainty bound on the predicted heat transfer rates for each pipe will be plus or minus three standard deviations from the mean since these limits will encompass 99.7% of the Q_{ca} Normally distributed random variables. If the observed heat transfer rate lies in this region of plus or minus three standard deviations of Q_{ca}, the probabilistic design equation is credited as having predicted the occurrence of the experimental result, Q_{ob}. If Q_{ob} falls outside the three standard deviation bounds, the probabilistic design equation will be considered inadequate in the prediction of the occurrence of Q_{ob}. Referring to the data of Appendix B, each of the 135 observed heat transfer rates, Q_{ob}, were within the three standard deviations of Q_{ca}. If we assume that the three standard deviation bound on the variability of the calculated heat transfer rate to be correct, then the probability of observing Q_{ob} within these bounds will be .9972. From 135 tests, all the observed heat transfer rates were within these bounds. The probability of observing 135 observed heat transfer rates within the three standard deviation bound and 0 outside the bound is $(.9972)^{135}$ or .668. This indicates a high probability that the calculated variability of the observed heat transfer rate, S_q, is correct

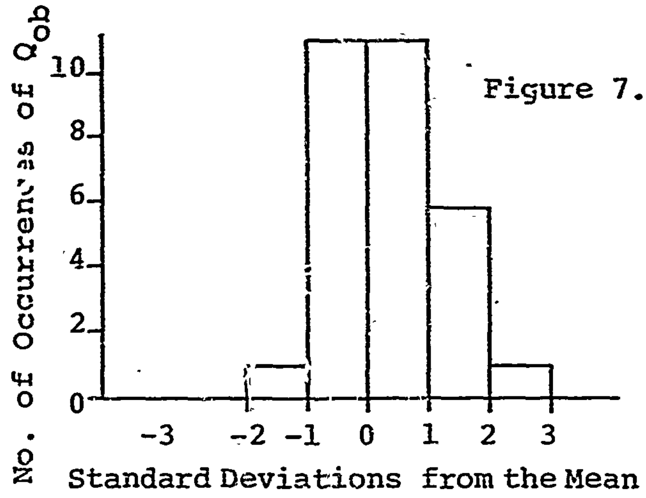

Figure 7.4. Distribution of Q_{ca} about Q_{ob} for 100-Mesh Stainless Steel, Two Layer Wicks at a Mean Wattage of 50.566

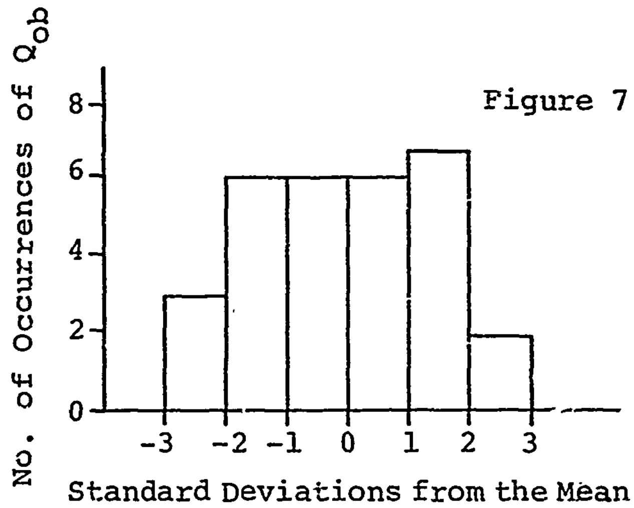

Figure 7.5. Distribution of Q_{ob} about Q_{ca} for 100-Mesh Stainless Steel, Two Layer Wicks at a Mean Wattage of 81.333

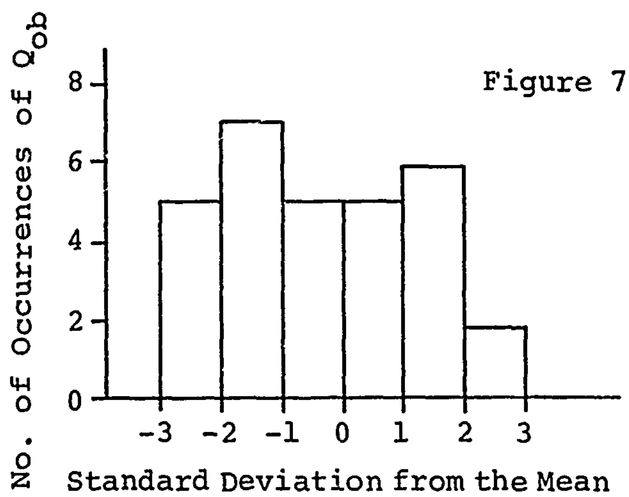

Figure 7.6. Distribution of Q_{ob} about Q_{ca} for 100-Mesh Stainless Steel, Two Layer Wicks at a Mean Wattage of 116.799

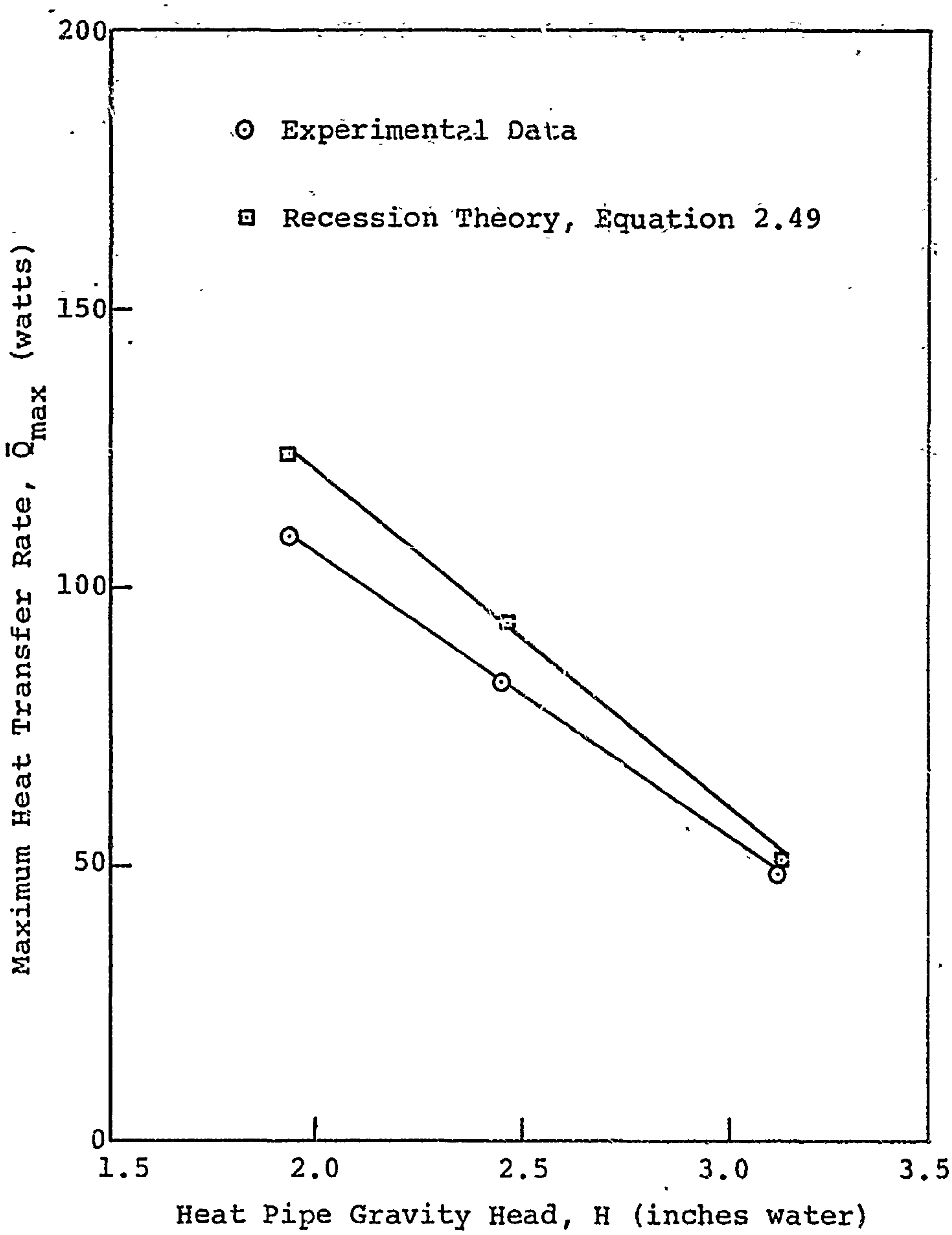

Figure 7.7. Comparison of the Mean, Maximum Heat Transfer Rate with Experimental Data from Data Set 1 (100 mesh stainless steel two layer wicks, tight wrap)

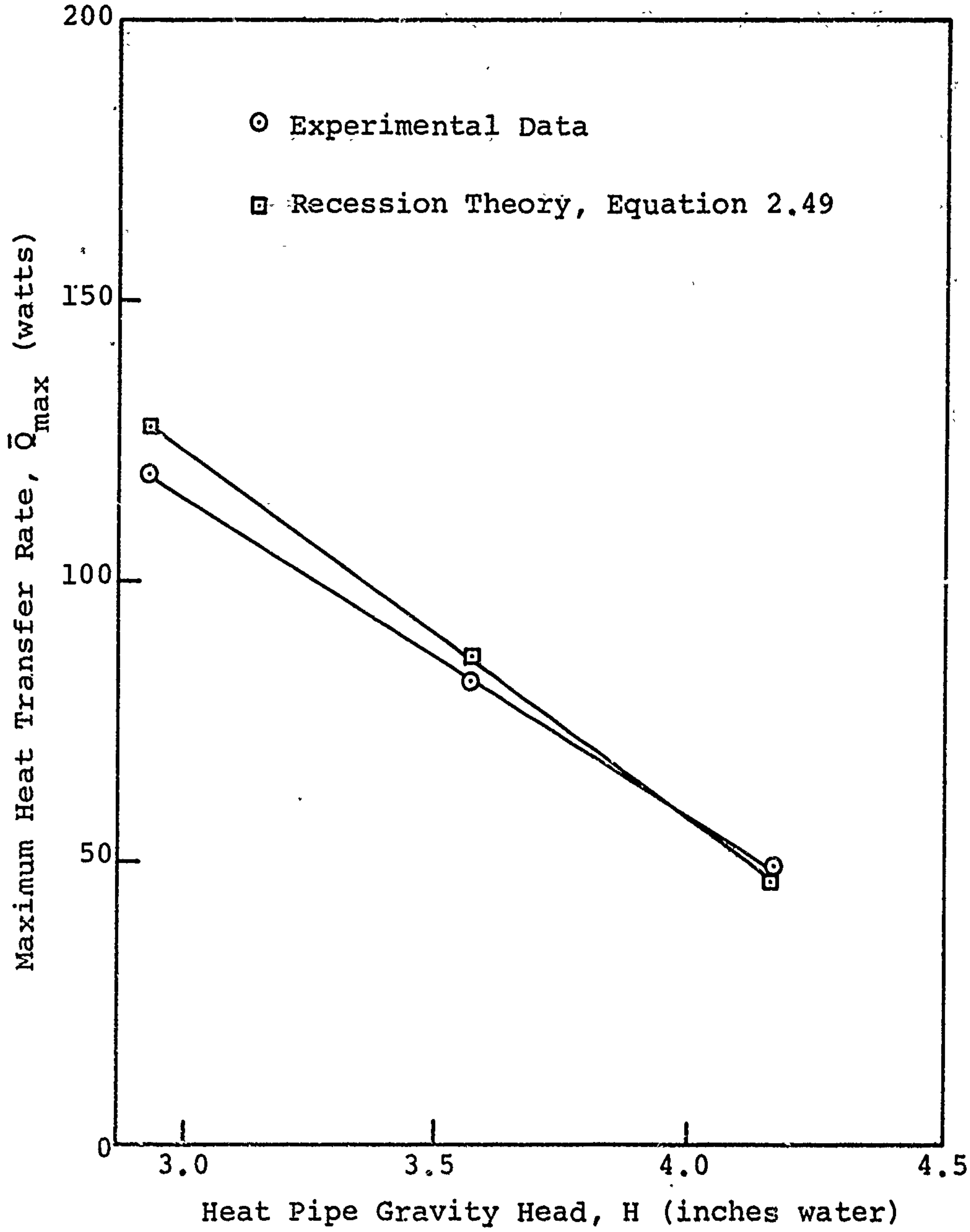

Figure 7.8. Comparison of the Mean, Maximum Heat Transfer Rate with Experimental Data from Data Set 2 (100 mesh stainless steel two layer wicks)

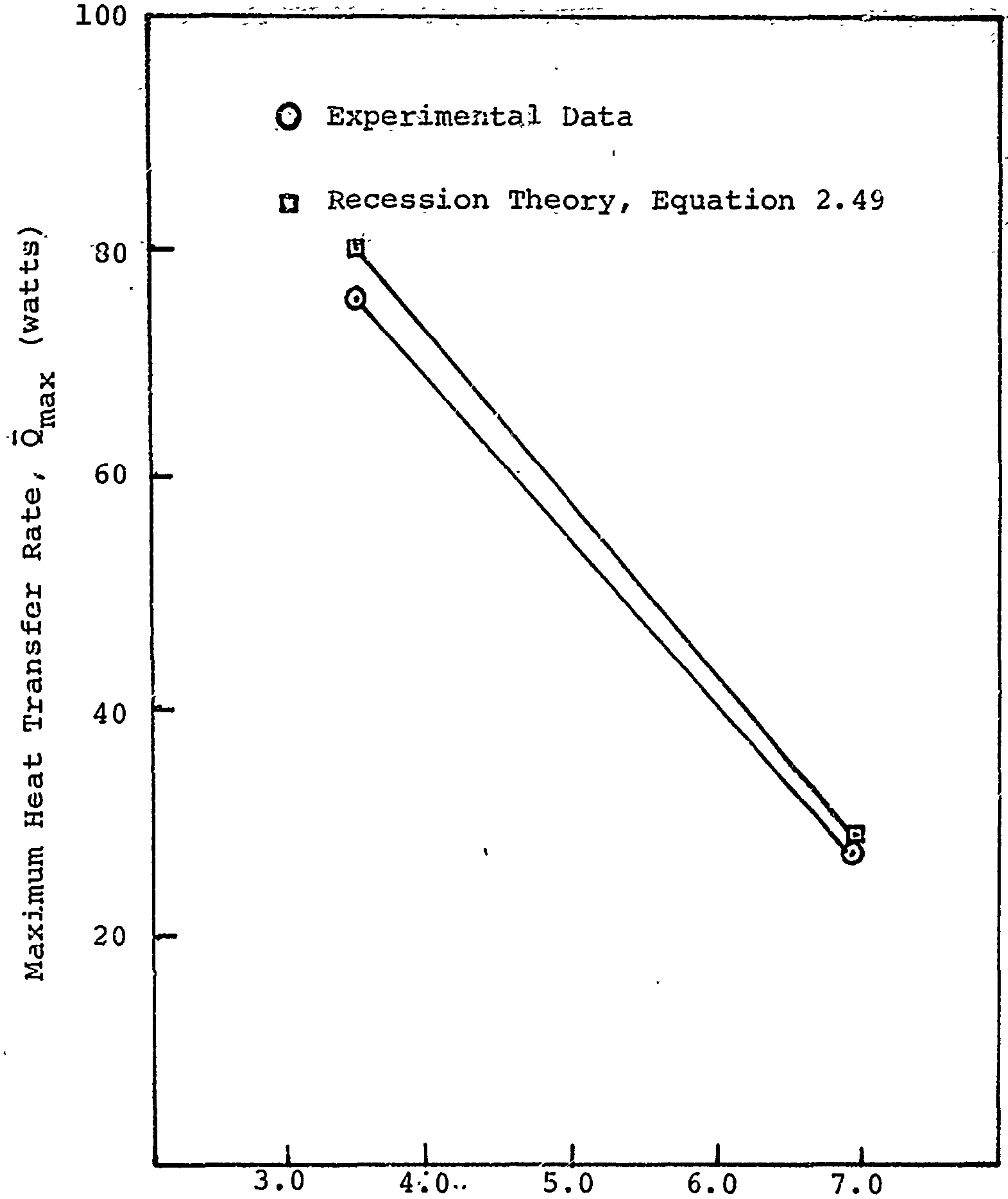

Figure 7.9. Comparison of the Mean, Maximum Heat Transfer Rate with Experimental Data from Data Set 3 (200 mesh stainless steel 3 layer wicks)

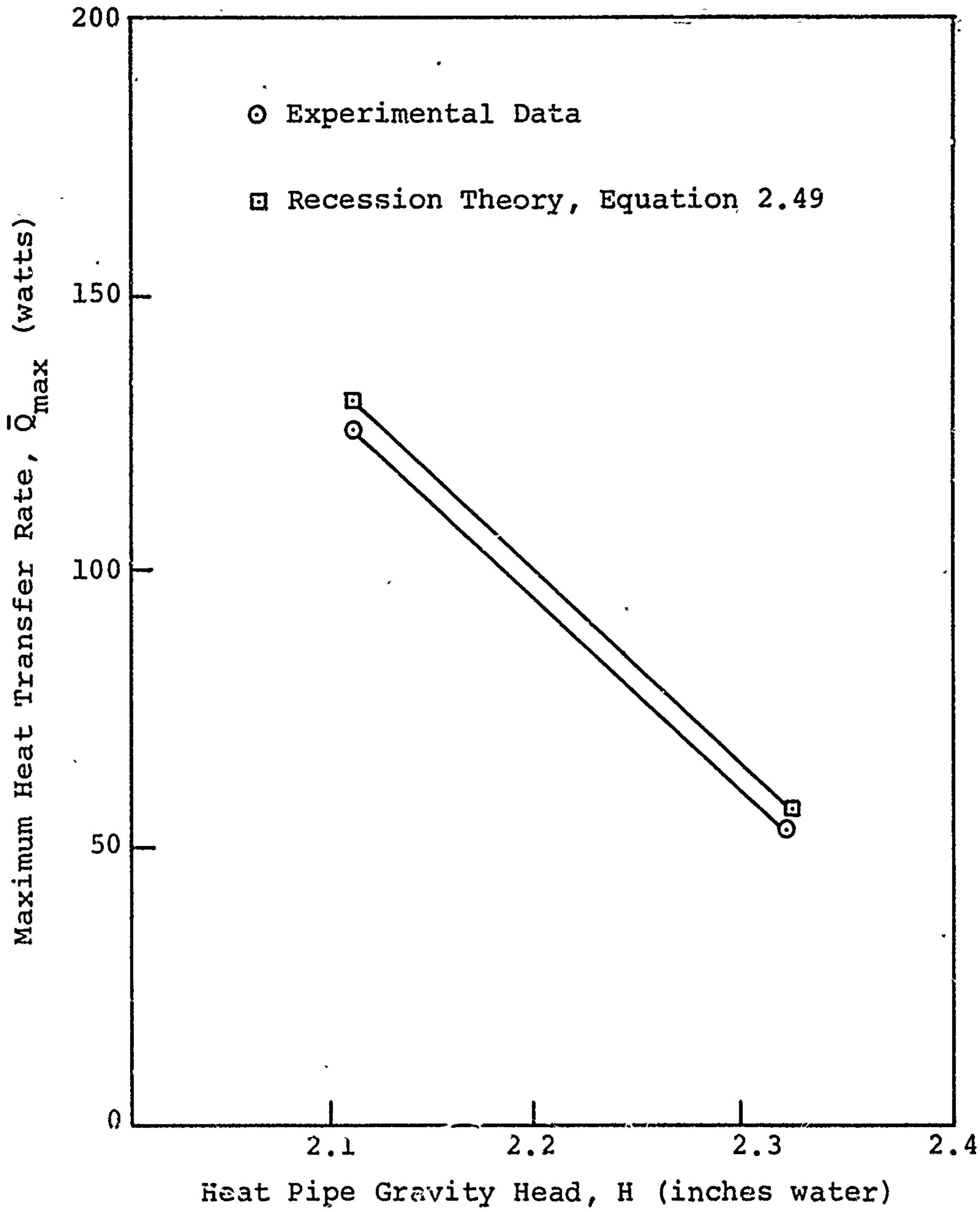

Figure 7.10. Comparison of the Mean, Maximum Heat Transfer Rate with Experimental Data from Data Set 4 (50-mesh stainless steel two layer wicks)

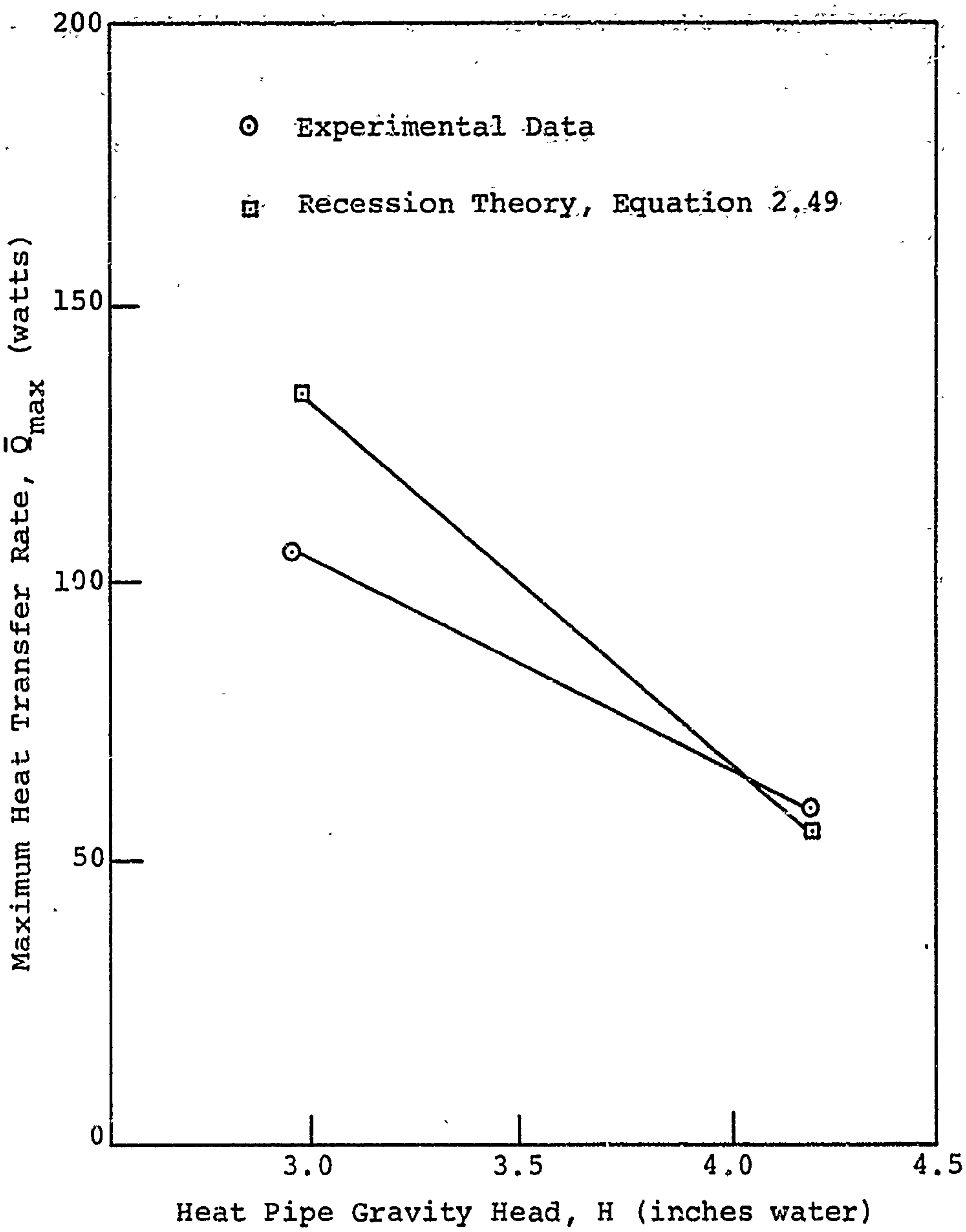

Figure 7.11 Comparison of the Mean, Maximum Heat Transfer Rate with Experimental Data from Data Set 5 (100-mesh copper two layer wick)

according to data from 135 tests. Figures 7.4, 7.5, and 7.6 show the distribution of the observed heat transfer rate, Q_{ob}, about the mean calculated heat transfer rate, Q_{ca} for data set 2. The distribution of Figure 7.4 did not reject the Komogrov-Smirnov significance test when tested for Normality and neither did the distributions of Figures 7.5 and 7.6. However, as heat transfer rate increased, the occurrence of Q_{ob} appeared more likely at the tails of the distributions and the resulting distributions became flatter than expected.

The consistency of predicting the range of occurrence of Q_{ob} using Equation 2.56 is evident. However, some basic numerical problems may result in applications to low heat transfer rates at high gravity effect and also to low heat transfer rates at high permeabilities. Upon examination of our mathematical model below, we can readily see how problems

$$Q = N_\ell \frac{K}{L'(A)_r}\left(\frac{2}{r_{fr}} - \frac{\rho_\ell g H}{g_c \sigma}\right)$$

arise. Shown below are two sample calculations using data from data set 2. One calculation has a high gravity head

$$Q = N_\ell \frac{K}{L'(A)_r}\left(\frac{24.}{4.069 \times 10^{-3}} - \frac{62.4\ (2.96)}{4.4 \times 10^{-3}(12)}\right) \text{(Low Gravity Loss)} \quad (7.3)$$

$$Q = N_\ell \frac{K}{L'(A)_r}\ (5900 - 3500)$$

$$Q = N_\ell \frac{K}{L'(A)_r}\left(5900 - \frac{62.4\ (4.21)}{4.4 \times 10^{-3}(12)}\right) \text{(High Gravity Loss)} \quad (7.4)$$

$$= N_\ell \frac{K}{L'(A)_r}\ (5900 - 5000)$$

loss while the other has a low gravity loss. Notice at the high gravity head loss the subtraction of the two rather large numbers. This shows the classic numerical problem of loss of significance when subtracting two nearly identical numbers. Such a problem was discussed in Chapter 6 and if one refers to Table 6.3 of Chapter 6 the sensitivity of this computation to error at relatively small standard deviations can be realized. Input standard deviations for the surface tension term are on the order of 5% and the gravity terms are approximately 1%. As shown on the previous page, these particular values of standard deviation lead to problems at low heat flow since the surface tension and gravity terms are on the order of magnitude of 5000. If one refers to Chapter 6, Table 6.3, we can observe a reliable prediction of the mean of the difference function. Despite the high resultant standard deviation, the error in the mean (calculated by simulation) is small in comparison (about 10%). We may conclude that although low heat flow (near wick dry out) standard deviation calculations may be unreliable, the mean heat flow calculation is quite good as indicated by the data discussed earlier in this chapter. If calculations must be made in the low heat flux range (less than 50 watts and near burn out), the resultant calculated standard deviations of heat flow will probably be conservative. Another numerical problem results at high permeabilities and low critical heat transfer rates. This is exemplified in data set 4 of the appendix (50 mesh stainless steel wicks). The permeability was large and the capillary pumping term was small resulting in a loss of significance in the difference term.

This resulted in extremely large calculations of standard deviation and seemed too conservative as indicated by the data.

We have been examining the prediction of heat transfer rate knowing the properties of the particular wick tested. If one wishes to design a heat pipe using the manufacturing technique of Chapter 3, then the wick properties of Table 4.23 should be used. These property values give the range of occurrence of wick properties for a particular heat pipe manufactured. Table 7.2 shows the mean calculated wattage and standard deviation at various values of H, using the three techniques mentioned in Chapter 6. The wattage values of Table 7.2 give the range of maximum heat transfer rate one might expect if a heat pipe was designed and operated at the particular gravity effect, H. Notice that the calculated standard deviations are quite high due to the high standard deviations of the input properties of Table 4.23. The three techniques used to solve the probabilistic design equation were quite close. The simulated results were slightly higher than the rest due to high variability in the denominator random variables. Now that the variability of the manufacturing process has been described, its applicability to design will be discussed.

7.2 Results of the Probabilistic Design

Assume that our design specification required that a particular heat pipe of this design operate at 75 watts at a gravity head of 2.96" H_2O. Referring to data set 2, the results of the probabilistic model (H = 2.96" H_2O) yields

Mean heat flow 125.707 watts

TABLE 7.2

THE OVERALL RESULTS OF THE PROBABILISTIC DESIGN EQUATION USING DESIGN PROPERTIES FROM TABLE 4.23

Data Set	H Inches	Sh Watts	Overall Mean Observed Wattage	Qcalc Sim. Watts	S_{qc} Sim. Watts	Qcalc P.D.& Exact Watts	S_{qc} Exact Watts	S_{qc} P.D. Watts
1	3.36	0.042	49.2	49.838	18.547	46.937	17.214	16.957
1	2.50	0.042	80.4	88.652	28.593	84.314	26.885	26.586
1	1.85	0.042	110.4	123.554	36.111	118.542	34.523	34.250
2	4.21	0.042	50.6	48.787	17.351	46.449	16.164	16.040
2	3.61	0.042	81.3	83.365	20.501	80.979	19.449	28.476
2	2.96	0.042	116.8	125.707	24.678	122.281	23.750	23.636
3	7.11	0.042	25.8	26.530	12.383	24.534	11.455	11.323
3	3.77	0.042	76.6	81.524	17.513	79.180	16.943	16.849
4	2.31	0.042	55.0	54.121	65.539	47.099	59.362	59.031
4	2.15	0.042	121.2	129.864	70.333	122.308	63.741	63.403
5	4.34	0.042	56.3	54.238	10.865	53.275	10.309	10.281
5	3.16	0.042	102.7	130.896	14.065	129.999	14.042	14.026

Notation: Q_{calc}, Sim-Calculated wattage using simulation, S_{qc}, sim - standard deviation of calculated wattage using simulation Q_{calc}, P.D.& Exact - Calculated wattage using partial derivative and exact techniques.(algebra of moments technique).

Standard deviation	24.678 watts
Distribution	Normal (passes Kolmogorov significance test)

Assuming the estimates of the mean and standard deviation to be perfect, the probability of failure for this heat pipe at 75 watts is

$$\frac{125.707-75}{24.678} = 2.06 = .98$$

$$1 - .98 = \text{probability of failure}$$
$$= .02$$

Since 30 samples were required for the estimation of the mean and standard deviation of the heat flows these estimates are by no means perfect. Due to the randomness of these estimates we will quote a maximum probability of failure at some confidence level. Using tolerance theory,[17] we may conclude that the upper tolerance limit of the probability of failure for this heat pipe design is .10 at a confidence of 99%, or that we are 99% confident that the probability of failure does not exceed .10. These tolerance limit values were computed from a table based on a given mean, standard deviation and sample size. This result indicates that the maximum amount of failures one might expect from 100 units of this design is 10 units. If this probability of failure is unacceptable, we can decrease the probability of failure by changing design parameters such that the meam heat flow is larger. For example, we can enlarge the wick area and one might calculate a heat flow of 150.00 watts at a standard deviation of 25 watts with a maximum probability of failure of .025 or 175 watts at a standard deviation of 30 watts with a .005 probability of failure. The difference between the mean calculation and the specification will indicate the risk one takes in designing a certain heat flow. The design distribution can be manipulated to minimize the risk of producing below specification. The reliability of this design is an initial start up reliability. An increase in failure probability may occur due to gas generation in the heat pipe. The resulting gas may block the condenser.

7.3 Heat Pipe Temperature Drop

The heat pipe thermal analog circuit appears in Figure 7.12. Applying this analysis to our low mass flow water heat pipes, we are allowed to neglect the evaporation temperature loss ($T_{ew} - T_{ev}$), the vapor flow loss ($T_{ev} - T_{cv}$) and the condensation temperature loss ($T_{cv} - T_{cw}$). These conclusions were a result of inserting the maximum expected mass flow rate, (.7 lbm/hr) into the pressure loss equation, 7.5 (derived from kinetic theory) and the Clausius equation, 7.6.

$$\Delta P = \frac{m\alpha}{g_c 2\pi r L} \sqrt{\frac{2\pi R T g_c}{M}} \qquad (7.5)$$

where R = Universal Gas Constant
M = Molecular Weight

$$\Delta T = T \, \Delta P / \rho h_{fg} J \qquad (7.6)$$

Figure 7.12 shows the general thermal analog circuit and our thermal circuit is reduced to

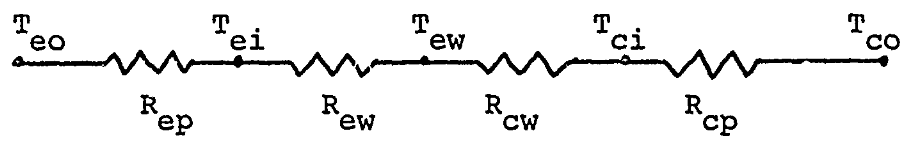

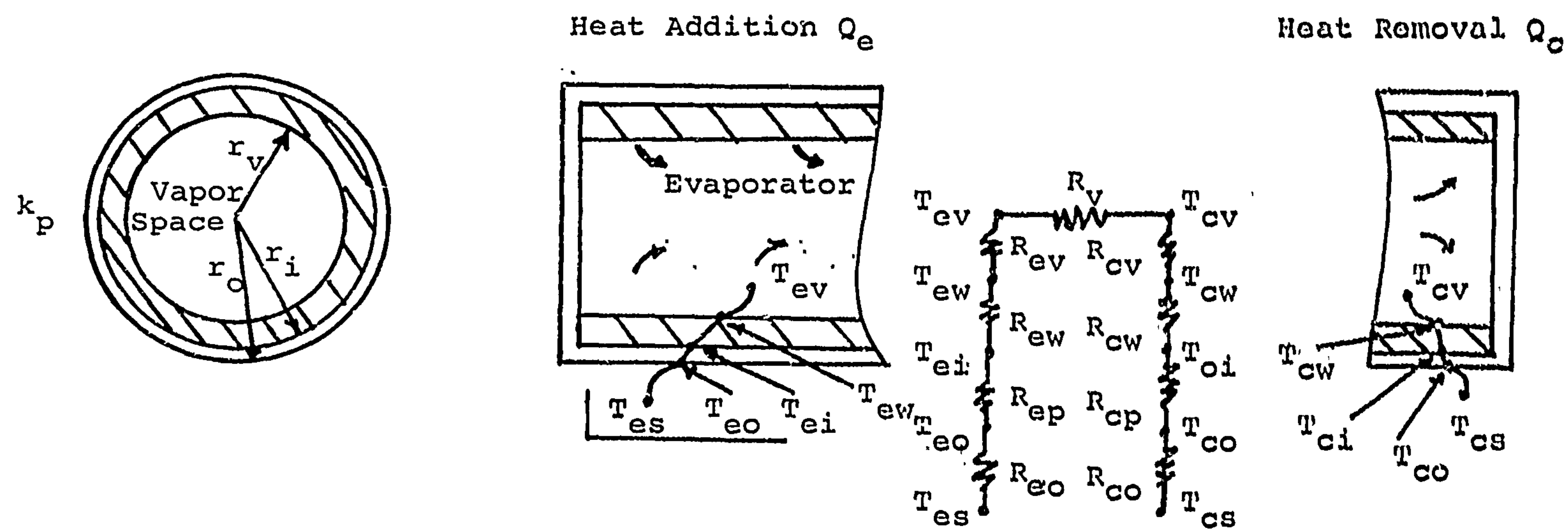

T_{es} evaporator surroundings
T_{cs} condenser surroundings
T_{eo} evaporator outside surface
T_{co} condenser outside surface
T_{ei} evaporator inside pipe surface
T_{ci} condenser inside pipe surface
T_{ew} evaporator wick-vapor interface
T_{cw} condenser wick-vapor interface
T_{ev} evaporator vapor
T_{cv} condenser vapor

R_{eo} evaporator outside surface
R_{ep} evaporator pipe = $(\ell n\ r_i/r_v)/2\pi k_{op} L_e$
R_{ew} evaporator wick-liquid = $(\ell n\ r_i/r_v)/2\pi k_{ow} L_e$
R_{ev} evaporation
R_v viscous vapor flow
R_{cv} condensation
R_{cw} condenser wick-liquid = $(\ell n\ r_i/r_v)/2\pi k_{ow} L_c$
R_{cp} condenser pipe = $(\ell n\ r_o/r_i)/2\pi k_{cp} L_c$
R_{co} condenser outside surface

Figure 7.12. Cross Section of a Heat Pipe Showing the Temperature Distribution, Nomenclature, and the Corresponding Thermal Analog Circuit for Heat Flow

where

$$R_{ep} = \ell n \frac{r_o/r_i}{2\pi k_p L_E}$$

$$R_{cw} = \ell n \frac{r_i/r_v}{2\pi k_w L_c} \qquad (7.8)$$

$$R_{ew} = \ell n \frac{r_i/r_v}{2\pi k_w L_E} \qquad (7.9)$$

$$R_{cp} = \ell n \frac{r_o/r_i}{2\pi k_p L_c} \qquad (7.10)$$

This model should adequately describe temperature loss assuming the fully wetted wick. For the fully recessed situation near burn out, the evaporator wick resistance is modified as follows

$$R_{EW} = R_{PRW} \times R_{FRW}/R_{PRW} \times R_{FRW}$$

$$R_{PRW} = \ell n\ r_e/(r_o + 1/4(r_i - r_o))/2\pi k_\ell (L_e - L_{fr})$$

$$R_{FRW} = \ell n\ r_i/(r_o + .41\ (r_i - r_o)/2\pi k_\ell (L_{fr})$$

It is assumed that the fully and partially recessed areas of the evaporator wick section combine in parallel to form a total resistance.

The thermal conductivity of the wick-fluid matrix is difficult to determine, but may be approximated by

$$k_w = \varepsilon k_\ell + (1 - e) k_s \qquad (7.11)$$

assuming that the wick is well bonded to the pipe wall (little wick-pipe thermal resistance). This equation is inaccurate in our particular case because of the poor pipe-wick contact and oxide coatings which yield a high thermal resistance as shown in Figure 7.13. It is therefore assumed that the wick contact resistance with the wall is on the same order of magnitude as that of the fluid and thermal conductivity of the wick is essentially that of the liquid.

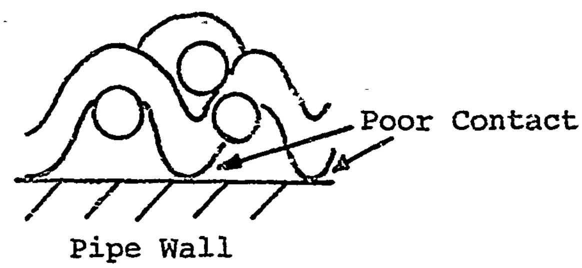

Figure 7.13. Wick Contact with Pipe Wall

As shown in Table 7.3 the stainless steel wick temperature loss predictions (using conductivity of the fluid as the wick conductivity) were always slightly higher than the observed temperature losses. The stainless steel wick has sufficient rigidity to allow some parallel heat paths to exist. However, the above assumption (conductivity of the wick equal to conductivity of the fluid) yields a conservative result and is more indicative of reality than the predictions of Equation 7.11.

The copper wicks, on the other hand, seemed to be described accurately by the fluid conductivity assumption. It is theorized that the copper wick lacks the rigidity for even mediocre thermal

TABLE 7.3

TEMPERATURE LOSS PREDICTION (Recession Model)

Data Set	Wattage	Obs. DT °F	S obs. DT °F	Calc. DT °F	S Calc. DT °F
1	42-59	8.309	3.432	8.297	3.177
1	70-90	9.369	3.293	15.046	5.046
1	100-130	12.799	3.271	21.939	8.386
2	42-59	6.799	1.788	7.163	2.608
2	70-90	9.033	1.564	12.438	3.132
2	100-130	12.099	2.411	18.835	3.803
3	20-30	2.000	0.707	2.582	1.235
3	60-80	4.799	1.923	8.070	1.743
4	50-60	7.399	1.341	16.362	21.767
4	100-130	14.600	2.191	41.899	23.400
5	45-55	7.400	1.516	7.789	1.638
5	90-120	16.400	1.949	18.980	2.352

Note:
a) Obs DT - mean observed temperature loss
b) S obs DT - standard deviation of observed temperature loss
c) Calc. DT - calculated mean temperature loss using recession model
d) S calc. DT - standard deviation of the calculated temperature loss

contact with the pipe wall and that essentially no parallel heat flow paths exist.

Figure 7.14 shows a typical wire mesh heat pipe temperature distribution. Refer to the appendix data sets for vapor temperature and temperature loss.

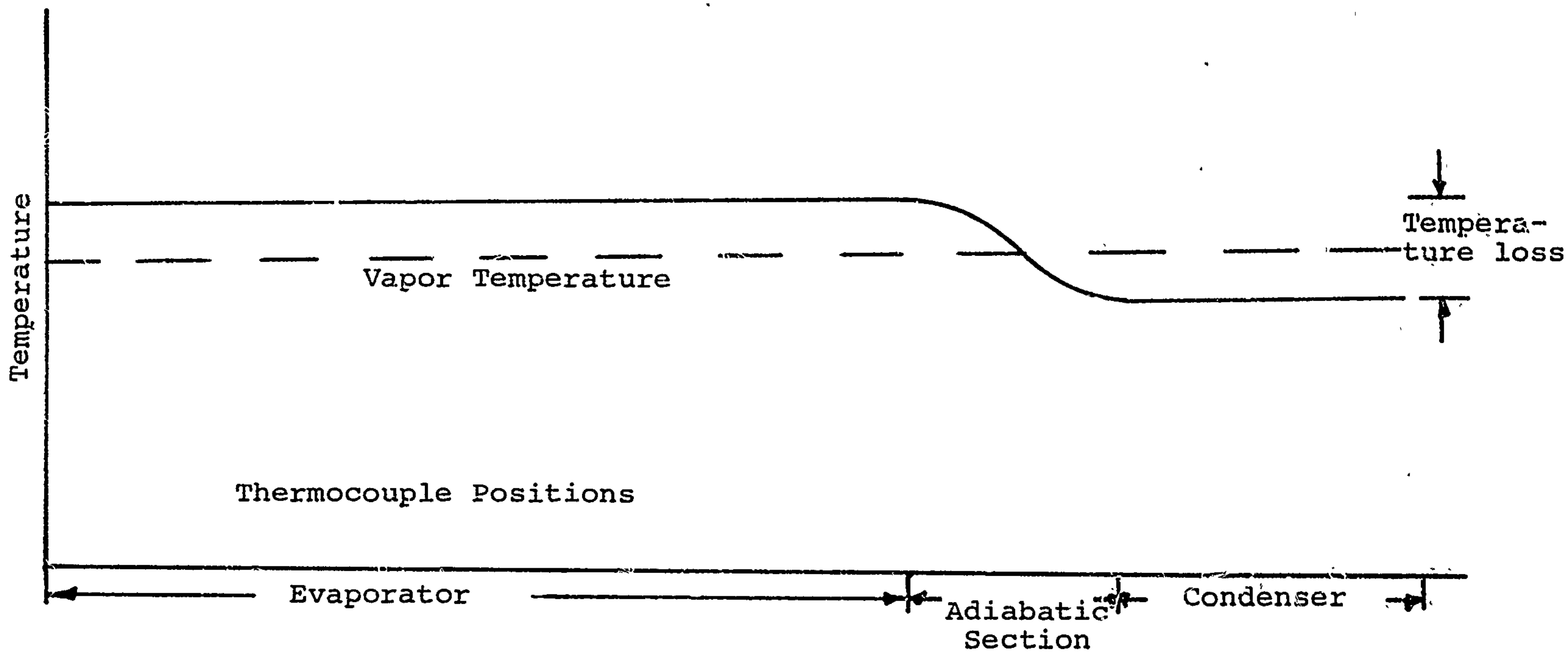

Figure 7.14. General Heat Pipe Temperature Distribution (The temperature loss is presented in each of the data sets of Appendix A, along with the heat pipe vapor temperature. No vapor temperature losses were observed.)

CHAPTER 8

CONCLUSIONS

8.1 Probabilistic Design

The probabilistic approach to design is illustrated in this work. For any given deterministic design equation,

$$A = F(x_1, x_2, \ldots x_n)$$

that describes the behavior of some physical phenomenon, we may transform into the probabilistic domain where

$$RA = F(R_{x_1}, R_{x_2}, \ldots R_{x_n})$$

R indicates the particular variable to be random and described by some probability function

The random result of the probabilistic design equation, RA, indicates the uncertainty of the design quantity to be predicted as a function of the input parameter uncertainties. The value of the probabilistic design is that it eliminates the requirement for safety factors (which are arbitrarily conceived and may not describe the situation at hand) in favor of a quantitative measure of the range of a design results. One can therefore indicate the probability of manufacturing a successful design hence predict it's reliability.

Three methods for the solution of the probabilistic design equations are mentioned. They are

a) Simulation

b) Algebra of moments

c) Taylor approximation

These methods work well in prediction of most design function variabilities but caution must be exercised in the handling of certain functions such as RA-RB and 1/RA at large coefficients of variation.

8.2 Heat Pipe Design

The recession model is quite reliable in the prediction of the mean heat flow capability of the wire mesh wick heat pipe. The prediction of heat flow standard deviations was good at high heat flows (therefore low gravity components). At low heat flows the magnitude of the gravity and surface tension terms approach each other to form the classical numerical problem mentioned in Chapter 6. At these low heat flows, prediction of the standard deviation is conservative. The recession model is by no means perfect and the descrepancy of standard deviation predictions at low heat flows is inherent to this particular model.

Uncertainty in the description of heat pipe wicking properties is discussed. A "rule of thumb" for predicting uncertainties in heat pipe properties is listed below in Table 8.1. The variability of these properties are a result of experimental and manufacturing variability. It should be mentioned that the property data generated in this work describes the wicks manufactured by the process mentioned in Chapter 3. Other types of wire mesh designs may have significantly different properties.

TABLE 8.1

UNCERTAINTY OF WICK PROPERTIES
AS A % OF THE MEAN PROPERTY

Property	Standard Deviation in % of Mean
Permeability, K	10%
Critical radius, re	5%
Wick cross sectional area, A	3%
Porosity, e	3%
Tortuosity, b	10%

REFERENCES

1. Haugen, E. B.,"Probabilistic Approaches to Design," Wiley & Sons, 1968.

2. Kreith, F., "Principles of Heat Transfer," International Textbook Company, Scranton, Pennsylvania, 1965.

3. Haring, R. E., and Greenkorn, R. A., "A Statistical Model of a Porous Medium with Non-Uniform Pores," AICHE Journal, May 1970.

4. Holm, F. W., and Miller, P. L., "Thermal Scale Modeling of a Heat Pipe," ASME publication 70-ht/spT-14, March 26, 1970.

5. Phillips, E. C., and Hinderman, J. D., "Determination of Properties of Capillary Media Useful in Heat Pipe Design," ASME-AICHE Heat Transfer Conference, Minneapolis, Minnesota, August 3-6, 1969.

6. Kemme, J. E., "Heat Pipe Design Considerations," ASME-AICHE Heat Transfer Conference, Minneapolis, Minnesota, August 3-6, 1969.

7. Feldman, K. T., "Analysis and Design of Heat Pipes," Lecture notes, UCLA, June 22-26, 1970.

8. Kunz, H. R., and Langston, L. A., "Vapor Chamber Fin Studies," NASA Contractor Report CR-812, June 1967.

9. Chun, K. R., "Some Experiments on Screen Wick Dry-Out Limits," ASME publication 71WA/HT-6, November 28, 1971.

10. Seban, R. A., and Abhat, A., "Steady and Maximum Evaporation from Screen Wicks," ASME Winter Annual Meeting, ASME Paper 71 WA/HT-12, November 23, 1971.

11. Chats, J. C., and Strevkert, J. H., "Performance of a Wick-Limited Heat Pipe," ASME-AICHE Heat Transfer Conference, Minneapolis, Minnesota, August 3-6, 1969.

12. Birnie, C., Jr., Private Communication, Department of Mechanical Engineering, The Pennsylvania State University, University Park, June 15, 1971.

13. Benner, R., Private Communication, Department of Mechanical Engineering, Lehigh University, Bethlehem, Pennsylvania, June 17, 1971.

14. Kemme, J. E., Private Communication, Los Alamos Scientific Laboratory, Los Alamos, New Mexico, March 8, 1971.

15. Stoeker, University of Illinois, Urbana, September 15, 1971.

16. Brownlee, K. A., "Statistical Theory and Methodology in Science and Engineering," Wiley & Sons, 1965.

17. Miller, I., and Freund, J. E., "Probability and Statistics for Engineers," Prentice-Hall, Inc., New Jersey, 1965.

18. Davis, H. T., Private Communication, Department of Mathematics and Statistics, The University of New Mexico, Albuquerque, 19 .

19. Van Andel, E., "Heat Pipe Design Theory," EURATOM CCR, Direct Conversation Division, Ispra, Italy.

20. Roberts, C. C., and Feldman, K. T., "Predicting Performance of Heat Pipes at High Heat Flux," to be presented at ASME Winter Annual Meeting, New York, November 1972.

APPENDIX A

BASIC RAW DATA

DATA NOMENCLATURE

The following is an explanation of data format.

K	Wick permeability as described by Darcy	(Ft^2)
SK	Standard deviation of permeability	(Ft^2)
RE	Effective capillary critical radius based on two layers of screen	(inches)
SR	Standard deviation of critical radius	(inches)
A	Flow area of the wick	(Ft^2)
SA	Standard Deviation of flow area	(Ft^2)
I LAYER	Capillary pressure capability of one layer of wire mesh	(in. H_2O)
II LAYER	Capillary pressure capability of two layers of wire mesh	(in. H_2O)

SUB TEST FORMAT

VAPOR TEMP	Heat pipe vapor temperature at equilibrium	(°F)
H	Total gravity head loss experienced by heat pipe	(in. H_2O)
SH	Standard deviation head loss	(in. H_2O)
ALPP	Darcy effective flow length (L') for non recession model $K = \frac{\mu L' \dot{m}}{\rho A \Delta P}$	(Ft)
SRALPP	Standard deviation of Darcy effective flow length non recessed model	(Ft)

Note: Each of the standard deviations are a result of experimental error in determination of the particular properties

ALPPR	Darcy effective flow length for recession model	(Ft)
SRALPR	Standard Deviation for Darcy effective flow length recession model	(Ft)
RL	Distance from the evaporator edge to the beginning of the fully recessed region of the wick	(Ft)
SRL	Standard deviation for RL	(Ft)
CALC WATTS R	Heat pipe wattage capability using the recession model Eq( )	(Watts)
SWR	Standard deviation of CALC WATTS R	(Watts)
CALC WATTS	Heat pipe wattage capability using non recessed model Eq( )	(Watts)
SW	Standard deviation of CALC WATTS	(Watts)
OBS WATTS	Experimentally observed wattage capability of a heat pipe with the above mentioned properties	(Watts)
DT CALC	Calculated temperature drop from evaporator surface to condenser surface. All vapor temperature drops were negligible	(°F)
SDT	Standard deviation of DT CALC	(°F)
OBS DT	Experimentally observed temperature drop along a heat pipe with the above mentioned properties	(°F)

TEST DATA SHEET FOR DATA SET #1

TEST #	17	18	19
K	3.5840 E-09	6.6540 E-09	5.2460 E-09
SK	1.9260 E-10	2.1580 E-10	2.8740 E-10
RE	4.0550 E-03	4.8090 E-03	4.2470 E-03
SR	1.0000 E-04	1.0000 E-04	1.0000 E-04
A	2.2830 E-04	2.3540 E-04	2.3750 E-04
SA	5.0400 E-06	6.2900 E-06	5.2000 E-06
I LAYER	5.0000	4.6250	4.1250
II LAYER	5.6250	4.7500	5.3640

(42-59W)
SUB TEST)

VAPOR TEMP	140	140	146
H	3.0600	3.2700	3.7400
SH	0.0417	0.0417	0.0417
ALPP	1.0400	1.0400	1.0400
SRALPP	0.0300	0.0300	0.0300
ALPPR	1.3260	1.3380	1.3430
SRALPR	0.0651	0.0769	0.0700
RL	1.0410	1.2080	0.7910
SRL	0.3210	0.4500	0.2890
CALC WATTS R	48.1120	49.0530	42.4140
SWR	5.3890	7.9690	5.6810
CALC WATTS	60.0870	60.8100	54.0170
SW	5.7640	8.4360	6.3500
OBS WATTS	55.0000	52.0000	53.0000
DT CALC	8.3830	8.6460	7.1740
SDT	1.0700	1.6870	1.0530
OBS DT	10.0000	7.0000	8.0000

(CONTINUED)

TEST DATA SHEET CONTINUED FOR DATA SET # 1

(70 - 90W
SUB TEST)

VAPOR TEMP	165	166	182
H	2.5000	2.2500	2.7600
SH	0.0417	0.0417	0.0417
ALPP	1.0400	1.0400	1.0400
SRALPP	0.0300	0.0300	0.0300
ALPPR	1.3380	1.3600	1.3440
SRALPR	0.0748	0.0965	0.0722
RL	1.1240	1.2080	0.8330
SRL	0.4270	0.5760	0.2830
CALC WATTS R	67.0410	101.8750	85.6470
SWR	7.2360	14.4850	9.2860
CALC WATTS	83.7070	127.7850	100.4470
SW	8.0990	18.4170	12.4160
OBS WATTS	78.0000	84.0000	80.0000
DT CALC	11.9080	18.2870	14.7720
SDT	1.4090	3.0880	1.7190
OBS DT	15.0000	9.0000	8.0

(100 - 130)W
SUB TEST)

VAPOR TEMP	198	185	204
H	1.8000	1.8700	2.0800
SH	0.0417	0.0417	0.0417
ALPP	1.0400	1.0400	1.0400
SRALPP	0.0300	0.0300	0.0300
ALPPR	1.4140	1.4280	1.3720
SRALPR	0.1300	0.1490	0.0696
RL	1.2080	1.2080	0.8540
SRL	0.7490	0.8100	0.3270
CALC WATTS R	96.3000	136.1640	122.2110
SWR	12.0020	22.0540	12.0210
CALC WATTS	118.9330	169.8960	155.1590
SW	10.6320	26.3460	16.6560
OBS WATTS	110.0000	110.0000	100.0000
DT CALC	17.1850	24.3230	20.9000
SDT	2.2210	4.2000	2.0280
OBS DT	18.0000	13.0000	10.0000

146

TEST DATA SHEET FOR DATA SET #1

TEST #	20	21
K	5.2440 E-09	5.4870 E-09
SK	2.6850 E-10	1.4950 E-10
RE	4.9060 E-03	4.3660 E-03
SR	1.0000 E-04	1.0000 E-04
A	2.5030 E-04	2.4450 E-04
SA	1.1040 E-05	4.7900 E-05
I LAYER	4.2500	4.5000
II LAYER	4.6250	5.2500

(42-59W)
SUB TEST)

VAPOR TEMP	138	147
H	2.9600	3.7500
SH	0.0417	0.0417
ALPP	1.0400	1.0400
SRALPP	0.0300	0.0300
ALPPR	1.3340	1.3260
SRALPR	0.0645	0.0648
RL	1.0410	0.9990
SRL	0.3080	0.3070
CALC WATTS R	48.1020	41.9380
SWR	5.3550	4.9170
CALC WATTS	60.1170	52.9920
SW	5.6620	5.7160
OBS WATTS	43.0000	43.0000
DT CALC	7.5660	6.4070
SDT	0.9680	0.7900
OBS DT	6.0000	3.0000

(CONTINUED)

147

TEST DATA SHEET CONTINUED FOR DATA SET # 1

(70 - 90W
SUB TEST)

VAPOR TEMP	178	157
H	2.3900	2.7300
SH	0.0417	0.0417
ALPP	1.0400	1.0400
SRALPP	0.0300	0.0300
ALPPR	1.3630	1.3310
SRALPR	0.0749	0.0680
RL	1.1660	0.9990
SRL	0.4370	0.3140
CALC WATTS R	78.5490	83.5200
SWR	8.9850	7.0820
CALC WATTS	97.8670	104.2500
SW	10.9480	7.6330
OBS WATTS	87.0000	73.0000
DT CALC	12.6340	12.9560
SDT	1.6100	1.1420
OBS DT	8.0000	7.0000

(100 - 130)W
SUB TEST)

VAPOR TEMP	192	192
H	1.6000	1.9800
SH	0.0417	0.0417
ALPP	1.0400	1.0400
SRALPP	0.0300	0.0300
ALPPR	1.4110	1.3490
SRALPR	0.1300	0.0707
RL	1.1660	1.0830
SRL	0.7490	0.4390
CALC WATTS R	120.1130	129.5810
SWR	14.5570	10.555
CALC WATTS	149.8650	161.2640
SW	15.3920	9.3140
OBS WATTS	128.0000	104.0000
DT CALC	18.2170	20.0970
SDT	1.7020	1.5970
OBS DT	13.0000	10.0000

148

TEST DATA SHEET FOR DATA SET #2

TEST #	22	23	24
K	6.909 E-09	7.479 E-09	6.850 E-09
SK	4.862 E-10	2.634 E-10	3.748 E-10
RE	4.139 E-03	3.786 E-03	3.645 E-03
SR	1.000 E-04	1.000 E-04	1.000 E-04
A	2.475 E-04	2.584 E-04	2.555 E-04
SA	1.479 E-05	6.340 E-05	1.190 E-05
I LAYER	4.625	5.500	5.250
II LAYER	5.500	6.000	6.250

(42-59W)
SUB TEST)

VAPOR TEMP	156.000	156.000	155.000
H	43.300	4.740	4.650
SH	0.042	0.042	70.042
ALPP	1.040	1.040	1.040
SRALPP	0.030	0.030	0.030
ALPPR	1.324	1.317	1.323
SRALPR	.064	0.067	0.064
RL	.999	1.187	0.999
SRL	.2846	0.270	0.273
CALC WATTS	R36.840	44.557	56.165
SWR	7.502	8.735	9.430
CALC WATTS	46.516	56.569	71.074
SW	8.743	10.500	10.562
OBS WATTS	46.090	48.000	48.500
DT CALC	5.671	7.185	8.922
SDT	1.272	1.470	1.640
OBS DT	5.000	5.000	7.000

(CONTINUED)

TEST DATA SHEET CONTINUED FOR DATA SET # 2

(70 - 90W
SUB TEST)

VAPOR TEMP	192.000	169.000	189.000
H	3.840	3.760	3.890
SH	0.042	0.042	0.042
ALPP	1.040	1.040	1.040
SRALPP	0.030	0.030	0.030
ALPPR	1.327	1.329	1.330
SRALPR	0.067	0.069	0.068
RL	1.104	1.208	1.083
SRL	0.340	0.374	0.351
CALC WATTS R	62.268	104.462	101.620
SWR	10.270	11.761	13.471
CALC WATTS	77.506	129.862	126.742
SW	13.294	15.189	17.383
OBS WATTS	75.000	82.000	84.000
DT CALC	9.894	17.290	16.571
SDT	1.760	2.024	2.362
OBS DT	10.000	8.000	8.000

(100 - 130)W
SUB TEST)

VAPOR TEMP	198.000	194.000	187.000
H	2.850	3.130	2.990
SH	0.042	0.042	0.042
ALPP	1.040	1.040	1.040
SRALPP	0.030	0.030	0.030
ALPPR	1.357	1.348	1.351
SRALPR	0.077	0.069	0.073
RL	1.083	1.208	1.020
SRL	0.404	0.453	0.430
CALC WATTS R	127.166	151.798	158.986
SWR	15.435	14.060	16.870
CALC WATTS	158.640	191.804	199.124
SW	19.603	18.773	21.956
OBS WATTS	101.000	110.000	114.000
DT CALC	19.936	25.203	25.577
SDT	2.492	2.299	2.743
OBS DT	12.000	12.000	10.000

150

TEST DATA SHEET FOR DATA SET #2

TEST #	25	26	27
K	8.379 E-09	7.184 E-09	6.250 E-09
SK	5.015 E-10	3.601 E-10	4.357 E-10
RE	4.265 E-03	4.053 E-03	3.639 E-03
SR	1.000 E-04	1.000 E-04	1.000 E-04
A	2.336 E-04	2.558 E-04	2.469 E-04
SA	1.124 E-05	1.189 E-05	1.674 E-05
I LAYER	4.750	4.000	5.250
II LAYER	5.350	5.675	6.250

(42-59W)
SUB TEST)

VAPOR TEMP	159.000	156.000	140.000
H	4.300	4.160	4.730
SH	0.042	0.042	0.042
ALPP	1.040	1.040	1.040
SRALPP	0.030	0.030	0.030
ALPPR	1.329	1.391	1.347
SRALPR	0.057	0.101	0.075
RL	1.062	0.729	0.916
SRL	0.279	0.332	0.272
CALC WATTS R	43.536	49.895	45.583
SWR	7.900	8.098	8.396
CALC WATTS	53.920	68.235	58.079
SW	10.754	8.432	9.692
OBS WATTS	51.000	51.000	57.000
DT CALC	6.433	7.833	6.992
SDT	1.114	1.421	1.461
OBS DT	6.000	5.000	6.000

(CONTINUED)

151

TEST DATA SHEET CONTINUED FOR DATA SET # 2

(70 - 90W
SUB TEST)

VAPOR TEMP	166.000	186.000	168.000
H	3.970	3.760	4.080
SH	0.042	0.042	0.042
ALPP	1.040	1.040	1.040
SRALPP	0.030	0.030	0.030
ALPPR	1.323	1.382	1.396
SRALPR	0.0646	0.105	0.089
RL	1.083	0.749	0.958
SRL	0.3191	0.330	0.325
CALC WATTS R	62.783	76.951	76.970
SWR	9.587	11.413	11.977
CALC WATTS	78.854	99.996	96.957
SW	10.926	14.798	15.126
OBS WATTS	82.000	85.000	91.000
DT CALC	9.243	12.118	12.107
SDT	1.562	1.861	2.084
OBS DT	11.000	8.000	8.000

(100 - 130)W
SUB TEST)

VAPOR TEMP	198.000	192.000	185 000
H	3.100	3.000	3.640
SH	0.042	0.042	0.042
ALPP	1.040	1.040	1.040
SRALPP	0.030	0.030	0.030
ALPPR	1.342	1.385	1.392
SRALPR	0.078	0.101	0.113
RL	1.166	0.729	0.958
SRL	0.464	0.332	0.332
CALC WATTS R	123.787	126.594	91.236
SWR	14.974	16.363	12.654
CALC WATTS	154.466	167.072	114.119
SW	19.230	24.198	14.898
OBS WATTS	114.000	116.000	118.000
DT CALC	18.670	20.174	14.153
SDT	2.480	3.136	2.008
OBS DT	12.000	11.000	12.000

TEST DATA SHEET FOR DATA SET #2

TEST #	29	30	31
K	8.116 E-09	6.081 E-09	6.326 E-09
SK	4.052 E-10	2.641 E-10	2.126 E-10
RE	3.961 E-03	3.958 E-03	3.859 E-03
SR	1.000 E-04	1.000 E-04	1.000 E-04
A	2.441 E-04	2.402 E-04	2.359 E-04
SA	1.117 E-05	9.200 E-6	7.890 E-06
I LAYER	4.500	4.750	4.750
II LAYER	5.750	5.750	5.900

(42-59W)
SUB TEST)

VAPOR TEMP	166.000	155.000	175.000
H	4.460	4.120	4.180
SH	0.042	0.042	0.042
ALPP	1.040	1.040	1.040
SRALPP	0.030	0.030	0.030
ALPPR	1.332	1.329	1.328
SRALPR	0.065	0.065	0.065
RL	0.895	0.958	0.958
SRL	0.271	0.279	0.289
CALC WATTS R	46.369	49.950	54.853
SWR	9.131	6.951	7.775
CALC WATTS	59.364	63.329	69.723
SW	10.683	7.892	8.965
OBS WATTS	54.000	58.000	53.000
DT CALC	7.011	7.501	8.089
SDT	1.478	1.133	1.226
OBS DT	6.000	3.000	10.000

(CONTINUED)

153

TEST DATA SHEET CONTINUED FOR DATA SET # 2

(70 - 90W
SUB TEST)

VAPOR TEMP	192.000	167.000	194.000
H	3.970	3.640	3.540
SH	0.042	0.042	0.042
ALPP	1.040	1.040	1.040
SRALPP	0.030	0.030	0.030
ALPPR	1.339	1.341	1.339
SRALPR	0.073	0.075	0.074
RL	0.937	0.958	0.979
SRL	0.310	0.337	0.344
CALC WATTS R	77.526	72.873	88.706
SWR	11.672	8.557	9.884
CALC WATTS	97.116	91.406	111.176
SW	15.573	11.531	13.286
OBS WATTS	79.000	93.000	77.000
DT CALC	12.030	11.130	13.328
SDT	1.859	1.351	1.525
OBS DT	8.000	5.000	12.000

(100 - 130)W
SUB TEST)

VAPOR TEMP	200.000	198.000	206.000
H	3.180	2.770	2.900
SH	0.042	0.042	0.042
ALPP	1.040	1.040	1.040
SRALPP	0.030	0.030	0.030
ALPPR	1.352	1.352	1.348
SRALPR	0.069	0.072	0.069
RL	0.917	1.102	0.999
SRL	0.358	0.435	0.398
CALC WATTS R	136.161	122.527	130.109
SWR	14.388	11.518	11.607
CALC WATTS	171.234	153.882	163.779
SW	19.563	16.004	16.587
OBS WATTS	118.000	130.000	114.000
DT CALC	20.837	18.605	19.395
SDT	2.201	1.751	1.710
OBS DT	1.500	10.000	13.000

154

TEST DATA SHEET FOR DATA SET #2

TEST #	33	34	35
K	8.214 E-09	7.324 E-09	8.154 E-09
SK	4.302 E-10	2.834 E-10	2.877 E-10
RE	4.140 E-03	4.337 E-03	4.539 E-03
SR	1.000 E-04	1.000 E-04	1.000 E-04
A	2.426 E-04	2.294 E-04	2.334 E-04
SA	8.500 E-06	8.470 E-06	6.270 E-06
I LAYER	4.625	4.750	4.625
II LAYER	5.500	5.250	5.000

(42-59W)
SUB TEST)

VAPOR TEMP	175	165	179
H	4.210	3.990	4.210
SH	0.042	0.042	0.042
ALPP	1.040	1.040	1.040
SRALPP	0.030	0.030	0.030
ALPPR	1.318	1.317	1.319
SRALPR	0.062	0.068	0.062
RL	1.062	1.187	1.021
SRL	0.238	0.259	0.233
CALC WATTS R	47.540	40.836	51.748
SWR	8.899	6.668	8.755
CALC WATTS	60.319	51.572	75.837
SW	10.298	7.681	10.232
OBS WATTS	48.500	48.000	50.000
DT CALC	7.203	5.937	7.551
SDT	1.419	1.032	1.331
OBS DT	5.000	8.000	8.000

(CONTINUED)

TEST DATA SHEET CONTINUED FOR DATA SET # 2

(70 - 90W
SUB TEST)

VAPOR TEMP	190	182	180
H	3.830	3.660	3.680
SH	0.042	0.042	0.042
ALPP	1.040	1.040	1.040
SRALPP	0.030	0.030	0.030
ALPPR	1.324	1.322	1.329
SRALPR	0.065	0.064	0.066
RL	1.083	1.268	0.999
SRL	0.263	0.288	0.257
CALC WATTS R	66.836	58.804	86.713
SWR	9.729	7.904	10.211
CALC WATTS	82.935	72.906	108.077
SW	12.166	9.899	12.433
OBS WATTS	80.000	77.000	77.000
DT CALC	10.388	8.740	12.910
SDT	1.522	1.191	1.528
OBS DT	8.000	8.000	8.000

(100 - 130)W
SUB TEST)

VAPOR TEMP	202	194	189
H	3.250	2.970	3.18
SH	0.042	0.042	0.042
ALPP	1.040	1.040	1.040
SRALPP	0.030	0.030	0.030
ALPPR	1.331	1.335	1.333
SRALPR	0.058	0.061	0.050
RL	1.104	1.208	1.042
SRL	0.304	0.359	0.290
CALC WATTS R	115.933	101.329	123.185
SWR	12.139	9.497	11.304
CALC WATTS	143.664	125.615	153.237
SW	14.569	11.017	13.306
OBS WATTS	118.000	109.000	114.000
DT CALC	17.309	14.895	18.203
SDT	1.813	1.388	1.607
OBS DT	13.000	10.000	10.000

TEST DATA SHEET FOR DATA SET #2

TEST #	36	37	38
K	7.475 E-09	6.698 E-09	6.566 E-09
SK	5.334 E-10	3.146 E-10	3.085 E-10
RE	4.141 E-03	3.870 E-03	4.337 E-03
SR	1.000 E-04	1.000 E-04	1.000 E-04
A	2.421 E-04	2.416 E-04	2.401 E-04
SA	1.300 E-05	1.022 E-05	8.750 E-06
I LAYER	5.000	5.250	4.675
II LAYER	5.500	5.875	5.250

(42-59W)
SUB TEST)

VAPOR TEMP	172.000	165.000	180.000
H	4.220	4.170	3.730
SH	0.042	0.042	0.042
ALPP	1.040	1.040	1.040
SRALPP	0.030	0.030	0.030
ALPPR	1.316	1.317	1.318
SRALPR	0.067	0.062	0.063
RL	1.208	1.166	1.166
SRL	0.251	0.257	0.275
CALC WATTS R	43.123	61.611	50.960
SWR	8.549	8.793	6.935
CALC WATTS	54.369	77.503	64.387
SW	9.742	9.927	8.150
OBS WATTS	47.000	54.000	53.000
DT CALC	6.593	9.413	7.740
SDT	1.418	1.471	1.140
OBS DT	5.000	7.000	7.000

(CONTINUED)

157

TEST DATA SHEET CONTINUED FOR DATA SET #2

(70 - 90W
SUB TEST)

VAPOR TEMP	194.000	175.000	195.000
H	3.380	3.380	3.460
SH	0.042	0.042	0.042
ALPP	1.040	1.040	1.040
SRALPP	0.030	0.030	0.030
ALPPR	1.327	1.327	1.324
SRALPR	0.067	0.067	0.065
RL	1.208	1.187	1.208
SRL	0.332	0.332	0.305
CALC WATTS R	95.714	101.988	65.902
SWR	12.006	11.386	7.876
CALC WATTS	119.515	127.300	82.085
SW	15.745	13.903	10.315
OBS WATTS	75.000	77.000	76.000
DT CALC	14.956	15.862	10.206
SDT	2.086	1.850	1.249
OBS DT	10.000	9.000	12.000

(100 - 130)W
SUB TEST)

VAPOR TEMP	195.000	205.000	205.000
H	2.940	2.650	2.86
SH	0.042	0.042	0.042
ALPP	1.040	1.040	1.040
SRALPP	0.030	0.030	0.030
ALPPR	1.338	1.346	1.336
SRALPR	0.063	0.068	0.061
RL	1.208	1.208	1.208
SRL	0.392	0.443	0.373
CALC WATTS R	126.022	152.780	102.459
SWR	14.558	14.981	8.918
CALC WATTS	155.837	189.397	127.379
SW	17.116	15.879	11.376
OBS WATTS	110.000	119.000	118.000
DT CALC	19.456	23.582	15.716
SDT	2.273	2.344	1.377
OBS DT	10.000	14.000	18.000

158

TEST DATA SHEET FOR DATA SET #2

TEST #	39	40	41
K	7.192 E-09	5.951 E-09	6.235 E-09
SK	3.193 E-10	3.363 E-10	2.832 E-10
RE	4.051 E-03	3.878 E-03	3.877 E-03
SR	1.000 E-04	1.000 E-04	1.000 E-04
A	2.392 E-04	2.416 E-04	2.363 E-04
SA	6.880 E-06	1.134 E-05	7.780 E-06
I LAYER	5.000	5.250	4.750
II LAYER	5.625	5.875	5.875

(42-59W)
SUB TEST)

VAPOR TEMP	175.000	160.000	174.000
H	4.010	4.560	4.310
SH	0.042	0.042	0.042
ALPP	1.040	1.040	1.040
SRALPP	0.030	0.030	0.030
ALPPR	1.317	1.315	1.322
SRALPR	0.063	0.062	0.062
RL	1.187	1.146	0.979
SRL	0.260	0.228	0.225
CALC WATTS R	58.780	34.876	46.413
SWR	8.036	6.665	7.214
CALC WATTS	74.435	44.341	59.278
SW	9.548	7.920	8.667
OBS WATTS	53.000	50.000	51.000
DT CALC	8.892	5.299	6.853
SDT	1.287	1.089	1.130
OBS DT	8.000	8.000	8.000

(CONTINUED)

TEST DATA SHEET CONTINUED FOR DATA SET #2

(70 - 90W
SUB TEST)

VAPOR TEMP	187.000	175.000	180.000
H	4.010	3.900	3.630
SH	0.042	0.042	0.042
ALPP	1.040	1.040	1.040
SRALPP	0.030	0.030	0.030
ALPPR	1.328	1.321	1.332
SRALPR	0.067	0.064	0.067
RL	1.208	1.187	0.958
SRL	0.341	0.278	0.253
CALC WATTS R	108.078	65.546	80.464
SWR	10.049	8.549	8.619
CALC WATTS	134.972	81.772	101.040
SW	13.158	11.076	11.275
OBS WATTS	84.000	73.000	78.000
DT CALC	16.639	10.205	12.094
SDT	1.597	1.384	1.327
OBS DT	10.000	10.000	10.000

(100 - 130)W
SUB TEST)

VAPOR TEMP	195.000	189.000	190.000
H	2.770	3.160	3.120
SH	0.042	0.042	0.042
ALPP	1.040	1.040	1.040
SRALPP	0.030	0.030	0.030
ALPPR	1.340	1.334	1.337
SRALPR	0.063	0.060	0.059
RL	1.208	1.208	0.950
SRL	0.402	0.357	0.273
CALC WATTS R	140.222	104.590	108.881
SWR	10.791	10.281	9.333
CALC WATTS	174.624	129.736	136.060
SW	13.838	12.980	11.979
OBS WATTS	115.000	120.000	125.000
DT CALC	21.447	16.122	16.206
SDT	1.665	1.616	1.366
OBS DT	14.000	18.000	12.000

160

TEST DATA SHEET FOR DATA SET # 2

TEST #	42	43	44
K	6.954 E-09	7.483 E-09	6.081 E-09
SK	3.122 E-10	4.465 E-10	2.298 E-10
RE	3.969 E-03	4.140 E-03	3.969 E-03
SR	1.000 E-04	1.000 E-04	1.000 E-04
A	2.426 E-04	2.382 E-04	2.353 E-04
SA	1.169 E-05	1.236 E-06	7.960 E-06
I LAYER	5.365	4.750	5.000
II LAYER	5.750	5.500	5.750

(42-59W)
SUB TEST)

VAPOR TEMP	165.000	185.000	176.000
H	4.440	4.210	4.170
SH	0.042	0.042	01042
ALPP	1.040	1.040	1.040
SRALPP	0.030	0.030	0.030
ALPPR	1.318	1.323	1.322
SRALPR	0.062	0.059	0.059
RL	1.041	0.895	0.894
SRL	0.226	0.229	0.224
CALC WATTS R	40.253	40.468	45.587
SWR	7.542	8.214	6.703
CALC WATTS	51.350	51.983	58.509
SW	9.047	9.800	8.129
OBS WATTS	53.000	45.000	45.000
DT CALC	6.107	5.986	6.683
SDT	1.236	1.313	1.049
OBS DT	10.000	8.000	5.000

(CONTINUED)

TEST DATA SHEET CONTINUED FOR DATA SET #2

(70 - 90W
SUB TEST)

VAPOR TEMP	185.000	192,000	198.000
H	3.810	3.490	3.420
SH	0.042	0.042	0.042
ALPP	1.040	1.040	1.040
SRALPP	0.030	0,030	0.030
ALPPR	1.327	1.343	1.341
SRALPR	0.065	0.077	0.760
RL	1.020	0.874	0.895
SRL	0.256	0.256	0.255
CALC WATTS R	75.292	85.704	83.753
SWR	9.646	10.709	8.474
CALC WATTS	94.157	108.543	105.741
SW	12.601	14.156	11.220
OBS WATTS	86.000	88.000	72.000
DT CALC	11.656	13.420	12.483
SDT	1.561	1.702	1.305
OBS DT	8.000	10.000	8.000

(100 - 130)W
SUB TEST)

VAPOR TEMP	190.000	205.000	198.000
H	3.140	3.000	3.070
SH	0.042	0.042	0.040
ALPP	1.040	1.040	1.040
SRALPP	0.030	0.030	0.030
ALPPR	1.319	1.333	1.329
SRALPR	0.061	0.064	0.063
RL	1.020	0.854	0.874
SRL	0.285	0.264	0.254
CALC WATTS R	116.538	118.852	102.627
SWR	10.946	12.124	8.546
CALC WATTS	145.170	149.571	129.286
SW	13.833	15.507	11.046
OBS WATTS	114.000	121.000	120.000
DT CALC	17.811	17.700	15.137
SDT	1.715	1.846	1.245
OBS DT	8.000	13.000	10.000

TEST DATA SHEET FOR DATA SET #2

TEST #	45	46	47
K	8.702 E-09	8.338 E-09	6.427 E-09
SK	3.439 E-10	2.742 E-10	3.796 E-10
RE	4.143 E-03	4.140 E-03	4.051 E-03
SR	1.000 E-04	1.000 E-04	1.000 E-04
A	2.337 E-04	2.270 E-04	2.387 E-04
SA	6.280 E-06	4.900 E-06	1.001 E-05
I LAYER	4.875	4.875	4.050
II LAYER	5.500	5.500	5.625

(42-59W)
SUB TEST)

VAPOR TEMP	168.000	170.000	179.000
H	4.078	4.280	4.140
SH	0.042	0.042	0.042
ALPP	1.040	1.040	1.040
SRALPP	0.036	0.030	0.030
ALPPR	1.317	1.325	1.346
SRALPR	0.058	0.060	0.064
RL	0.937	0.854	0.708
SRL	0.232	0.221	0.215
CALC WATTS R	65.462	40.704	44.146
SWR	9.656	7.538	7.281
CALC WATTS	83.766	52.739	57.578
SW	11.397	9.220	8.816
OBS WATTS	51.000	50.000	52.000
DT CALC	9.530	5.725	6.495
SDT	1.446	1.092	1.157
OBS DT	6.000	10.000	6.000

(CONTINUED)

TEST DATA SHEET CONTINUED FOR DATA SET # 2

(70 - 90W
SUB TEST)

VAPOR TEMP	185.000	200.000	190.000
H	3.460	3.580	3.480
SH	0.042	0.042	0.042
ALPP	1.040	1.040	1.040
SRALPP	0.030	0.030	0.030
ALPPR	1.337	1.347	1.367
SRALPR	0.075	0.077	0.082
RL	0.937	0.833	0.687
SRL	0.261	0.244	0.228
CALC WATTS R	99.720	84.430	78.652
SWR	10.273	9.422	9.171
CALC WATTS	125.386	106.740	101.497
SW	13.540	12.510	12.328
OBS WATTS	81.000	83.000	83.000
DT CALC	14.706	12.143	11.786
SDT	1.542	1.354	1.433
OBS DT	8.000	10.000	10.000

(100 - 130)W
SUB TEST)

VAPOR TEMP	190.000	205.000	190.000
H	2.970	2.680	2.910
SH	0.042	0.042	0.042
ALPP	1.040	1.040	1.040
SRALPP	0.030	0.030	0.030
ALPPR	1.326	1.337	1.356
SRALPR	0.067	0.066	0.0679
RL	0.916	0.812	0.666
SRL	0.270	0.260	0.227
CALC WATTS R	135.919	149.236	109.447
SWR	10.797	10.381	10.220
CALC WATTS	170.892	189.573	140.463
SW	13.992	13.625	13.463
OBS WATTS	112.000	130.000	125.000
DT CALC	19.941	21.276	16.187
SDT	1.538	1.423	1.512
OBS DT	12.000	13.001	14.000

164

TEST DATA SHEET CONTINUED FOR DATA SET # 2

(70 - 90W
SUB TEST)

VAPOR TEMP	189.000	180.000	190.000
H	3.580	2.950	3.310
SH	0.042	0.042	0.042
ALPP	1.040	1.040	1.040
SRALPP	0.030	0.030	0.030
ALPPR	1.349	1.352	1.348
SRALPR	0.077	0.080	0.078
RL	0.812	0.812	0.833
SRL	0.233	0.260	0.254
CALC WATTS R	82.475	113.993	71.195
SWR	8.437	9.536	6.899
CALC WATTS	104.588	145.198	90.239
SW	11.175	12.906	9.238
OBS WATTS	80.000	89.000	80.000
DT CALC	12.401	16.294	10.092
SDT	1.282	1.435	0.998
OBS DT	10.000	10.000	10.000

(100 - 130)W
SUB TEST)

VAPOR TEMP	192.000	192.000	190.000
H	3.040	2.700	2.540
SH	0.042	0.042	0.042
ALPP	1.040	1.040	1.040
SRALPP	0.030	0.030	0.030
ALPPR	1.337	1.337	1.339
SRALPR	0.064	0.066	0.066
RL	0.791	0.812	0.792
SRL	0.236	0.262	0.261
CALC WATTS R	111.588	133.755	110.377
SWR	8.870	9.888	7.484
CALC WATTS	141.818	169.661	140.466
SW	11.636	12.848	9.801
OBS WATTS	121.000	110.000	110.000
DT CALC	16.592	18.949	15.487
SDT	1.270	1.402	1.040
OBS DT	12.000	10.000	15.000

TEST DATA SHEET FOR DATA SET #2

TEST #	48	49	50
K	6.204 E-09	8.246 E-09	6.412 E-09
SK	2.576 E-10	2.674 E-10	1.968 E-10
RE	3.887 E-03	4.257 E-03	4.257 E-03
SR	1.000 E-04	1.000 E-04	1.010 E-04
A	2.387 E-04	2.261 E-04	2.236 E-04
SA	6.000 E-06	7.510 E-06	6.290 E-06
I LAYER	4.875	4.500	4.500
II LAYER	5.875	5.365	5.365

(42-59W)
SUB TEST)

VAPOR TEMP	176.000	174.000	176.000
H	4.210	3.780	3.870
SH	0.042	0.042	0.042
ALPP	1.040	1.040	1.040
SRALPP	0.030	0.030	0.030
ALPPR	1.331	1.330	1.330
SRALPR	0.061	0.062	0.062
RL	0.812	0.833	0.830
SRL	0.216	0.235	0.233
CALC WATTS R	54.535	6[illegible].828	43.227
SWR	7.240	7.782	5.839
CALC WATTS	70.427	79.545	55.724
SW	8.826	9.459	7.127
OBS WATTS	49.000	58.000	43.000
DT CALC	8.067	8,728	6.031
SDT	1.127	1.188	0.862
OBS DT	6.000	10.000	7.000

(CONTINUED)

166

TEST DATA SHEET FOR DATA SET #2

TEST #	51	52	53
K	8.337 E-09	7.463 E-09	7.775 E-09
SK	3.730 E-10	1.382 E-10	3.343 E-10
RE	4.140 E-03	4.140 E-03	4.245 E-03
SR	1.000 E-04	1.000 E-04	1.000 E-04
A	2.373 E-04	2.324 E-04	2.392 E-04
SA	6.270 E-06	5.320 E-06	9.780 E-06
I LAYER	5.000	4.750	4.500
II LAYER	5.500	5.500	5.365

(42-59W)
SUB TEST)

VAPOR TEMP	168.000	184.000	185.000
H	4.160	4.020	3.980
SH	0.042	0.042	0.042
ALPP	1.040	1.040	1.040
SRALPP	0.030	0.030	0.030
ALPPR	1.315	1.323	1.330
SRALPR	0.057	0.059	0.061
RL	0.999	0.896	0.833
SRL	0.235	0.232	0.233
CALC WATTS R	50.830	50.886	49.416
SWR	8.118	7.406	8.126
CALC WATTS	64.889	65.495	63.716
SW	9.722	9.112	9.813
OBS WATTS	48.000	54.000	49.000
DT CALC	7.529	7.362	7.378
SDT	1.255	1.116	1.297
OBS DT	8.000	6.000	5.000

(CONTINUED)

TEST DATA SHEET CONTINUED FOR DATA SET #2

(70 - 90W
SUB TEST)

VAPOR TEMP	177.000	192.000	194.000
H	3.610	3.560	3.660
SH	0.042	0.042	0.042
ALPP	1.040	1.040	1.040
SRALPP	0.030	0.030	0.030
ALPPR	1.330	1.343	1.347
SRALPR	0.073	0.076	0.077
RL	0.979	0.874	0.833
SRL	0.260	0.247	0.245
CALC WATTS R	86.563	79.212	69.306
SWR	9.649	8.123	9.610
CALC WATTS	108.494	99.799	87.654
SW	12.643	10.782	12.113
OBS WATTS	86.000	82.000	85.000
DT CALC	13.060	11.655	10.487
SDT	1.466	1.202	1.416
OBS DT	10.000	6.000	8.000

(100 - 130)W
SUB TEST)

VAPOR TEMP	189.000	202.000	202.000
H	2.860	2.990	2.990
SH	0.042	0.042	0.042
ALPP	1.040	1.040	1.040
SRALPP	0.030	0.030	0.030
ALPPR	1.324	1.332	1.337
SRALPR	0.063	0.064	0.065
RL	0.950	0.854	0.812
SRL	0.287	0.256	0.257
CALC WATTS R	140.225	116.434	116.188
SWR	11,067	8.609	10.409
CALC WATTS	175.901	147.187	146.990
SW	14.331	11.205	13.472
OBS WATTS	18.000	125.000	125.000
DT CALC	20.936	16.966	17.341
SDT	1.606	1.209	1.559
OBS DT	10.000	10.000	10.000

TEST DATA SHEET FOR DATA SET #3

TEST #	54	55	56
K	3.074 E-09	2.584 E-09	3.796 E-09
SK	2.845 E-10	1.483 E-10	6.949 E-10
RE	2.336 E-03	2.396 E-03	2.525 E-03
SR	1.000 E-04	1.000 E-04	1.000 E-04
A	1.614 E-04	1.579 E-04	1.688 E-04
SA	1.294 E-05	5.390 E-06	8.570 E-06
I LAYER	8.000	7.000	
II LAYER	9.750	9.500	

(20-30W)
SUB TEST)

VAPOR TEMP	152.000	146.000	164.000
H	7.230	7.100	7.010
SH	0.042	0.042	0.042
ALPP	1.040	1.040	1.046
SRALPP	0.030	0.030	0.030
ALPPR	1.227	1.239	1.225
SRALPR	0.055	0.056	0.055
RL	0.937	0.729	0.999
SRL	0,180	0.148	0.193
CALC WATTS R	26.665	20.406	25.080
SWR	6.529	4.382	8.379
CALC WATTS	32.035	24.953	30.116
SW	7.399	5.118	9.191
OBS WATTS	26.500	25.000	25.400
DT CALC	2.878	2.136	2.779
SDT	0.779	0.479	0.976
OBS DT	2.000	1.000	2.000

(CONTINUED)

169

TEST DATA SHEET CONTINUED FOR DATA SET # 3

(70 - 90W
SUB TEST)

VAPOR TEMP	150.000	192.000	200.000
H	2.860	3.620	3.980
SH	0.042	0.042	0.047
ALPP	1.040	1.040	1.040
SRALPP	0.030	0.030	0.030
ALPPR	1.257	1.255	1.255
SRALPR	0.075	0.069	0.074
RL	0.854	0.749	1.083
SRL	0.377	0.216	0.498
CALC WATTS R	92.933	74.076	99.119
SWR	13.026	7.632	20.465
CALC WATTS	110.930	88.276	117.492
SW	15.865	9.227	23.810
OBS WATTS	78.000	70.000	75.000
DT CALC	10.231	7.952	11.474
SDT	1.588	0.839	2.384
OBS DT	4.000	3.000	4.000

170

TEST DATA SHEET FOR DATA SET

TEST #	57	58
K	2.798 E-09	3.171 E-09
SK	9.819 E-11	2.146 E-10
RE	2.162 E-03	2.603 E-03
SR	1.000 E-04	1.000 E-04
A	1.677 E-04	1.682 E-04
SA	6.440 E-06	7.860 E-06
I LAYER	9.250	7.350
II LAYER	10.250	8.750

(20-30W)
SUB TEST)

VAPOR TEMP	162.000	175.000
H	7.360	6.850
SH	0.042	0.042
ALPP	1.040	1.040
SRALPP	0.030	0.030
ALPPR	1.222	1.222
SRALPR	0.055	0.055
RL	1.100	1.062
SRL	0.181	0.070
CALC WATTS R	34.337	18.559
SWR	6.742	5.653
CALC WATTS	41.373	22.590
SW	7.892	6.496
OBS WATTS	29.000	24.000
DT CALC	3.842	2.060
SDT	0.797	0.659
OBS DT	3.000	2.000

(CONTINUED)

171

TEST DATA SHEET CONTINUED FOR DATA SET #3

(60 - 80W)
SUB TEST)

VAPOR TEMP	203.000	194.000
H	4.350	4.050
SH	0.042	0.042
ALPP	1.040	1.046
SRALPP	0.030	0.030
ALPPR	1.244	1.242
SRALPR	0.067	0.067
RL	1.208	1.083
SRL	0.376	0.314
CALC WATTS R	92.092	75.657
SWR	9.862	9.050
CALC WATTS	107.954	89.044
SW	11.745	10.827
OBS WATTS	81.000	79.000
DT CALC	10.581	8.688
SDT	1.168	1.082
OBS DT	5.000	8.000

172

TEST DATA SHEET FOR DATA SET #4

TEST #	59	60	61
K	2.729 E-08	3.209 E-08	3.291 E-08
SK	1.339 E-09	1.381 E-09	1.265 E-09
RE	7.921 E-03	8.278 E-03	8.675 E-03
SR	1.000 E-04	1.000 E-04	1.000 E-04
A	5.314 E-04	5.203 E-04	5.406 E-04
SA	1.890 E-05	2.091 E-06	1.860 E-06
I LAYER	2.365	2.365	2.000
II LAYER	2.875	2.750	2.625

(50-60W)
SUB TEST)

VAPOR TEMP	182.000	195.000	188.000
H	2.480	2.290	2.250
SH	0.042	0.042	0.042
ALPP	1.040	1.040	1.040
SRALPP	0.030	0.030	0.030
ALPPR	1.328	1.328	1.342
SRALPR	0.064	0.063	0.076
RL	1.041	1.166	0.916
SRL	0.403	0.439	0.442
CALC WATTS R	35.003	68.111	38.561
SWR	26.410	32.289	31.797
CALC WATTS	44.122	85.004	48.406
SW	30.879	37.535	37.576
OBS WATTS	55.000	56.000	56.000
DT CALC	-10.778	21.366	11.904
SDT	8.668	10.562	10.533
OBS DT	8.000	8.000	8.001

(CONTINUED)

TEST DATA SHEET FOR DATA SET #4

(100-130 W)
SUB TEST)

VAPOR TEMP	200.000	200.000	200.000
H	2.250	2.230	2.100
SH	0.042	0.042	0.042
ALPP	1.040	1.040	1.040
SRALPP	0.030	0.030	0.030
ALPPR	1.348	1.345	1.364
SRALPR	0.085	0.082	0.098
RL	1.083	1.117	0.937
SRL	0.440	0.449	0.464
CALC WATTS R	133.845	286.371	118.182
SWR	29.706	32.232	33.356
CALC WATTS	163.944	103.088	144.277
SW	40.669	44.143	45.878
OBS WATTS	115.000	120.000	123.000
DT CALC	45.000	28.965	40.421
SDT	10.006	10.608	11.280
OBS DT	18.000	14.000	14.000

174

TEST DATA SHEET FOR DATA SET #4

TEST #	62	63
K	2.822 E-08	3.231 E-08
SK	8.494 E-10	9.071 E-10
RE	8.675 E-03	8.675 E-03
SR	1.000 E-04	1.006 E-04
A	5.438 E-04	5.295 E-04
SA	1.001 E-05	1.100 E-05
I LAYER	1.875	2.250
II LAYER	2.625	2.625

(50-60W)
SUB TEST)

VAPOR TEMP	176.000	170.000
H	2.300	2.240
SH	0.042	0.042
ALPP	1.040	1.040
SRALPP	0.030	0.030
ALPPR	1.355	1.331
SRALPR	0.084	0.065
RL	0.791	1.124
SRL	0.432	0.448
CALC WATTS R	23.412	158.707
SWR	23.637	29.374
CALC WATTS	30.089	73.392
SW	30.476	34.452
OBS WATTS	53.000	55.000
DT CALC	7.027	18.544
SDT	8.365	9.631
OBS DT	8.000	8.000

(CONTINUED)

175

TEST DATA SHEET FOR DATA SET #4

(100-130W)
SUB TEST)

VAPOR TEMP	195.000	184.000
H	2.030	2.120
SH	0.042	0.042
ALPP	1.040	1.040
SRALPP	0.030	0.030
ALPPR	1.378	1.351
SRALPR	0.108	0.087
RL	0.812	1.124
SRL	0.458	0.471
CALC WATTS R	147.351	123.177
SWR	27.892	29.889
CALC WATTS	183.923	149.780
SW	38.544	40.569
OBS WATTS	122.000	126.000
DT CALC	50.058	41.568
SDT	9.374	9.913
OBS DT	12.006	15.000

176

TEST DATA SHEET FOR DATA SET #5

TEST #	64	65	66
K	6.737 E-09	6.031 E-09	6.421 E-09
SK	2.587 E-10	4.131 E-10	4.344 E-10
RE	3.888 E-03	3.888 E-03	3.888 E-03
SR	1.000 E-04	1.000 E-04	1.000 E-04
A	3.092 E-04	2.759 E-04	2.939 E-04
SA	9.650 E-06	1.719 E-05	1.053 E-05
I LAYER	5.750	5.250	5.250
II LAYER	5.875	5.875	5.875

(45-55W)
SUB TEST)

VAPOR TEMP	175.000	201.000	185.000
H	4.310	4.580	4.490
SH	0.042	0.042	0.042
ALPP	1.040	1.040	1.040
SRALPP	0.030	0.030	0.030
ALPPR	1.308	1.307	1.305
SRALPR	0.055	0.055	0.055
RL	1.208	1.208	1.145
SRL	0.245	0.230	0.735
CALC WATTS R	61.077	30.988	45.768
SWR	9.506	8.860	10.015
CALC WATTS	77.575	39.683	58.129
SW	11.395	10.535	11.815
OBS WATTS	53.000	45.000	55.000
DT CALC	9.561	4.284	6.803
SDT	1.587	1.320	1.650
OBS DT	7.000	5.000	8.000

(CONTINUED)

177

TEST DATA SHEET CONTINUED FOR DATA SET #5

(90-120W
SUB TEST)

VAPOR TEMP	185.000	201.000	180.000
H	3.550	3.590	3.750
SH	0.042	0.042	0.042
ALPP	1.040	1.040	1.040
SRALPP	0.030	0.030	0.030
ALPPR	1.327	1.328	1.327
SRALPR	0.068	0.068	0.068
RL	1.208	1.208	1.200
SRL	0.308	0.315	0.302
CALC WATTS R	112.410	94.374	87.366
SWR	11.538	12.657	11.942
CALC WATTS	140.247	118.145	109.325
SW	15.031	16.431	15.490
OBS WATTS	104.000	105.000	110.000
DT CALC	17.930	13.421	13.764
SDT	1.911	1.985	1.997
OBS DT	15.000	15.000	19.000

178

TEST DATA SHEET FOR DATA SET #5

TEST #	67	68
K	6.400 E-09	6.577 E-09
SK	3.475 E-10	3.111 E-10
RE	3.971 E-03	3.888 E-03
SR	1.000 E-04	1.000 E-04
A	2.836 E-04	2.893 E-04
SA	1.474 E-05	1.037 E-05
I LAYER	5.165	5.250
II LAYER	5.750	5.875

(45-55W
SUB TEST)

VAPOR TEMP	190.000	186.000
H	3.950	4.380
SH	0.042	0.042
ALPP	1.040	1.040
SRALPP	0.030	0.030
ALPPR	1.308	1.308
SRALPR	0.055	0.055
RL	1.124	1.208
SRL	0.263	0.240
CALC WATTS R	71.543	52.877
SWR	10.360	9.568
CALC WATTS	90.255	67.271
SW	12.109	11.431
OBS WATTS	55.000	55.000
DT CALC	10.302	7.715
SDT	1.710	1.487
OBS DT	8.000	9.000

(CONTINUED)

TEST DATA SHEET CONTINUED FOR DATA SET #5

(90 - 120 W
SUB TEST)

VAPOR TEMP	195.000	186.000
H	3.650	3.490
SH	0.042	0.042
ALPP	1.040	1.040
SRALPP	0.030	0.030
ALPPR	1.327	1.328
SRALPR	0.068	0.067
RL	1.208	1.020
SRL	0.301	0.279
CALC WATTS R	91.632	113.258
SWR	11.601	11.854
CALC WATTS	114.474	141.463
SW	15.102	15.440
OBS WATTS	95.000	100.000
DT CALC	13.395	16.866
SDT	1.822	1.857
OBS DT	15.000	18.000

180

APPENDIX B

COMPUTER PROGRAM

58.05

```
/ID 016367080,ME699     ROBERTS,CHARLES
/JOB TIME=10,GO
      DIMENSION AAN(400),F(400),OBF(400),DIFF(400),X(400)
      COMMON  RHOF,UL,AL,H1L,RE,SR,HFG,AK,SK,SAL
      DO 681 II=1,10
      READ,RV
      READ,SRV
      RV=RV/2.
      SRV=SRV/2.
      READ,H1L
      H1L=H1L/12.
      READ,AL
      READ,SAL
      READ,AK
      READ,SK
      READ,RE
      READ,SR
      READ 100,RHOF,HFG
      READ 100,SIGMA,UL
      READ 100,H,SH
      READ 100,TT,ALPP
  100 FORMAT(E20.7,E20.7)
  200 FORMAT(E20.7,E20.7,E20.7)
      WRITE(6,102)
  102 FORMAT(6X,'AK',15X,'SK',15X,'RE',15X,'SR',15X,'H',15X,'SH',/)
      WRITE(6,101)  AK,SK,RE,SR,H,SH
  101 FORMAT(2X,1PE12.5,4X,1PE12.5,4X,1PE12.5,4X,1PE12.5,4X,1PE12.5,
     14X,1PE12.5,/)
      SRALPP=.03
      DO 400 KL=1,3
      WRITE(6,103)
  103 FORMAT(6X,'ALPP',/)
      WRITE(6,104) ALPP
  104 FORMAT(2X,1PE12.5,/)
      PRINT,SRALPP
      WRITE(6,165)
  165 FORMAT(6X,'TEMP',/)
      WRITE(6,166) TT
  166 FORMAT(2X,1PE12.5,/)
```


181

```
      G=32.139
      GC=32.174
      ANL=RHOF*SIGMA*HFGZUL
      C=GC*60.*17.57
      WRITE(6,155)
155   FORMAT(6X,'AREA',15X,'ANL',/)
      WRITE(6,156) AL,ANL
156   FORMAT(2X,1PE12.5,4X,1PE12.5,/)
      PRINT,SAL
      WRITE(6,201)
201   FORMAT(2X,'HEAT FLOW,WATTS',2X,'PERMEABILITY,FTSQ',2X,'CRITICAL
     1RADIUS,IN',5X,'HEIGHT',3X,'AREA',8X,'LIQUID FLOW PATH',/)
      N=200
      XXXX=RANF(23782)
      DO 10 I=1,N
      RK=(GAUS(0)*SK)+AK
      RR=(GAUS(0)*SR)+RE
      RH=(GAUS(0)*SH)+H
      RALPP=(GAUS(0)*SALPP)+ALPP
      RAL=(GAUS(0)*SAL)+AL
      AKP=RK*RAL/RALPP
      GF1=24./RR
      GF2=RHOF*(RH/12.)/SIGMA
      GFAC=GF1-GF2
      QBAR=ANL*AKP*GFAC
      QBAR=QBAR*C
      WRITE(6,202)   QBAR,RK,RR,RH,RAL,RALPP
202   FORMAT(2X,1PE12.5,6X,1PE12.5,6X,1PE12.5,6X,1PE12.5,
     16X,1PE12.5,6X,1PE12.5)
      X(I)=QBAR
10    CONTINUE
      PRINT 600
600   FORMAT('SAMPLE SIZE IS')
      PRINT 610,N
610   FORMAT(1H,I5)
      Z=N
      SUM=0.
      DO 180 I2=1,N
180   SUM=SUM+X(I2)
      EXBAR=SUM/Z
      SUMSQ=0.
      DO 190 I3=1,N
190   SUMSQ=SUMSQ+(X(I3)-EXBAR)**2
      SUMSQN=SUMSQ/(Z-1)
      SQSIG=SQRT(SUMSQN)
      PRINT 555,EXBAR,SQSIG
555   FORMAT(//'MEAN VALUE =',F20.3//,'STANDARD DEVIATION=',F20.3//)
      FF=SUMSQ/Z
      X1=0.
      X2=0.
      X3=0.
      X4=0.
      DO 20 I=1,N
      X1=X1+X(I)
      X2=X2+X(I)**2
      X3=X3+X(I)**3
20    X4=X4+X(I)**4
```


182

```
      CM3=X3/Z-3*(X2/Z)*(X1/Z)+2*(X1/Z)**3
      ALPHA=CM3/(SQRT(FF*3))
      PRINT 666,ALPHA3
  666 FORMAT(//'COEFFICIENT OF SKEWNESS =',F20.8//)
      CM4=X4/Z-4*(X1/Z)*(X3/Z)+6*(X2/Z)*(X1/Z)**2-3*(X1/Z)**4
      ALPHA4=CM4/(FF**2)
      PRINT 300,ALPHA4
  300 FORMAT(//'COEFFICIENT OF KURTOSIS =',F20.8//)
      C2=RHOF/(SIGMA*12.)
      C3=24.
      Q=C*ANL*(AK*AL/ALPP)*(C3/RE-C2*H)
      PRINT,Q
      A4=AK*AL
      A5=A4/ALPP
      A3=C3/RE-C2*H
      CALL QUOT(S1,0.,SR,1.,RE)
      S1=S1*C3
      S2=C2*SH
      CALL SUMDIF(S3,S1,S2)
      CALL PROD(S4,SK,SAL,AK,AL)
      CALL QUOT(S5,S4,SRALPP,A4,ALPP)
      CALL PROD(S6,S5,S3,A5,A3)
      S6=C*ANL*S6
      PRINT,S6
      QB=C3/RE-C2*H
      PQWA=C*ANL*(AK/ALPP)*QB
      PQWK=C*ANL*(AL/ALPP)*QB
      PQWLP=-C*ANL*(AL*AK/(ALPP**2))*QB
      QC=C*ANL*(AK*AL/ALPP)
      PQWH=QC*(-C2)
      PQWRE=QC*(-C3/(RE**2))
      S7=(PQWA**2)*(SAL**2)+(PQWK**2)*(SK**2)+(PQWLP**2)*(SRALPP**2)
     1+(PQWH**2)*(SH**2)+(PQWRE**2)*(SR**2)
      S7=SQRT(S7)
      PRINT,S7
      CALL RECESS(FXBAR,SQSIG,ALPPN,SRALPN,H,SH)
      ALPP=ALPPN
      SRALPP=SRALPN
      PRINT,SRALPP
      CALL DELTAT(PV,SRV,EXBAR,SQSIG)
  400 CONTINUE
  681 CONTINUE
      CALL EXIT
      END
```


183

```
      FUNCTION GAUS(K)
C     RANDOM NUMBER GENERATOR PACKAGE.    RANF(K) GIVES UNIFORM RANDOM
C     NUMBERS, GAUS(K) GIVES NORMALLY DISTRIBUTED (0,1) NUMBERS.
C     IF RANF HAS BEEN INITIALIZED, GAUS SHOULD NOT BE INITIALIZED.
C
      DATA ISET/0/
      DATA TWOPI/6.28318/
      IF(ISET)10,10,20
   10 ISET=1
      A=SQRT(-2.*ALOG(RANF(K)))
      B=RANF(0)*TWOPI
      GAUS=A*SIN(B)
      STORE=A*COS(B)
      RETURN
   20 ISET=0
      GAUS=STORE
      RETURN
      END
```


184

```
      FUNCTION RANF(N)
C
C     FORTRAN ROUTINE TO GENERATE FLOATING RANDOM NUMBERS OVER THE
C     RANGE OF 0.0 TO 1.0.
C     ROUTINE BY HARRY [illegible] MURPHY, JR., 22 FEBRUARY 1969.
C
      EQUIVALENCE (IX,RX)
C
      DATA IX/32771/
C
    1 IF (N) 4,2,3
    2 IX=MOD(1021*IX+3,1048576)
      RANF=FLOAT(IX)/1048576.0
      RETURN
C
    3 IX=MOD(N,1048576)
C
    4 RANF=RX
      RETURN
      END
```


185

```
      SUBROUTINE KSTST(N,X,EXBAR,SQSIG)
      DIMENSION AAN(400),F(400),CDF(400),DIFF(400),X(400)
      DO 36 I=1,N
 36   F(I)=0.
      L=N+1
      M=N+10
      DO 114 I=L,M
 114  X(I)=0.
      U=EXBAR
      S=SQSIG
      PRINT 777,N
 777  FORMAT(//'SAMPLE SIZE=',I5)
 5    Z=-1.00E+10
      Y=0.
 3    DO 2 I=1,N
      IF(X(I)-Z) 1,2,2
 1    K=I-1
      X(K)=X(I)
      X(I)=Z
      Y=1.
 2    Z=X(I)
      IF (Y) 5,6,4
 4    GO TO 5
 6    CONTINUE
      P=0.
      DO 51 I=1,N
      Q=1.
      K=I+1
      IF   (X(I))  62,51,62
 62   IF(X(I)-X(K))   31,32,31
 32   DO 53 J=I,N
      L=J+1
      L2=J+2
 53   X(L)=X(L2)
      Q=Q+1.
      P=P+1.
      IF(X(I)-X(K)) 31,32,31
 31   CONTINUE
      F(I)=Q
 51   CONTINUE
      L=P
      M=N-L
      CFZ=0.
      DO 71 I=1,M
      B=N
      OBSF=F(I)/B
      CFZ=CFZ+OBSF
 71   CBF(I)=CFZ
      DO 41 I=1,M
      UU=(X(I)-U)/S
      R=0.
      IF  (UU)   131,131,132
 131  UU=ABS(UU)
      R=1.
 132  CONTINUE
      ZU=1./(SQRT(6.28318)*EXP(UU**2/2.))
      T=1./(1.+.33267*UU)
```


186

```
      PX=1.-  (.4361336*T-.120167*(T**2)+.9372980*(T**3))* ZU
      IF (R)  134,134,135
135   PX=1.-PX
134   CONTINUE
41    AAN(I)=PX
      DO 81 I=1,M
      DIFF(I)=ABS(AAN(I)-CBF(I))
81    CONTINUE
      PRINT 888
888   FORMAT('OBSERVED DATA       FREQUENCY          OBSERVED FUNCTION
     1NORMAL FUNCTION          ABSOLUTE DIFFERENCE')
      DO 96 I=1,M
96    PRINT 999,X(I),F(I),OBF(I),AAN(I),DIFF(I)
999   FORMAT(1H,F15.8,5X,F10.5,5X,F15.8,5X,F15.8,5X,F15.8)
      DIFMX=0.
      DO 83 I=1,M
      IF (DIFMX-DIFF(I)) 86,83,83
86    DIFMX=DIFF(I)
83    CONTINUE
      PRINT 400,DIFMX
400   FORMAT(//'MAXIMUM ABSOLUTE DIFFERENCE=',F20.8)
      TEST=1.63/(SQRT(B))
      PRINT 403,TEST
403     FORMAT(//'KOLMOGOROV CRITICAL VALUE AT 99 PERCT CL=',F15.8/)
      RETURN
      END
```


187

```
      SUBROUTINE DELTAT(RV,SRV,Q,SQ)
      DIMENSION DT(120)
      COMMON /CBLK/RECESL,SRESSL
      C1=60./17.57
      Q=C1*Q
      SQ=C1*SQ
      RKW=.396766
      ROI=.43/.393
      N=100
      RKP=218.
      RLE=14.5/12.
      RLC=7./12.
      DO 5 I=1,N
      RRV=(GAUS(0)*SRV)+RV
      RVC=(.393-RRV)*((GAUS(0)*.018)+.25)+RRV
      RIVE=.393/RVC
      RIVER=(.393-RRV)*((GAUS(0)*.03)+.41)+RRV
      RIVER=.393/RIVER
      RECL=(GAUS(0)*SRESSL)+RECESL
      RESE=ALOG(RIVE)/(6.28318*RKW*(RLE-RECL))
      RESER=ALOG(RIVER)/(6.28318*RKW*RECL)
      RIVC=.393/RRV
      RQ=(GAUS(0)*SQ)+Q
      RRPE=ALOG(ROI)/(6.28318*RKP*RLE)
      RRWE=RESER*RESE/(RESER+RESE)
      RRWC=ALOG(RIVC)/(6.28318*RKW*RLC)
      RRPC=ALOG(ROI)/(6.28318*RKP*RLC)
      SUMR=RRPE+RRWE+RRWC+RRPC
    5 DT(I)=RQ*SUMR
      CALL MEAN(N,DT,DDT,SDT)
      PRINT 100,DDT,SDT
  100 FORMAT(//'MEAN DT=',F15.8//,'STDV DT=',F15.8//)
      RETURN
      END
```


188

```
      SUBROUTINE AKVAL(N,X,AL,SAL,AK,SK)
      DIMENSION X(400)
      PRINT 501
501   FORMAT('DATA IS')
      DO 14 J=1,N
14    PRINT 621,X(J)
621   FORMAT(1H,F15.8)
      PRINT 16
16    FORMAT('SAMPLE SIZE IS')
      PRINT 610,N
610   FORMAT(1H,I5)
      DO 33 I=1,N
      A=(GAUS(0)*SAL)+AL
   33 X(I)=6.133E-04*(2.0/X(I))*(2.205E-03/A)*(1./62.265)*(2./62.265)*
     1(1./32.2)
      Z=N
      SUM=0.
      DO 181 I2=1,N
181   SUM=SUM+X(I2)
      EXBAR=SUM/Z
      SUMSQ=0.
      DO 191 I3=1,N
191   SUMSQ=SUMSQ+(X(I3)-EXBAR)**2
      SUMSQN=SUMSQ/(Z-1)
      SQSIG=SQRT(SUMSQN)
      PRINT 106,EXBAR,SQSIG
106   FORMAT(//'MEAN VALUE =',F20.8//,'STANDARD DEVIATION=',F20.8//)
      AF=SUMSQ/Z
      X1=0.
      X2=0.
      X3=0.
      X4=0.
      DO 21 I=1,N
      X1=X1+X(I)
      X2=X2+X(I)**2
      X3=X3+X(I)**3
21    X4=X4+X(I)**4
      CM3=X3/Z-3*(X2/Z)*(X1/Z)+2*(X1/Z)**3
      ALPHA3=CM3/(SQRT(AF**3))
      PRINT 203,ALPHA3
203   FORMAT(//'COEFFICIENT OF SKEWNESS =',F20.8//)
      CM4=X4/Z-4*(X1/Z)*(X3/Z)+6*(X2/Z)*(X1/Z)**2-3*(X1/Z)**4
      ALPHA4=CM4/(AF**2)
      PRINT 301,ALPHA4
301   FORMAT(//'COEFFICIENT OF KURTOSIS =',F20.8//)
      AK=EXBAR
      SK=SQSIG
      RETURN
      END
```


190

```
      SUBROUTINE RVALU(N,X,RE,SR)
      DIMENSION X(400)
      PRINT 500
500   FORMAT('DATA IS')
      DO 13 J=1,N
13    PRINT 620,X(J)
620   FORMAT(1H,F15.8)
      PRINT 15
15    FORMAT('SAMPLE SIZE IS')
      PRINT 611,N
611   FORMAT(1H,I5)
      CONST=288.*4.92345E-03/62.2389
      DO 162 I=1,N
162   X(I)=CONST/X(I)
      Z=N
      SUM=0.
      DO 182 I2=1,N
182   SUM=SUM+X(I2)
      EXBAR=SUM/Z
      SUMSQ=0.
      DO 192 I3=1,N
192   SUMSQ=SUMSQ+(X(I3)-EXBAR)**2
      SUMSQN=SUMSQ/(Z-1)
      SQSIG=SQRT(SUMSQN)
      PRINT 107,EXBAR,SQSIG
107   FORMAT(//'MEAN VALUE =',F20.8//,'STANDARD DEVIATION=',F20.8//)
      AF=SUMSQ/Z
      X1=0.
      X2=0.
      X3=0.
      X4=0.
      DO 22 I=1,N
      X1=X1+X(I)
      X2=X2+X(I)**2
      X3=X3+X(I)**3
22    X4=X4+X(I)**4
      CM3=X3/Z-3*(X2/Z)*(X1/Z)+2*(X1/Z)**3
      ALPHA3=CM3/(SQRT(AF**3))
      PRINT 204,ALPHA3
204   FORMAT(//'COEFFICIENT OF SKEWNESS =',F20.8//)
      CM4=X4/Z-4*(X1/Z)*(X3/Z)+6*(X2/Z)*(X1/Z)**2-3*(X1/Z)**4
      ALPHA4=CM4/(AF**2)
      PRINT 302,ALPHA4
302   FORMAT(//'COEFFICIENT OF KURTOSIS =',F20.8//)
      SR=SQSIG
      RE=EXBAR
      RETURN
      END
```


191

```
      SUBROUTINE MVALU(N,X,AL,SAL)
      DIMENSION X(400)
      PRINT 600
  600 FORMAT('SAMPLE SIZE IS')
      PRINT 610,N
  610 FORMAT(1H,I5)
      PI=3.14159/576.
      D1=.786
      DO 30 I=1,N
   30 X(I)=PI*(D1**2-X(I)**2)
      Z=N
      SUM=0.
      DO 180 I2=1,N
  180 SUM=SUM+X(I2)
      EXBAR=SUM/Z
      SUMSQ=0.
      DO 190 I3=1,N
  190 SUMSQ=SUMSQ+(X(I3)-EXBAR)**2
      SUMSQN=SUMSQ/(Z-1)
      SQSIG=SQRT(SUMSQN)
      PRINT 555,EXBAR,SQSIG
  555 FORMAT(//'MEAN VALUE =',F20.8//,'STANDARD DEVIATION=',F20.8//)
      FF=SUMSQ/Z
      X1=0.
      X2=0.
      X3=0.
      X4=0.
      DO 20 I=1,N
      X1=X1+X(I)
      X2=X2+X(I)**2
      X3=X3+X(I)**3
   20 X4=X4+X(I)**4
      CM3=X3/Z-3*(X2/Z)*(X1/Z)+2*(X1/Z)**3
      ALPHA=CM3/(SQRT(FF*3))
      PRINT 666,ALPHA3
  666 FORMAT(//'COEFFICIENT OF SKEWNESS =',F20.8//)
      CM4=X4/Z-4*(X1/Z)*(X3/Z)+6*(X2/Z)*(X1/Z)**2-3*(X1/Z)**4
      ALPHA4=CM4/(FF**2)
      PRINT 300,ALPHA4
  300 FORMAT(//'COEFFICIENT OF KURTOSIS =',F20.8//)
      SAL=SQSIG
      AL=EXBAR
      RETURN
      END
```


192

```
      SUBROUTINE MEAN(N,X,EXBAR,SGSIG)
      DIMENSION X(400)
      PRINT 600
600   FORMAT('SAMPLE SIZE IS')
      PRINT 610,N
610   FORMAT(1H,I5)
      Z=N
      SUM=0.
      DO 180 I2=1,N
180   SUM=SUM+X(I2)
      EXBAR=SUM/Z
      SUMSQ=0.
      DO 190 I3=1,N
190   SUMSQ=SUMSQ+(X(I3)-EXBAR)**2
      SUMSQN=SUMSQ/(Z-1)
      SQSIG=SQRT(SUMSQN)
      PRINT 555,EXBAR,SGSIG
555   FORMAT(//'MEAN VALUE =',F20.8//,'STANDARD DEVIATION=',F20.8//)
      RETURN
      END
```


193

```
      SUBROUTINE RECESS(Q,SQ,ALPPN,SRALPN,H,SH)
      DIMENSION Y(200)
      COMMON RHOF,UL,AL,H1L,RE,SR,HFG,AK,SK,SAL
      COMMON /CBLK/RECESL,SRESSL
      AMO=(Q*.05692/(HFG*60.))
      SAMO=SQ*.05692/(HFG*60.)
      EL=14.5/12.
      SEL=.03
      FH=H/12.
      SFH=SH/12.
      X=0.
      DX=.25/12.
      C1=(UL*.5*AMO)/((RHOF**2)*32.2*AK*AL)+(9.5/24.)*FH
      A=(AMO*UL)/(AK*32.2*(RHOF**2)*EL*3.*AL/4.)
      B=FH/2.
      N=58
      DO 3 I=1,N
      X=X+DX
      PD=-A/2.*(X**2)+(EL*A+B)*X+C1
      IF (PD-H1L) 5,6,6
    5 OPD=PD
      PRINT,PD
      OX=X
    3 CONTINUE
    6 RECESL=EL-OX
      ALPPN=RECESL**2/(5.25*EL)+2.*EL/3.+.5
      NN=100
      DO 9 I=1,NN
      RK=(GAUS(0)*SK)+AK
      RA=(GAUS(0)*SAL)+AL
      RAMO=(GAUS(0)*SAMO)+AMO
      RH=(GAUS(0)*SFH)+FH
      RTH=(GAUS(0)*.052)+.75
      RC=(UL*.5*RAMO)/((RHOF**2)*32.2*RK*RA)+(9.5/24.)*RH
      AA=(RAMO*UL)/(RK*32.2*(RHOF**2)*EL*RTH*RA)
      RB=RH/2.
      RPD=-(AA/2.)*(OX**2)+(EL*AA+RB)*OX+RC
      Y(I)=RPD
    9 CONTINUE
      CALL MEAN(NN,Y,XBAR,SX)
      PD=XBAR
      SPD=SX
      SLOPE=-A*OX+EL*A+B
      BB=SPD**2+SH**2
      SRESSL=SQRT(BB)/SLOPE
      DO 10 I=1,NN
      RRECSL=(GAUS(0)*SRESSL)+RECESL
      RTHRD=(GAUS(0)*.014)+.19
      REL=(GAUS(0)*SEL)+EL
      RTTH=(GAUS(0)*.048)+2./3.
      RALPPN=(RRECSL**2)*RTHRD/REL+RTTH*REL+.5
   10 Y(I)=RALPPN
      CALL MEAN(NN,Y,XBAR,SX)
      SRALPN=SX
      PRINT,SRALPN
      PRINT,OX
      PRINT,SRESSL
      RETURN
      END
```


194

```
SUBROUTINE SUMDIF(SA,SB,SC)
SA=SB**2+SC**2
SA=SQRT(SA)
RETURN
END
```

```
SUBROUTINE CUOT(SA,SB,SC,BBAR,CBAR)
SA=((CBAR**2)*(SB**2)+(BBAR**2)*(SC**2))/(CBAR**4)
SA=SQRT(SA)
RETURN
END
```

```
SUBROUTINE PROD(SA,SB,SC,BBAR,CBAR)
SA=(BBAR**2)*(SC**2)+(CBAR**2)*(SB**2)+(SB**2)*(SC**2)
SA=SQRT(SA)
RETURN
END
```



```
SUBROUTINE XSQARE(SX2,SX,XBAR)
SX2=4.*XBAR*XBAR*SX*SX+2.*SX**4
SX2=SQRT(SX2)
RETURN
END
```

APPENDIX C

HEAT PIPE EXPERIMENTAL TEST PROCEDURES

The following is a step-by-step procedure for the testing of a water heat pipe.

1. The heat pipe is thoroughly cleaned using trichloroethylene, alcohol, and water.

2. A wick is saturated with fresh distilled water and inserted into the pipe.

3. The wick is inserted with the seam facing down and is forced against the evaporator plug.

4. The pipe is then filled with distilled water to further saturate the clearance area between the wick and the pipe wall.

5. The water is drained and 30 cc of excess water is injected.

6. The condenser plug is inserted and sealed.

7. The pipe is then evacuated to 23 inches of Hg.

8. The evaporator is lowered and full power (100 watts) applied. The start up is observed to avoid premature burnout.

9. When the pipe pressure reaches 0 psi, the condenser valve is opened to vent any non-condensible residual gases.

10. After venting and resealing, the calorimeter is turned on and the system allowed to reach an equilibrium at the particular power level to be tested.

11. The evaporator is raised in increments of one fourth inch until a wick burnout is attained. A burnout is defined

as a sudden temperature rise of more than 10°F at the extreme end of the evaporator after equilibrium is reached.

12. A second measurement is made to determine the burnout height within one eighth inch of the true height.

13. Data recorded at this time are:

a. Heat pipe temperature distribution

b. Calorimeter flow and temperature rise

c. Pipe vapor pressure

d. Burnout height

14. The power is now disengaged and the evaporator seal broken.

15. The gravity head is measured at the various burnout heights, as shown in Figure 3.5.

16. The permeability is measured, as described in Figure 3.9. Thirty flow readings are recorded. Permeability is calculated according to the formula $K = uL'\dot{m}/\rho A\Delta p$, where Δp is assumed to be the linear head loss through the wick.

17. The wick is removed from the pipe and portions of it are placed in the wick apparatus, as described in Figure 3.12. If five consecutive identical readings are observed, they are considered to be the mean and the standard deviation is chosen to be one half the least count of the instrument. r_{fr} is calculated as: $r_{fr} = 2\sigma/\rho GH$.

18. The data are compiled for reduction.

The procedure for wire mesh wick manufacture is as follows.

1. The raw wire mesh is cut to size and the retainer rod is welded to an edge.

2. The wire mesh is inserted into the mandrel, wrapped in the wrapping apparatus (Figure 3.15) and welded.

4. The wick is cleaned as follows:

   a. Ultrasonic cleaner with alkanox.

   b. Rinse with tirchloroethylene.

   c. Rinse in methanol.

   d. Rinse in distilled water.

5. The wick is oxidized in air at 850°F for two hours.

6. Storage is under distilled water.

198